



Norwegian University  
of Life Sciences

**Master's Thesis 2023 30 ECTS**

Faculty of Science and Technology

# **Vibration Behaviour of Pedestrian Bridges with Different Construction Systems**

Hassan Mazloum

Construction Engineering and Architecture

## Acknowledgements

This thesis marks the end of a five-year education on the Master`s degree in Structural Engineering and Architecture at the Norwegian University of Life Science - NMBU.

Primarily, I want to thank God for the gift of life and His mercies. I also want to thank my family for giving me strength and support throughout this period of research and writing. I would like to express my most profound gratitude to my primary supervisor, Professor Ebenezer Ussher. Your support, patience, and guidance made this thesis a possibility and a reality. I would also like to thank Dr Xiaojun Gu (Scott) for his time and expertise when conducting for the thesis. Furthermore, I want to thank Viken Municipality and Statens Vegvesen in Norway for giving their time and effort to provide data and files that helped complete this thesis. Finally, my appreciation goes to NMBU and my fellow students. Thank you all for great years, discussions, assistance, and memories.

Oslo, June 7, 2023



---

Hassan Mazloun

## Abstract

The design of pedestrian bridges is continuously being developed and the mechanical properties influence the dynamic properties in the SLS. Pedestrian induced vibrations have been a major concern regarding design criteria and construction. The opening of the Millennium bridge in London in 2000 made headlines regarding the matter and several researchers and papers have been assessing vibrations on pedestrian bridges due to pedestrian loading. Thus, the main goal of this thesis is to contribute to the global community researching the matter with the implementation of field tests and numerical solutions with the use of FE-modelling.

The procedure in this thesis involved field tests on two bridges with different systems and materials. The field tests estimated natural frequencies, mode shapes and their respective damping ratios. Results from the field test modal analyses were used to validate a FE-Model and the verified model employed to perform a parametric study that showed the development of frequencies and modes as the span changed. Following the modal analyses time-history response analyses computing the Vibration Dose Values (VDV) and Root Mean Square (RMS) were evaluated and compared with the ISO 10137. The accelerations recorded in the field tests were then compared to calculated accelerations in different national and international guidelines. The guideline compared in this thesis includes Statens Vegvesens Handbook N185, the Eurocodes, the UK-NA to Eurocode 1, ISO 10137, SÉTRA, and the JRC.

The modes in both running and walking corresponded both in terms of mode shapes and natural frequencies. The frequency discrepancies were low for both activities resulting in acceptable results. Very good correspondence was also achieved between test and FE results. Furthermore, the calculated running accelerations were more in line with the limits of all guidelines. The walking acceleration did not satisfy all the guideline within the same margins. However, the damping ratios in the respective guidelines, implemented in the guideline calculations were not correspondent with the effective damping ratios from the field results, resulting in high accelerations.

## Acronyms:

AMA	Analytical Modal analysis
DFT	Discrete Fourier Transform
DLF	Dynamic Load Factor
DOF	Degrees of Freedom
EFDD	Enhanced Frequency Domain Decomposition
EOM	Equation of Motion
FDD	Frequency Domain Decomposition
FE	Finite Element
FEM	Finite Element Method
HHI	Human-Human Interaction
HSI	Human – Structure Interaction
ISO	International Organisation for Standardization
JRC	Joint Research Centre
MAC	Modal Assurance Criterion
MOE	Modulus of Elasticity
OMA	Operational Modal Analysis
RMS	Root Mean Square
SÉTRA	Service d’Etudes Techniques des Routes et Autoroutes
SLS	Serviceability Limit State
SSI	Stochastic Subspace Identification
UK-NA	The United Kingdom National Annex.
ULS	Ultimate Limit State

## List of figures:

Figure 1.1: The London Millennium Bridge .....	2
Figure 2.1: a drawing of the most classic MDOF system with two degrees of freedom.....	12
Figure 2.2: a SDOF system with a vibration absorber attached (Chopra, 2014) .....	15
Figure 2.3: Model calibration illustrated graphically.....	24
Figure 2.4: The typical walking force shape after Andriacchi et al. (Andriacchi, et al., 1977) .....	30
Figure 2.5: the figure illustrates the placement of the different structures described above. The figure is extracted from Hartford County (Miller, u.d.) .....	40
Figure 2.6: Examples of pre-stressed transversal glulam slab. Illustration to the left is extracted from a doctorate thesis (Ekholm, 2013) and from a glulam book: “Limtreboka” (Norsk Limtreprodusenters forening, 2015) .....	42
Figure 3.1: Nordre Finstad bridge photographed from the road below, and blueprints of the bridge () courtesy of Viken Municipality.....	45
Figure 3.2: Modelled bridge extracted from the blueprints, courtesy of Statens Vegvesen – Norwegian Public Road Administration.....	47
Figure 3.3: Photographs of the bridge on the left side of the road (top) and the span of the bridge crossing the river (bottom).....	47
Figure 3.4: illustration of placement of the double-sided tape for securing the sensors.....	49
Figure 3.5: Distribution of the sensors on the timber bridge with the same spacing and distances. ....	49
Figure 3.6: Reference sensor marked with a red ribbon. ....	50
Figure 3.7: The testing procedure illustrated with roving sensors, reference sensors and data readers. ....	51
Figure 3.8: The finished geometry for the timber deck with nodes, lines, and surfaces. ....	52
Figure 3.9: the placement of reference and roving sensors on the bridge according to the physical placement on the bridge deck .....	53
Figure 3.10: an overview of the test placements. This acts as a basis for the time-history results presented later. ....	56
Figure 4.1: the ratio for span and width, $d/L$ to determine the value for K in equation 4.2. ....	59

Figure 4.2: Dynamic factor load factor $\psi$ at the y-axis can be extracted depending on the span length L on the x-axis due to the damping $\xi$ .	60
Figure 4.3: Graph that gives $k_{vert}$ depending on $f_{vert}$ .	63
Figure 4.4: The acceleration in the vertical direction based on the frequency ranges. This is the basis for calculations in Table 4.6.	67
Figure 5.1: A graph of the damping development for each mode in the walking scenario. Values are based on field test from Table 5.1.	76
Figure 5.2: A graph of the damping development for each mode in the running scenario. Values are based on field test from Table 5.1.	77
Figure 5.3: Illustrates the frequency graph for running from ARTeMIS with marked amplitudes.	79
Figure 5.4: Illustrates the frequency graph for walking from ARTeMIS with marked amplitudes.	80
Figure 5.5: The different VDV values calculated on each of the sensors distributed on the bridge deck for walking.	83
Figure 5.6: The different RMS values calculated on each of the sensors distributed on the bridge deck for walking.	83
Figure 5.7: The different VDV values calculated on each of the sensors distributed on the bridge deck for running.	84
Figure 5.8: The different RMS values calculated on each of the sensors distributed on the bridge deck for running.	85
Figure 5.9: The graph represents the frequencies at each mode for the different spans studied.	94
Figure 5.10: Calculated peak walking acceleration for all field tests conducted on the timber bridge.	96
Figure 5.11: Calculated peak running acceleration for all field tests conducted on the timber bridge.	96
Figure A. 1: The timber bridge deck seen from the above.	108

Figure A. 2: Cross section of the timber bridge deck blueprints courtesy of Viken Municipality .....	108
Figure A. 3: Cross section of the timber bridge including deck and columns. ....	109
Figure A. 4: Longitudinal section (left) and cross section (right) of the concrete abutments on each side of the timber bridge.....	110
Figure A. 5: Illustrations with dimensions of the oval columns and connections of the concrete fundaments.....	111
Figure B. 1: Longitudinal section of the steel bridge with truss configuration. ....	112
Figure B. 2: The steel bridge seen from above and marked with lines where the floor beams are placed.....	112
Figure B. 3: Cross section of the bridge showing both the top and bottom chords. ....	112
Figure C. 1: Details regarding accelerometer Model 39B31 and Model 393B12 .....	113
Figure C. 2: Details regarding amplifiers Model MX440B and Model MX840B.....	114
Figure C. 3: The specifications for the MX1601B amplifier. ....	115
Figure D. 1: Acceleration calculations made in accordance with the guidelines presented.....	116

## List of tables:

Table 2.1: table by Ingólfsson comparing the walking average walking characteristics according to different researchers. ....	34
Table 4.1: determination of factor K based on the span width ratio in Figure 4.1. If there is only one slab, the factor for K is 1.0. ....	60
Table 4.2: Damping ratios for timber bridges according to Eurocode 5. ....	62
Table 4.3: Recommended values for the site usage factor $k_1$ . ....	65
Table 4.4: Recommended values for the route redundancy factor $k_2$ . ....	65
Table 4.5: Recommended values for the structure height factor $k_3$ . ....	65
Table 4.6: An overview of calculations for different frequency ranges according to Figure 4.4. ....	67
Table 4.7: Advised damping ratios ( $\xi$ ) for different materials according to SÉTRA. ....	70
Table 4.8: Comfort classes and their respective degrees of comfort followed by the acceleration value for the vertical direction. ....	71
Table 4.9: Frequency range for the vertical direction according to the JRC guideline ....	71
Table 4.10: Different materials` minimum and average damping ratios according to the JRC guideline. ....	72
Table 4.11: Summary of all acceleration limits in the presented guidelines. ....	73
Table 4.12: Summary of available frequency ranges in the guideline mentioned in Chapter 4. ....	73
Table 5.1: An overview of the field test results with all parameters and mode shapes for both running and walking. ....	74
Table 5.2: Damping ratios for timber in three of the guidelines mentioned in Chapter 4. ....	77
Table 5.3: Frequency ranges based on guidelines presented in Chapter 4. ....	78
Table 5.4: An overview of the field test results with all parameters and mode shape for both running and heel-drop for the steel bridge. ....	81
Table 5.5: Advised damping values for steel in UK-NA and SÉTRA. ....	81
Table 5.6: VDV values ( $m/s^{1.75}$ ) above which various degrees of adverse comments may be expected in residential buildings. ....	82
Table 5.7: Timber bridge comparison of Field test results and FE-Model for mode one. ....	87
Table 5.8: Timber bridge comparison of Field test results and FE-Model for mode two. ....	88



Table 5.9: Timber bridge comparison of Field test results and FE-Model for mode three. ....	89
Table 5.10: Steel bridge comparison of Field test results and FE-Model for mode one. ....	90
Table 5.11: Parametric study result for timber deck span 10 m. ....	92
Table 5.12: Parametric study result for timber deck span 15 m. ....	92
Table 5.13: Parametric study result for timber deck span 20 m. ....	93
Table 5.14: Parametric study result for timber deck span 25 m. ....	93
Table 5.15: Acceleration limits in the comfort criteria for guidelines presented in Chapter 4....	95
Table 5.17: Comparison of calculated acceleration and the guideline of each guideline presented in Chapter 4. ....	96
Table 5.18: Comparison of acceleration from field tests, calculated acceleration according to guidelines, and acceleration limits for walking. ....	98
Table 5.19: Comparison of acceleration from field tests, calculated acceleration according to guidelines, and acceleration limits for running. ....	99

## Table of contents

Acknowledgements.....	i
Abstract.....	ii
Acronyms: .....	iii
List of figures:.....	iv
List of tables:.....	vii
1 Introduction.....	1
1.1 Background.....	1
1.2 State of the Art.....	3
1.3 Problem Statement and Research Questions .....	6
1.4 Study Objectives.....	7
1.5 Limitations and assumptions .....	8
1.6 Thesis outline .....	8
2 Theory.....	10
2.1 Structural dynamics.....	10
2.2 FEM – Finite Element Method .....	16
2.3 Operational Modal Analysis – OMA.....	19
2.4 Dynamic loading: pedestrian traffic.....	29
2.5 Interaction mechanisms.....	37
2.6 Bridges in different construction systems .....	39
3 Methodology .....	43
3.1 Choice of method.....	43
3.2 Thesis approach.....	44
4 Existing and emerging methods of assessing pedestrian and other bridge vibration performance .....	57
4.1 Statens Vegvesen Handbooks:.....	58
4.2 Eurocodes.....	61
4.3 UK – NA to Eurocode 1.....	64
4.4 ISO 10137 .....	66
4.5 SÉTRA Technical guide: Assessment of vibrational behaviour of footbridges under pedestrian loading.....	68
4.6 JRC – Design of Lightweight Footbridges for Human Induced Vibrations .....	71
4.7 Compendium of Comfort criteria:.....	73

5	Results and Discussion.....	74
5.1	Field experiment results – OMA .....	74
5.2	Time history calculations: VDV and RMS .....	82
5.3	Numerical results – FEM .....	86
5.4	Effect of changes in span length .....	91
5.5	Guideline Evaluation .....	95
6	Conclusion and Further Work.....	100
6.1	Summary and results.....	100
6.2	Further work: Recommendations .....	102
	References .....	103
	Appendix A: Blueprints for timber bridge.....	108
	Appendix B: Blueprints for Steel bridge.....	112
	Appendix C: Raw data on the accelerometers and amplifiers used to conduct the field tests.	113
	Appendix D: Acceleration calculation based on the guidelines. ....	115

# 1 Introduction

## 1.1 Background

Since the dawn of time, humans have moved from one place to another. Crossing certain obstacles required innovative technology and construction systems. The invention of the bridge made crossing these obstacles a reality. This innovation has been developed over the years and constructed in simple forms to advanced construction systems as the years went on. The design of pedestrian bridges has been so impressive that certain bridges have become tourist attractions and landmarks. The limitation is only in the eye of the creator when it comes to the possibilities available due to the modern technology and engineering methods of constructing bridge systems.

The design of lightweight and slender bridges is constantly developed regarding the ultimate limit state – ULS. Thus, the mechanical properties and the loading of the bridges have been problematic for the dynamic performance in the Serviceability Limit State – SLS. Vibrations due to pedestrian activity are being brought up and are frequently discussed in the field. The bridge's natural frequency and the pedestrian's walking frequency coincides, implementing the phenomenon known as resonance (Zivanovic, et al., 2005). This is a frequently occurring problem on different pedestrian bridges, which are also made of varied materials.

Looking further back in time, in 1821, Stevenson reported vibrations on a footbridge because of pedestrians and led horses passing on the bridge (Stevenson, 1821). This is the earliest indication of vibrations on pedestrian bridges. Moving centuries forward in time, one event that sparked the interest of many engineers was the opening of the Millennium Bridge in London in June 2000. The 325m long steel complex steel structure impacted the world on how vital the vibrational matter of pedestrian bridges is due to the resonance occurrence on the bridge. Due to the extensive media coverage and recognition of the happening on the Millennium Bridge, the problem of the vibration of pedestrian bridges became alarming; in fact, in 2002, an

international conference with the title *Footbridge 2002* was held in Paris and was devoted to the matter. Many articles presented state-of-the-art in footbridge-induced dynamic load (Schlaich, 2002). Despite the event striking over 20 years ago, this is still a frequent problem in the field, and many different load models, guidelines, and codes have been implemented to assess the situation.



*Figure 1.1: The London Millennium Bridge*

## 1.2 State of the Art

Different articles, papers, and other sources have studied ambient vibrations and vibrations in different systems. This section discusses various literature regarding various sources and research on the vibration characteristics of pedestrian bridges as the state of the art of this thesis.

As mentioned earlier, the Millennium Bridge sparked much interest in bridges when vibrations occurred on its opening day on the 10th of June 2000. Researchers were on a mission to understand the phenomena that occurred due to the swaying and loading of multiple pedestrians. In 2002 Aleksandar Pavic and a handful of researchers from the United Kingdom (UK) tested the Millennium Bridge for the vertical and lateral mode that gave them the opportunity to evaluate the Frequency response functions – FRFs (Pavic, et al., 2002). The procedure was done by two different shakers on the bridge. Dallard et al. Took a different approach to the testing by implementing moving platforms on which pedestrians walked, intending to account for the probability that a pedestrian's footfall rate will synchronize to the frequency of the platform in a swaying motion, otherwise known as a "lock-in" effect (Dallard, et al., 2001). Furthermore, Dillard et al. also took it upon themselves to improve the damping level to over 20 % critical. This was done by implementing fluid viscous dampers and tuned mass dampers.

In 2005 Zivanovic et al. took it upon themselves to research the human-induced dynamic loading of pedestrian bridges, also known as footbridges. Their report, which included the dominant load induced, paved the way for the excessive research of the Vibration serviceability of footbridges under human-induced excitation. Looking at early work back to the 1800s, Zivanovic et al. take on more than two hundred references of studies conducted on pedestrian bridges and assessed them through 6 different parts (Zivanovic, et al., 2005). The first three parts of the literature review are based on the material properties concerning the vibration path, source, and receiver. The fourth outlines the human–structure dynamic interaction phenomenon, the fifth part reviews the necessary procedures or recommendations, and the

sixth part reviews measures against excessive vibrations of footbridges. After reviewing over two hundred sources, one of the main findings was that forces induced by joggers have not been researched much in the past and running and low damping together increases the response of the structure. Furthermore, the report also discusses how the dynamic properties such as mass, stiffness and damping are important when estimating natural frequencies and mode shapes within implementation of Finite Element Modelling. However, the damping is obtained best with field test conducting.

Later, many guidelines were implemented to assess the vibrational problem in pedestrian bridges. As a result, different tests have been done on pedestrian bridges worldwide by implementing the various design codes. Using software for numerical analysis called SOFISTIK, Ramoul, and Spremic at the University of Belgrade, Serbia, the "Step by step" integration method was used to experiment on an arched steel bridge (Ramoul & Spremic, 2021). They were able to compare the numerical results with the load models in three different guidelines: Eurocode 1 pre-standard (EN 1991-2), SÉTRA Guide (Service d'Études techniques des routes et autoroutes), and the UK National Annex to EN-1991-2. This is one of the few experiments that found that many of the guidelines are adequate to some degree. However, the Eurocode does not define recommendations and data for the performance of dynamic analysis due to pedestrians. And the different guidelines analysed, all offered different results. The design recommendation in SÉTRA and UK-NA leads to slender structures with lower stiffness that ultimately fulfils the SLS criteria. Nonetheless, implementing the same solution in the Pre-standard of Eurocode 1 leads to discomfort in the comfort criteria and vibration dampers should be considered.

In South America, A dynamic study of timber footbridges with uncertain mechanical properties considering the Human Structure Interaction (HSI) induced by the pedestrians is presented in a study conducted by Garcia et. al and is extracted from *Asociación Argentina de Mecánica Computacional*, the Argentine Association of Computer Mechanics (García, et al., 2018). The study takes on the uncertain mechanical properties of timber footbridges due to the Human

structure interaction – HSI induced by pedestrians. To understand the matter, Garcia et al. used a stochastic approach. Using a *Probability Density Function (PDF)* of the timber properties formulated the researchers applied the *principle of maximum entropy (PME)* to address the matter of random distances between the finger joints. Pedestrians arrive at the footbridge under a Poisson distribution, and the arrival velocity is such that the footbridge dimension achieves a medium/low transit density. Stochastic properties of the HSI model are introduced through their PDFs. Changes in the natural frequencies and structure damping induced by the HSI are numerically obtained through the Finite Element Method (FEM) and Monte Carlo Simulations (MCS). The use of the Finite Element Method (FEM) has vastly improved over the years, and Finite Element Model Updating has paved the way for perfecting models for further use. The stochastic analysis performed by the authors resulted in extending the range of response starting from a beam modelled equivalently as the footbridge. Thus, it was discovered that when the beam`s stiffness increased, the first natural frequency change and the damping decrease. This led to the modification of the modal damping that was approximated in a linear relation. The velocity on arrival on the other hand did not modify the damping considerably.

Recently in 2022, Ussher et al. researched timber floors. Their interest in predicting vibration serviceability performances in lightweight timber floors highlighted the best design procedures and analysis methods in the European and North American hemispheres. The paper addressed the different variables and guideline values associated with the practices of the 21 first century to ensure good architectural and construction design choices and researched the dynamic effects occupancies floor motions have on timber floors (Ussher, et al., 2022). Ussher et al. recommends the development of design rules and methods that are international and accepted by international organizations, such as the ISO standards. The information out in public today is significant and applicable in many cases, but it needs more support for further investigation on issues in the 21<sup>st</sup> century. The dynamic time-history responses such as VDV and RMS are robust and reliable for assessment of the acceptable dynamic motions of timber floors. The methods are not fully developed but have come a far way and are worth investigating.



In Turkey, Altunisik et al. researched full-scale arch-type steel highway bridges. Finite element modelling and operational modal analysis were presented on the bridge. Using project drawings and Analytical Modal Analysis (AMA), they constructed a 3D FEM model in SAP2000 that generated natural frequencies and mode shapes in the three orthogonal directions (Altunişik, et al., 2011). They implemented the use of Operational Modal Analysis (OMA) as well by ambient vibrational testing of the bridge deck under natural excitation such as traffic, human walking, and wind loads. Lastly, the authors compared the dynamic characteristics of the bridge due to the analysis and the physical experiments. The author concluded that mode shapes found in the EFDD and SSI were close in matter of frequencies and mode shapes. This was confirmed for six modes. The Modal Assurance Criterion – MAC value compared was over 90% generally and the damping ratios was close in both SSI and EFDD. Ambient Vibration measurement using EFDD and SSI are enough to identify the mode of a highway bridge in steel and update of the Finite Element Model is essential to ensure the safety the analysis performed on the bridge.

### 1.3 Problem Statement and Research Questions

This thesis addresses various research questions with the goal of contributing to the global community researching the vibrational matter in pedestrian bridges. The conclusions made in the report are based on field experimental campaign and numerical studies verified with the experimental results.

Little documentation has been done on the vibration characteristics of pedestrian bridges built from different materials. However, said characteristics including the natural frequencies, mode shapes, and the effective damping are design precursors upon which demands may be estimated and verified with design guideline limits.

Currently the Vibration Dose Values (VDV) have become popular in assessing vibration serviceability in regulation to human interaction with structures. However, its application to bridge vibration serviceability is limited.

This study attempts to answer the following questions:

- 1) What are the modal characteristics of pedestrian bridges constructed from different systems and materials?
- 2) How do engineering design variables affect the modal responses of pedestrian bridges?
- 3) Are existing and emerging design guidelines including those that prescribe VDV, effective and reliable for assessing the vibration performance of pedestrian bridges under human footfall excitations?

#### 1.4 Study Objectives

The following objectives therefore underpin this thesis:

1. To procure data on the modal characteristics of pedestrian bridges designed and built with various construction systems – the targets are natural frequencies, mode shapes, damping ratios, frequency separations and time history responses.
2. To assess the effect of engineering design variables on the dynamic characteristics of pedestrian bridges - this objective considers the effect of span lengths, supporting systems, simple spans, continuous spans, and similar bridges in different materials.
3. To assess the reliability and robustness of existing and emerging design rules in evaluating the dynamic performance of pedestrian bridges under human footfall impacts.

## 1.5 Limitations and assumptions

Dynamic assessment of footbridges is a very complicated topic, making it a quite wide topic. Many parts of the field have been studied and assessed, making this thesis a contribution for comparison and further research. Thus, the work in this thesis is limited to the following:

- Coverage of serviceability state is the only state considered. In other words, the comfort criteria and loading of the bridge will be the focus. Load models from guidelines are not applied to models due to time constraints. The risk of structure failing in ULS will also be neglected.
- The calculations and measurements of the bridges in the respective cases are considered vibration in the vertical direction only. The transversal and longitudinal vibrations due to pedestrian activities are not a part of this thesis.
- Simplifications of the FE-Model are made. However, models are developed to represent real systems as close as possible. Curvatures and unknown dimensions are measured, calculated, and assumptions made where necessary. Unknown material properties are assumed to be the median values found in the literature.

## 1.6 Thesis outline

The thesis is divided into respective chapters and are described in the following paragraphs:

**Chapter 1:** this chapter presents the introduction of this study in which background information of the studied topic, state of the art, research questions and objectives and the limitations perceived are provided.

**Chapter 2:** introduces the theory of structural dynamics and the implementation of DOFs systems. Furthermore, the chapter describes the Finite Element Method and the application of

the method before describing Operational Modal Analysis and the theory behind that method of testing. Software for each respective analysis method is assessed and described. The theory behind dynamic excitation values and calculations from pedestrians and interaction mechanisms followed by construction types of pedestrian bridges concludes this chapter.

**Chapter 3:** describes how the approach answers the research questions and problem statements. How the results were derived, calculated, and presented, as well as figures and tables to understand the results, are also presented in this chapter.

**Chapter 4:** presents existing guideline comfort criteria and parameters, including calculating acceleration values according to the respective guidelines.

**Chapter 5:** presents all the results, validations, and calculations from field experiments, time-history analysis, numerical solutions, parametric studies, and guideline evaluations. The results are then compared and discussed through tables and figures.

**Chapter 6:** concludes the thesis based on the previous chapters. Results and validations are summed up, and recommendations for further work concerning the thesis are presented.

## 2 Theory

### 2.1 Structural dynamics

Structural dynamics involves the study of a given structure subjected to dynamic loads. Dynamic loads are loads applied to a structure as a function with respect to time. The response of the system depends on its dynamic properties such as stiffness, damping, and inertia. These contribute to forces depending on displacements, velocities, and accelerations opposing the motions. The responses are obtained by combining these forces and the equation below illustrates how the different dynamic properties result in the external force acting on a given system (Chopra, 2014):

$$p(t) = f_S + f_D + f_I \quad (2.1)$$

Where:

- $p(t)$  is the external force acting on the system,
- $f_S$  is the resisting force related to the displacement  $u$  times the stiffness  $k$ ,
- $f_D$  is the damping force related to the velocity times the damping,
- $f_I$  is the inertial force related to acceleration times the mass.

#### 2.1.1 SDOF - Single Degree of Freedom systems

A single degree of freedom as the name implies consists of a system in which oscillations occur about a single position. Here the equation of motion may be generalized. Due to the single scalar, an analysis consisting of a single degree of freedom gives an approximate result if the system has distributed mass and stiffness. The degrees of freedom normally point of motion, are associated with the mass and is the minimum of scalar quantities necessary to describe the mechanical configuration of a given system completely. Infinite degrees of freedom will give the most accurate representation of a system, and will be explained further in the next part of the chapter.

Newton's second law of motion, the EOM can be derived as the equation knowing that  $F = m * a$ , or in this case,  $p(t) = m\ddot{u}$ . Implementing this in the equation from above, results in the *Equation of Motion* for a SDOF system. This is illustrated below (Chopra, 2014)

$$p - f_S - f_D = m\ddot{u} \rightarrow p = m\ddot{u} + f_S + f_D \quad (2.1)$$

Incorporating the system dynamic properties, equation (2.1) may be re-written as:

$$m\ddot{u} + c\dot{u} + ku = p(t) \quad (2.2)$$

Where:

$m$ ,  $c$ , and  $k$  are the mass, damping and stiffness values and,  $u$ ,  $\dot{u}$  and  $\ddot{u}$  are the displacement velocity and acceleration, respectively.

### 2.1.2 MDOF - Multi Degree of Freedom systems

Complex structures have an infinite number of degrees of freedom. Multi degrees of freedom systems are introduced when a system requires two or more coordinates to describe the motion. However due to the complexity, it is possible to limit the masses, members, and node displacements to a finite number. This is done as an approximation and analyses done by either analytical or numerical tools.

Using the equation of motion, the matter of multi degree of freedom can be assessed, however it is assessed differently. Due to the elements now assembled by nodes, it leads to many members with interconnected masses, stiffnesses and damping (Chopra, 2014). Therefore, analysis involves formulation of matrices for the mass  $\mathbf{M}$ , the damping  $\mathbf{C}$ , and the stiffness  $\mathbf{K}$ . The EOM for a MDOF system can therefore be written as:

$$\mathbf{M}\ddot{\mathbf{u}} + \mathbf{C}\dot{\mathbf{u}} + \mathbf{K}\mathbf{u} = \mathbf{p}(t) \quad (2.3)$$

Where the  $\mathbf{p}(t)$  acts as the applied force vector. This system can be solved for  $N$  different equation depending on the displacement  $\mathbf{u}$  from the applied forces  $\mathbf{p}$ . In Figure 2.1 a MDOF system is presented with two masses ( $m$ ), linear springs ( $k$ ) and viscous dampers ( $c$ ) that are subjected to external forces  $p_1$  and  $p_2$ .

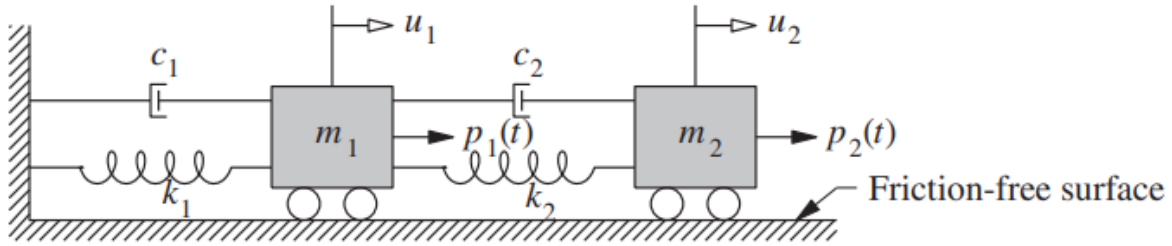


Figure 2.1: a drawing of the most classic MDOF system with two degrees of freedom.

As this thesis takes on the vibrations of pedestrian bridges and the interest lies in the natural frequencies, the modal analysis when performed should focus on the free vibration. Here the damping is neglected, and the natural frequencies of the bridge evaluated based on operating conditions including pedestrians and traffic.

#### Free Vibration

In the absence of damping, the proposed EOM for free vibration is represented by (Chopra, 2014):

$$M\ddot{u} + Ku = 0 \quad (2.5)$$

Where there is no external applied force in theory.

Taking an undamped structure, it will undergo simple harmonic motion if subjected to initial deflection that equals the deflection shape itself (Chopra, 2014). However, if free vibration is initiated and the displacements in the degrees of freedom are distributed appropriately, the characteristics shapes in term of deflection from free vibration exists and the relationship between the natural period for a vibration  $T_n$  and the ordinary and circular frequencies are given by  $f_n$ :

$$T_n = \frac{2\pi}{\omega_n} \quad f_n = \frac{1}{T_n} \quad (2.6) \text{ and } (2.7)$$

The free vibration of an undamped system defines the modal displacements in the natural vibration modes as follows:

$$u = u(t) = \phi_n q_n(t) \quad (2.8)$$

Where:

$\phi_n$  is the deflected shape and does not vary with time.

The variation of time in terms of displacements is described by the simple harmonic function:

$$q_n(t) = A_n \cos \omega_n t + B_n \sin \omega_n t \quad (2.9)$$

Where both  $A_n$  and  $B_n$  are constant found with solving the initial conditions associated with the motion.

Combining equation (2.8) and (2.9) results in the equation for displacement:

$$u(t) = \phi_n (A_n \cos \omega_n t + B_n \sin \omega_n t) \quad (2.10)$$

Where both  $\phi_n$  and  $\omega_n$  are unknown

Taking equation for  $u(t)$  and substituting it in equation (2.5) provides:

$$[\omega_n^2 m \phi_n + k \phi_n] q_n(t) = 0 \quad (2.11)$$

This equation can be satisfied through; First if  $q_n(t) = 0$  which then implies that  $u(t) = 0$  and the system is motionless. Or that the natural frequency  $\omega_n$  and the modes  $\phi_n$  must satisfy the following algebraic equation:

$$k \phi_n = \omega_n^2 m \phi_n \quad (2.12)$$

The solution of this equation provides a useful condition. This is called *the matrix eigenvalue problem* (Chopra, 2014). Since both the stiffness and mass matrixes are known, the remaining scalars to be determined are:  $\omega_n^2$  and  $\phi_n$ . The equation is then written as the following to indicate a formal solution:

$$[k - \omega_n^2 m] \phi_n = 0 \quad (2.13)$$



If the equation is solved as:

$$\det[k - \omega_n^2 m] = 0 \quad (2.14)$$

Then this is a non-trivial solution meaning there is no motion in the system, meaning that at least one of the solutions or one of the variables has a non-zero value. This equation is known as The *Characteristic Equation* or *Frequency Equation*. The equation has  $N$  real as well as positive roots for  $\omega_n^2$ . This is because both  $\mathbf{m}$  and  $\mathbf{k}$  are structural mass and stiffness matrixes that are symmetric and positive definite (Chopra, 2014). The  $N$  roots,  $\omega_n^2$  in equation (2.14) decides the natural frequency,  $\omega_n$  ( $n = 1, 2, 3, \dots, N$ ) of vibration where they traditionally are arranged from smallest to greatest ( $\omega_1 < \omega_2 < \dots < \omega_N$ ). *The Eigen values, Characteristic values, or Normal values* as they also are called, have corresponding mode shapes with each natural frequency which can be solved from equation (2.13).

Since many structures contain a vast number of DOFs, it is critical to express the nodal displacements, respectively. Using “modal analysis,” the system is idealized with “ $N$ ” degrees of freedom. The system is simplified with the help of equation (2.15) that with first glance is in basics the same as the EOM illustrated in the SDOF chapter. The method used results in linear independent systems of “ $N$ ” degrees of freedom equations. These are then solved separately.

$$M_n \ddot{q}_n + C_n \dot{q}_n + K_n q_n = p_n(t) \quad (2.15)$$

The displacement response of each “ $N$ ” DOF system is given by:

$$u(t) = \sum_{n=1}^N \phi_n q_n(t) \quad (2.16)$$

$q_n(t)$  is the modal coordinate for  $n$ :th mode.

At last, the equations for the  $n$  degrees of freedom are formulated. The generalized mass, stiffness, and damping matrices are then given for each mode as in equations (2.17-2.20):

$$M_n = \phi_n^T \mathbf{M} \phi_n, K_n = \phi_n^T \mathbf{K} \phi_n, C_n = \phi_n^T \mathbf{C} \phi_n, P_n(t) = \phi_n^T \mathbf{P}(t) \quad (2.17-2.20)$$

### 2.1.3 Damping

Even though damping is neglected when estimating the natural frequencies, damping can be implemented later in modal analysis and is therefore important to address.

When a system is exposed to damping it is defined as when the energy in the vibrating system is dissipated by different mechanisms. Damping in a structure makes the amplitude of the vibration decrease as the energy is dissipated through different mechanisms. Furthermore, there may be more than one mechanism present initiating the damping on the system. As explained earlier the damping is illustrated through the damping force in structural dynamics, however unlike stiffness the damping cannot be calculated through the structure and size of the elements in the system. Thus, the damping coefficient used is based on experimental data done beforehand (Chopra, 2014)

There are diverse ways of how damping occurs in a structure. This can be from the material properties and the material use in the system, where the energy is dissipated through the material an example would be deformation of the material. Another means is by friction in the system, this is a result of two dry surfaces sliding against each other (Chopra, 2014). An example of this is slipping of joints in the system. The last example would be tuned mass dampers. The latter is often portrayed as a *vibration absorber* where one spring and mass that decreases the unwanted vibration in a construction system. This is illustrated as follows in Figure 2.2:

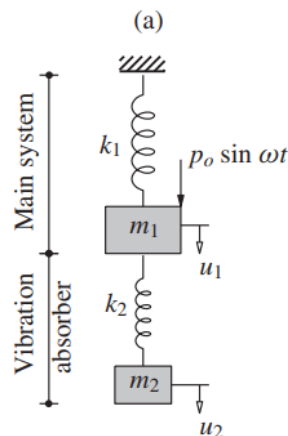


Figure 2.2: SDOF system with a vibration absorber attached (Chopra, 2014)

## 2.2 FEM – Finite Element Method

The Finite Element Method is a well-known technique using numerical analysis to obtain approximate solution to a variety of engineering problems (Ewins, 2000). Originally planned as a method for assessing stresses in complex airframe structure, the method was then applied to vast field of continuum mechanics – continuum here being a body of matter (solid, liquid or gas) or just a region of space where a phenomenon occurs.

### 2.2.1 How does the FEM work?

The idea of the method is based on a discretization process, where the problem in question is reduced from an infinite number of unknowns to a finite number of unknowns. In other words, by implementing the concept of degrees of freedom; the discretization process is about reducing great structures with infinite degrees of freedom to models with finite degrees of freedom. The degrees of freedom are connected through nodal points and the degrees of freedom for the proposed models are located at the nodes. The nodal values as well as the interpolation functions define the field variable within the element.

The finite number of unknowns is then divided into elements with approximating functions, where the functions are defined within the field variable specified points called nodal points, which makes the degrees of freedom.

*The Finite Element Method for Engineers* by Huebner et al. summarizes the steps in the finite element method as follows (Huebner, et al., 2001): *Discretize the Continuum* -- The first step is to divide the solution region into elements.

1. *Select Interpolation Functions* – In this step each node is assigned to the belonging element, and then an interpolation function to represent the variation of the field variable over the element is chosen.
2. *Find The Element Properties* – after the establishment of the FEM, the matrix equations expressing the properties of the elements are determined.

3. *Assemble the Element Properties to Obtain System Equations* – By combining the matrix equations expressing the behaviour of the elements, then a matrix equation expressing the behaviour of the entire system can be made. This is because the matrix representing the entire system have the same form equations as the individual elements, but they contain more terms since all nodes are included.
4. *Impose the Boundary Conditions* – The boundary conditions must be accounted for before the system equations are ready for solution. Known nodal values are imposed of the dependent nodal loads.
5. *Solve the System Equations* – A set of simultaneous equations is solved to obtain the unknown nodal values of the problem.
6. *Make Additional Computations If Desired* – Computing other important parameters with the solution is possible if desired.

There are many advantages of Finite Element modelling. The appealing futures in the engineering industry attract users because of these advantages. Some of the advantages are (IEEE, 2020):

**Modelling:** Complex structures and irregular shapes in systems can be simplified both on the exterior and interior plane. Critical factors such as loads and environment conditions affecting the system can be considered when modelling.

**Accuracy:** Modelling FE - models can be complex and challenging to do by hand, leading to inaccuracies. Therefore, FEM software can be done accurately and adequately to ensure reliable results.

**Boundaries:** Boundary conditions are assigned to a system to ensure the right conditions for system response and to mimic the physical model as much as possible. Both point and

distributed forces, temperatures, and constraints are all factors that affect the model and how the user wants.

**Visuals:** FEM software and models can easily detect flaws in the design process. The details in the design help spot irregularities, which can be problematic when performing calculations.

However, the FE-Model needs to be verified to be further used in calculations and design processes. The reason for that is the need of knowing if the information and analysis extracted from the model is correct. The validation can for example be compared to another test performed either physically or analytically to check if the result in each test corresponds. Different calculations on the FE-Model and for example the physical results are compared, and if more than one scenario aligns, then the FE-model can be used for further research.

### 2.2.2 FEM – software: SAP2000

SAP2000 is a structural analysis software developed by CSI – *Computer & Science INC* (Rivera, et al., 2015). The program takes usage of the finite element method to analyse linear and non-linear models. This type of analyses makes it possible for the software to divide the models such as buildings, bridges, transportation infrastructure, dams, sports facilities, and offshore systems into section for designs. Furthermore, the software considers different international standards and guidelines for analysis and design.

Although the layout may seem simple and user friendly, the user may have full control with sound knowledge in structural mechanics. When analysing a structure, the software discretises the model into respective segments. First the model is discretised into the phase of “node-element discretization” (Rivera, et al., 2015). Here the structural elements are identified as different section properties consisting of frames, shells, or solids. These are then connected by nodes in a global 2-d or 3-D-system. Each element will then be defined with properties that align with the physical material property of the structure. This will include properties that define geometry, stiffness, loads and other requirements. Boundary conditions are also defined

and assigned at appropriate locations to make the model as close as possible to the actual system. After that, a meshing procedure takes place where the elements are then connected by the nodes forming a complex structure that is solved by SAPs own analysis engine.

Modelling in SAP2000 comes with various possibilities. Linear or curved members, cables and post-tensioned tendons, link elements to model springs, dampers, isolators, framing, multi-layered shell, solid elements with isoperimetric formulation and nonlinear response are all different modelling options for object assembly in the software (CSI - Knowledge Base, 2022). Furthermore, there is also the possibility of section design if preferred structural members do not satisfy the need of the user, and these are provided by the extensive SAP2000 libraries.

On the analysis front, there are many techniques that are integrated in the software making it relatively easy for the user to analyse both linear and dynamic structures. This includes solvers for static, linear-elastic to more complex dynamic and nonlinear-inelastic analysis types.

### 2.3 Operational Modal Analysis – OMA

Engineering consists of many fields and practices. One of those fields is the study of modal properties of systems under Ambient vibrations. This is also known as Operational Modal Analysis (Brincker & Ventura, 2015). OMA is conducted under operation conditions and provides useful methods for modal analysis in different areas of engineering fields.

OMA measures only the output of the structure. The ambient and natural operating forces on the other hand, as input forces are not measured. OMA is used instead of mobility-based modal analysis. The reason being that OMA does not account for the input and when it is difficult to excite the structure artificially (Jacobsen, et al., 2007). OMA uses algorithms that assumes that the input forces are stochastic. In other words, the input forces are random that can be analysed statically, and therefore not be predicted precisely (Jacobsen, et al., 2007). However, in most civil engineering cases this is normal. This is found for example, in towers, bridges, buildings and structures that are constructed offshore. The forces acting upon those examples are the ambient and natural forces that can be wind, waves, traffic, or seismic micro-tremors.

It is worth noting that the input forces of any given structure are not measured in OMA and therefore must be considered to identify the deterministic signals so their influence over the modal parameter extraction process is reduced (Jacobsen, et al., 2007).

### 2.3.1 Fourier transforms

One of the most key features in signal processing is the Fourier transform. Fourier transforms make it possible to modify the characteristics of recorded signals, and many signal processing techniques implements this transform in one of its many forms. Fourier transforms then make the signals more adequate for further analysis (Brincker & Ventura, 2015). Understanding the fundamentals of the Fourier Transforms is therefore essential to understand the techniques behind signal processing during OMA. The idea of a Fourier series is to represent a signal periodically with respect to its harmonic factors. In short, it can be represented as the following (Brincker & Ventura, 2015):

$$y(t) = a_0 + \sum_{k=1}^{\infty} (a_k \cos \frac{2\pi kt}{T} + b_k \sin \frac{2\pi kt}{T}) \quad (2.21)$$

Where:

$k$  represents the  $k$ th harmonic component and the quantity,

The coefficients  $a_0$  and  $a_k$  are the harmonic components of the series and can be obtained through the following:

$$a_0 = \frac{1}{T} \int_{-\frac{T}{2}}^{\frac{T}{2}} y(t) dt, \quad a_k = \frac{2}{T} \int_{-\frac{T}{2}}^{\frac{T}{2}} y(t) \cos \frac{2\pi kt}{T} dt, \quad b_k = \frac{2}{T} \int_{-\frac{T}{2}}^{\frac{T}{2}} y(t) \sin \frac{2\pi kt}{T} dt \quad (2.22-2.24)$$

### Discrete Fourier transform:

The signals originated in the time domain (Ewins, 2000) and the desired spectral properties lie within the frequency domain. Furthermore, continuous data cannot be computed by the classical Fourier integral resulting in the introduction of the DFT – *Discrete Fourier Transform*. This transform makes it possible for the required modal analysis of discrete values.

The transform is defined for the discrete values  $N$  over the period  $T$  in the time series  $x(t_k)$  and is defined as follows:

$$X_n = \frac{1}{N} \sum_{k=1}^N x_k e^{-\frac{2\pi i n k}{N}} \quad (2.25)$$

and:

$$x(t_k) = x_k = \sum_{n=0}^{N-1} X_n e^{\frac{2\pi i n k}{N}} \quad (2.26)$$

Where:

$X_n$  is the discrete value of the times series  $x(t_k) = x_k$  at the time  $t = k\Delta$ ,

$k$  is the sample number and is numbered as:  $r = 0, 1, 2, 3 \dots, N - 1$

$N$  is the total sample number measured over the period  $T = \Delta N$ ,

$n$  is the frequency component and is numbered  $n = 0, 1, 2, 3 \dots, N - 1$

$\Delta$  is the interval between each sample. This interval is constant each time.

Algorithms such as the Enhanced Frequency Domain Frequency Decomposition (EFDD) and the Cur-Fit Frequency Domain Decomposition (CFDD) employed analytically or in commercial software for data analysis are developed based on the Fourier transform.

### Nyquist frequency

In Digital signal processing the signal is digitised by an analog-to-digital converter and the  $N$  number of discrete values is recorded. These values are then evenly spaced in the period  $T$ . If it is assumed that the sample in time  $T$  is periodic, a Finite Fourier transform is then calculated.

Furthermore, the basic relationship between the discrete values,  $N$  and the sampling length,  $T$  is also connected to a sampling rate  $\omega_s$  and the range and resolution for the frequency spectrum. The range of the whole spectrum is  $0 - \omega_{max}$ , whereas  $\omega_{max}$  is *The Nyquist frequency*, on the other hand the resolution lines are  $\Delta\omega$ . They are described as (Ewins, 2000):



$$\omega_{max} = \frac{\omega_s}{2} = \frac{1}{2} \left( \frac{2\pi N}{T} \right) \quad (2.27)$$

$$\Delta\omega = \frac{\omega_s}{N} = \frac{2\pi}{T} \quad (2.28)$$

To recover all the Fourier components a sampling rate is used. This sampling rate is twice as much as the highest waveform frequency. With the use of the Nyquist frequency a sample of the highest waveform frequency and with the use of two samples per cycle. The signal is demonstrated and reconstructed. The Nyquist frequency is the maximum frequency past which “Aliasing” will occur.

The Nyquist frequency was chosen as 200 Hz to enable the identification with a natural frequency up to 100 Hz. This is based on range of parameters advised by ISO 10137 (International Organization for Standardization - ISO, 2007).

### 2.3.2 Domain identification

The core of the OMA often deals with data processing and identification relevant dynamic properties. Here the modal parameters are estimated, and two methods of identification are discussed. The first being frequency, and the second time domain identification. They are assessed and explained together with the respective techniques below.

#### *Frequency domain identification: FDD and EFDD*

For the Frequency domain identification, each mode participates with some degree of frequency band interacting with adjustment modes. Within a band where a particular mode dominates enables the identification of the various dynamic properties associated with that particular mode (Brincker & Ventura, 2015). This is a technique where an approximate decomposition of the system is performed. The system is decomposed to sets of independent SDOF for each mode. The decomposition is executed by decomposing the estimated spectral density matrices. The process involves estimating the singular values from the auto spectral

density – ASD of the SDOF systems through modal coordinates and the area of the resonance peak through the mode shapes of the mode (Structural Vibration Solution - SVIBS, 2023).

According to the makers of ARTeMIS OMA, SVIBS, the FDD can be divided into simple steps explained as follows (Structural Vibration Solution - SVIBS, 2023):

1. The spectral densities matrices are first estimated from the raw time series data,
2. Single value decomposition of the spectral density matrices is performed,
3. Average the first singular value of all test setup and average the second and so on, this is if multiple tests are available,
4. Pick the peak on the average singular values. If the modes are well-separated, always pick on the first singular value. However, if the modes are repeated pick on the second, third and fourth singular value etc.
5. The last step is optional, but the singular values are inspected for each setup and the peak picking position is edited, if necessary, when performing multiple tests.

On the other hand, the EFDD – *Enhanced Frequency Domain Decomposition* is described as an expansion of the FDD technique. Compared to the FDD the EFDD improves the approximation of the natural frequencies and the mode shapes. However, this technique also includes damping unlike the simple FDD technique. The SDOF Power Spectral Density – PSD function with the help of the Inverse Discrete Fourier Transform, is taken back to the time domain. Furthermore, the natural frequency is then determined by the number of “zero-crossing” as a function of time, while the damping is estimated by the logarithmic decrement of the corresponding SDOF normalized auto correlation function (Jacobsen, et al., 2007) In EFDD the modal estimation is divided into two steps, the first step performs the FDD peak picking, while the second uses the FDD identified mode shapes to identify the SDOF spectral bell functions. With the help of the SDOF spectral bell functions, both the frequency and damping are estimated. The SDOF Spectral bell is identified with the help of the FDD mode shape. The mode shape is used as a reference vector to in a correlation analysis. This analysis is then based on the Modal Assurance Criterion – MAC. This is a scalar value bounded both by zero and one. This

real scalar then depicts the co-linearity between the two mode shape vectors (Allemang, 2003). The MAC will be described further later in the theory part.

### *Time domain identification – Stochastic Subspace Identification*

On the contrary to Frequency Domain Identification, OMA techniques in the time domain are based on the examination of response times histories and is often used when handling “noisy” data (Ren & Zong, 2004). working in the time domain, free decays are handled and are normally estimated as correlation function and random decrement functions. In other words, the signals present any time present in the mode of the free decay. Thus, all modes contribute to the time domain (Brincker & Ventura, 2015).

SSI – Stochastic Subspace Identification is one of the techniques within time domain identification. Here a parametric model is constructed from time series data. This mathematical model with different parameters can be adjusted so the model can fit into the data. Usually, the parameters used are picked so the deviation between the system response model and measurements are minimal and is referred to as model calibration. This can be illustrated through the following (SVIBS, 2023):

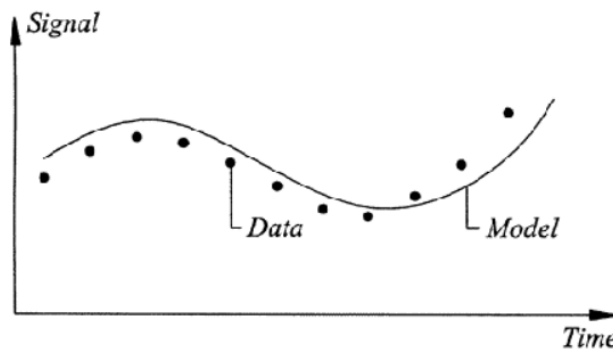


*Figure 2.3: Model calibration illustrated graphically.*

The linear and time- invariant time domain modal identification techniques is formulated in a general form as an innovation state space formulation:

$$\hat{x}_{t+1} = A\hat{x}_t + Ke_t \quad (2.29)$$

$$y_t = C\hat{x}_t + e_t \quad (2.30)$$

- Here the A-matrix contains the physical information,
- while the C-matrix obtains the information regarding the system response,
- the K-matrix covers the statistical information that allows the model to have correct correlation function and the correct spectral density function. This is known as covariance equivalent modelling.

The parameter number is important. A small number of parameters results in incorrect models of the dynamical and statistical behaviour. However, if the number is too great, then the model becomes over-specified resulting in high statistical uncertainties of the model parameters. Therefore, it is important to master the art of parametric model estimation so a model with reasonable numbers is determined (SVIBS, 2023).

#### *The Modal Assurance Criterion – MAC*

As mentioned earlier MAC is a scalar value that assist with the comparison of mode shapes and therefore making it a useful tool when performing modal analysis (Ewins, 2000). The technique compares the measured mode shapes acquired from experiments and the predicted mode shapes from mathematical models. When given a set of  $m_X$  experimental modes and  $m_A$  predicted modes, then a matrix of  $m_X \times m_A$  can be computed. The matrix then shows an indication of which predicted mode correspond with which experimental mode. Then a value of the correspondence is acquired. The value lies between 0 and 1, whereas 1 being the perfect correspondence. In general, a value of 0.9 is described as well-correlated modes. Values over 0.8 are acceptable, but values below 0.2 is described as non-correlative.

The MAC parameter is defined as:

$$MAC(A, X) = \frac{|\sum_{j=1}^n (\Psi_X)_j (\Psi_A)_j^*|^2}{(\sum_{j=1}^n (\Psi_X)_j (\Psi_X)_j^*) (\sum_{j=1}^n (\Psi_A)_j (\Psi_A)_j^*)} \quad (2.31)$$

Or:

$$MAC(A, X) = \frac{|(\Psi_X)^T (\Psi_A)|^2}{((\Psi_X)^T (\Psi_X)) ((\Psi_A)^T (\Psi_A))} \quad (2.32)$$

Where:

$\Psi_{Aj}$  is the mode shape vector from the predicted mode shape,

$\Psi_{Xj}$  is the mode shape vector from the experimental mode shape,

$\Psi^*$  is called the complex conjugate in the equation.

### 2.3.3 VDV – Vibrational Dose Value

One of the ways of assessing vibrations is by estimating the Vibrational Dose Value – VDV is a parameter used for the assessment of continuous, intermittent, occasional, and impulsive vibrations with limiting values for comparisons (BSI - British Standards, 2008). The magnitude of the vibration is combined with the time of occurrence. Because the method of computing the VDV uses fourth power instead of for example second power of the acceleration time history, it is more sensitive to peaks compared to other methods (International Organization for Standardization - ISO, 2003).

The VDV is illustrated as the following in ISO 2631:

$$VDV = \left( \int_0^T a_w^4(t) dt \right)^{\frac{1}{4}} \quad (2.33)$$

Where:

$a_w(t)$  is the instantaneous frequency-weighted acceleration,

$T$  is the duration of the measurement.

### 2.3.4 RMS – Root mean square

Another vibration serviceability indicator is the RMS – Root Mean Square and it is evaluated as the frequency weighted acceleration. The RMS is defined as:

$$a_w = \left[ \frac{1}{T} \int_0^T a_w^2(t) dt \right]^{\frac{1}{2}} \quad (2.34)$$

Where according to ISO 2631

$a_w(t)$  is the weighted acceleration as a function of time,

$T$  is the duration of the measurements in second.

### 2.3.5 Data conversion in OMA – signal processing

When processing signals in OMA transform is important. This valuable tool makes it possible to identify systems and process signals when performing tests. However, under certain circumstances there may occur some problems which may affect the quality of the results. Therefore, it is important to address the different methods that prevents these errors.

#### *Aliasing*

In digital spectral analysis there is a problem known as “aliasing.” This is a result from discretization of the originally continuous time history. During the discretisation process high frequencies may be misinterpreted if the sampling rate is too slow. In fact, the frequencies will instead appear as low frequencies which may not be distinguished from other low frequencies. The solution to this kind of problem is to implement via **anti-aliasing** filter. This subjects the original time signal to a low-pass filter that distinguishes the frequencies (Ewins, 2000).

#### *Leakage*

Another problem worth mentioning is leakage. Due to the need to only take a finite length of the time history and the assumption of periodicity, leakage may occur. Energy from the spectral lines may “leak” into spectral lines close to the true frequency and the spectrum is spread over several lines. This is a genuine problem when dealing with digital processing as well as Frequency Response Functions – FRF measurements. However, there are some ways to avoid it including (Ewins, 2000):

- Change of duration of the measurement sample length to match the periodicity in the signal.
- Increase the duration of measurement period,  $T$  this makes it possible to separate the frequency resolution and making it finer.
- Including more zeroes at the end of the measured sample. This is also known as Zero padding.

- Modifying the signal sample so the severity of the leakage is reduced. This is called windowing. Detailed discussions and explanation of the implementation of the various techniques in resolving or reducing signal processing errors and defects are discussed in various literature (Ewins, 2000).

### 2.3.6 ARTeMis Modal

ARTeMis Modal is a software for OMA developed by Structural Vibration Solution A/S (Structural Vibration Solutions - SVIBS, 2023). ARTeMis Modal platform is used for modal testing, modal analysis as well as modal problem-solving. Its user-friendly and open platform enables different measurements to be made. When for example measuring vibrations, the data procured through a data logger can be then transferred to ARTeMIS via the tester and subsequently to the Extractor from which modal parameters such as the mode shapes, natural frequencies, and damping ratios may be estimated. The software has algorithms with various techniques in modal parameter extraction including the Frequency Domain Decomposition (FDD), enhanced frequency domain decomposition (EFDD), the curve-fit frequency domain decomposition (CFDD) and the stochastic subspace identification (SSI). The options provided enables easy comparison of estimated modal parameters and therefore makes ARTeMIS attractive when performing modal analysis.

The software is applicable in the fields of Operational Modal Analysis, Experimental Modal Analysis, Operating Deflection Shapes and Structure Health Monitoring Analysis. This thesis focuses on using the OMA component of ARTeMIS for assessing the modal behaviour of two bridges.

In dealing with the signal processing problems mentioned above, ARTeMIS is developed with various filters and additional algorithms that provide quality assurance of estimated parameters including in-built functions that estimate and compare the Modal Assurance Criteria for various modes.

The software implements the use of MIMO (Multiple Input Multiple Output) techniques, where closely spaced modes and even repeated modes with a high degree of accuracy are estimated. Compared to both Single Input Multiple Output - SIMO, Multiple Input Single Output - MISO and Single Input Single Output – SISO, these techniques will have a tough time finding the separated poles because of poor mode separation.

ARTEMIS makes vibration testing easy, since there is no need for vibration shaker or impact hammer, simple or random tapping on the given structure in different random locations will provide a fair approximation of a multivariate white noise stochastic process. Also relying on the ambient or operating conditions of a structure may be enough in terms of exciting some relevant modes.

However, the limitations in such situations may vary and depend on the domain used when performing analysis (Bin Zahid, et al., 2020). In the frequency domain when implementing EFDD, the computation of modal damping is an issue that could lead to estimates that are considered biased. Furthermore, in the time domain, the modal parameters are sometimes difficult to extract when dealing with closely spaced modes.

#### 2.4 Dynamic loading: pedestrian traffic

Dynamic loading in this thesis will be referred to as the loads induced by pedestrian activity on the infrastructure. These will be walking as well as running. The different activities act differently and result in different reactions, as well as the number of people and the synchronization inducing the oscillation influence the responses of the structure. This chapter will discuss both walking and running as dynamic loads on bridges.

When taking a step on the surface of a bridge, the dynamic excitation by pedestrians turns into forces that varies due to time. Dynamic forces are more complex than they may seem. There are many different parameters that leads to this complexity. The frequency of pace, walking speed and step length all are some of the things considered when determining the dynamic



loading. However, these forces can be divided that acts in three different directions, and those are: lateral, longitudinal, and vertical. Since this thesis only focuses on the latter, only the vertical directions will be assessed and discussed.

### 2.4.1 Walking

Excitation of forces because of pedestrians walking is widely studied and assessed. Different researchers and projects have been made on the matter and the results have been proposed as the ground theory of the walking excitation.

A lot of measurements and tests have been conducted to quantify loads in the vertical direction induced by pedestrians on footbridges. In 1961 Harper et al. conducted research using a force plate where they measured the force of a single step (Harper, et al., 1969). The graphical shape of the force in relation to time acquired in the process was confirmed by many other researchers where some of the names were Galbraith and Barton, Blanchard et al., Ohlsson, Kerr and many others (Zivanovic, et al., 2005). The research conducted in the early sixties sparked the interest of another group of researchers. Andriacchi et al. in an equivalent manner with Harper et al. measured the vertical force with a force plate (Andriacchi, et al., 1977). They observed that an increase of walking velocity results in an increase in step length and peak force. In other words, the change of walking speed changes the dynamic walking effects. The research conducted showed the complexity of human-induced dynamic forces and how they depend on many parameters.

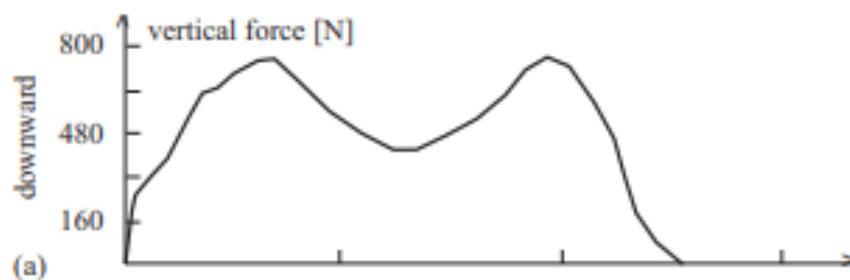


Figure 2.4: The typical walking force shape after Andriacchi et al. (Andriacchi, et al., 1977)

Individual step forces were then measured more advanced due to informative measurements of continuous walking comprising several steps. With the use of different methods including gait machines, floor strips and a platform induced with several force plates, measurements showed that the result were almost periodic. The average period equalled the reciprocal value of the (average) step frequency.

In 1982 broad research on the matter of human forces relevant to footbridge dynamic excitation was conducted by a researcher with the name of John E. Wheeler. Wheeler made a system of the work of researchers before him in relation to different modes of human movements (Wheeler, 1982). Figure 2.5 shows the different human movements as functions of time. The movements were divided into six stages where they started off as slow walk all the way up to running.

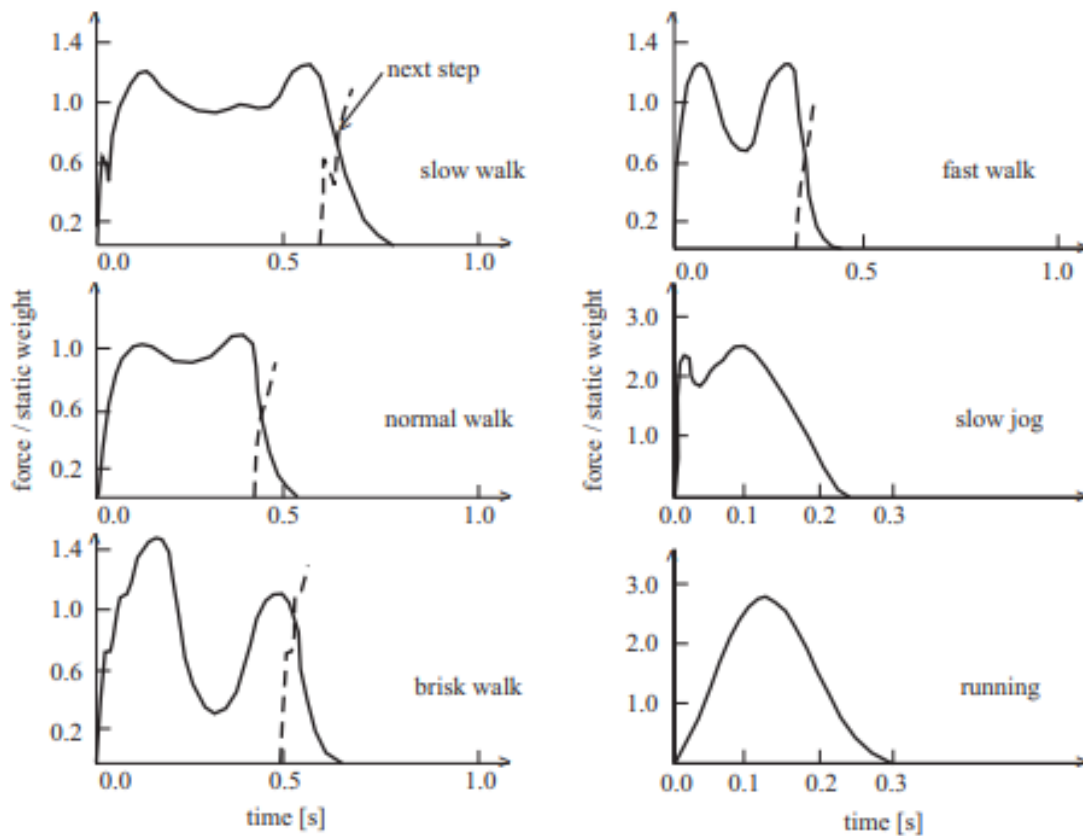


Figure 2.5: force patterns for human activities according to wheeler et al.

In addition, Wheeler presented the dependence of many walking parameters. These includes step-length, moving velocity, peak force, and contact time (the time while one foot has contact with the ground and the other is in the air) as a function of the pacing frequency. Figure 2.6 describes Wheeler’s work both the stride length, and the movement force varies with the frequency and speed (Wheeler, 1982).

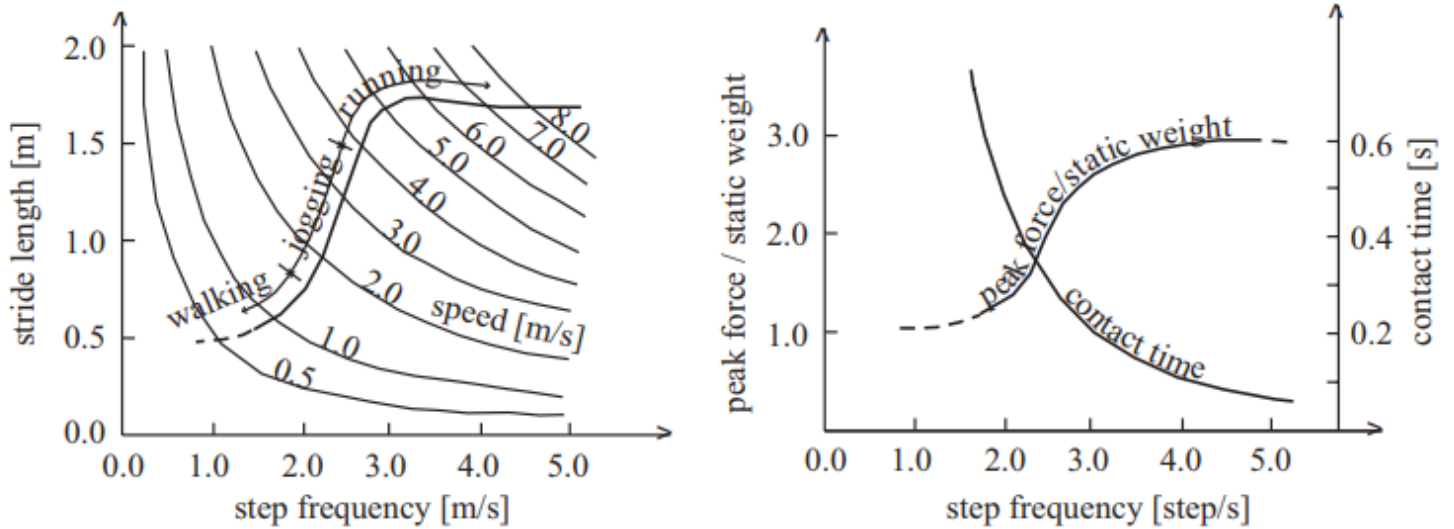


Figure 2.6: The dependence of walking parameters based on Wheeler’s work.

In 1978 Matsumoto et al. made a reliable statistical description of the frequencies produced when walking (Matsumoto, et al., 1978). The experiment results were illustrated in a normal distribution in figure 2.7. The test investigated a sample of 505 people where it was concluded that the frequency followed a normal distribution and the mean rate of pacing landed on 2.0 Hz followed by a standard deviation of 0.173 Hz.

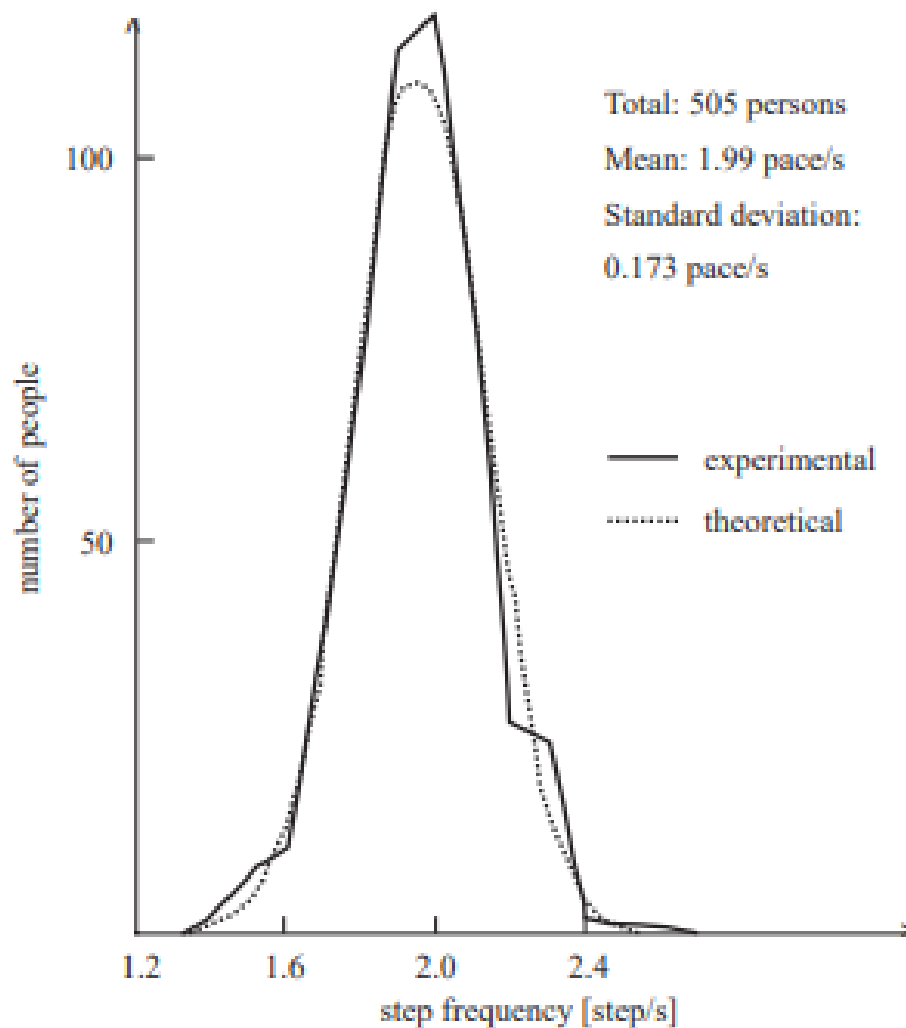


Figure 2.7: Normal distribution of pacing frequencies for normal walking by Matsumoto et al.

This opened the door to many measurements and experiments on the frequencies in the vertical direction. Much research teams did their own respective tests, some with fewer test subjects and different methods. In a PhD done by Einar Ingólfsson at The Technical University of Denmark – DTU, he made a description of the different researchers and proposed results as summarized in Table 1 (Ingólfsson, 2011):

*Table 2.1: table by Ingólfsson comparing the walking average walking characteristics according to different researchers.*

Study	N	Walking speed ( $\frac{m}{s}$ )			Pacing rate (Hz)		
		Men	Women	Total	Men	Women	Total
Matsumoto et al.	505	-	-	-	-	-	1.99
Zivanovic et al.	1976	-	-	-	-	-	1.87
Morgenroth	6000	1.49	1.41	1.45	-	-	-
Ricciardelli and Pizzimenti	116	1.44	1.37	1.41	1.81	1.86	1.84
Sahnaci and Kasperski	251	1.37	1.36	1.37	1.80	1.91	1.82
Pachi and Ji <sup>1</sup>	400	1.35	1.25	1.30	1.80	1.86	1.83
Pachi and Ji <sup>2</sup>	400	1.46	1.37	1.42	1.97	2.03	2.00
Zivanovic et al.	939	1.51	1.45	1.47	1.89	1.98	1.94
Butz	98	-	-	-	1.80	1.89	1.84
Venuti and Bruno <sup>3</sup>	-	1.34 $\alpha_G\alpha_T$			-	-	-

<sup>1</sup> Measured on two different pedestrian bridges,

<sup>2</sup> Measured on floors in two different shopping malls,

<sup>3</sup> The coefficients  $\alpha_G$  depends on the geographic location (1.05 for Europe, 1.01 for USA and 0.92 for Asia) and the  $\alpha_T$  depends on the travel purpose. (1.20 for Rush hour/Business, 1.11 for Commuters/events and 0.84 for Leisure/Shopping)

### 2.4.2 Runners/ joggers

Many of the research done earlier, were always based on excitation due to pedestrians walking. As important as this may be, it is important to take running into consideration. Running is not as frequently mentioned in the literature compared to walking.

In 1970 Galbraith and Barton took upon them self the task of measuring a single step force on an aluminium plate (Galbraith & Barton, 1970). The force excitation was a result from slowly walking to running. According to Galbraith and Barton the shape of the running force differs from the walking force shape. The difference was that the running force only had one peak compared to the walking force. Furthermore, the weight and step frequency of the test subjects were classified as important parameters. An increase in those parameters, meant an increase in the peak force amplitude.

The main difference in the two activities is that when walking both feet is connected to the ground. Running on the other hand is an activity where only one of the feet is initiating contact with the ground. This can be seen in Figure 2.8 where there is only one amplitude for running compared to walking.

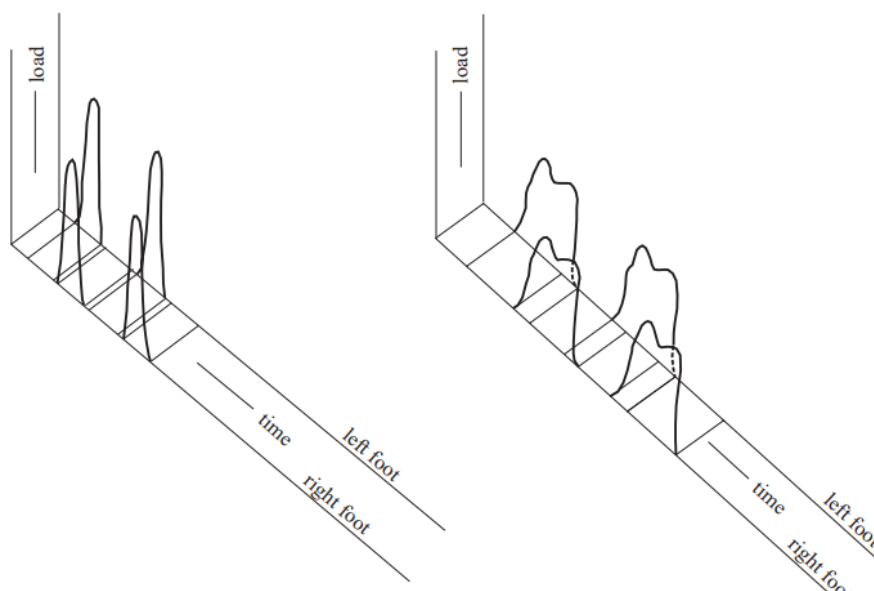


Figure 2.8: Successive running (to the left) and walking (to the right) forces based on research by Galbraith and Barton.

### 2.4.3 Groups of people

Until now, the dynamic loading induced by pedestrians were attributed to a single pedestrian. This brings up the question about how the dynamic loading will differ when multiple pedestrians are involved and what if their movements synchronize as well. Synchronization or “the lock-in” effect as it is also called is a phenomenon that occurs when the natural frequency is almost identical to the walking frequency of the pedestrians. The adaptation of the pedestrian to the natural frequency may then cause great excitation.

According to Dallard et al. after Researching the millennium bridge in London in 2001, there are two types of synchronization (Dallard, et al., 2001). There is synchronization among people as well as synchronization between the people and the structure. This is a reference to interaction mechanisms explained later in the thesis. These two types of synchronizations are different in nature, but they usually lead to the same results. The result then being an increase in the response of the structure. Dallard et al. concluded that to map the relationship between the crowd density and the structure it is important to identify the following (Dallard, et al., 2001):

1. The relationships between the crowd density, walking speed, walking frequency and probability of synchronisation,
2. The probability of lock-in and effective force per person in a crowd as a function of the amplitude and frequency of the bridge motion.

Back in 1987 both Backman and Amman respectively quantified the density of the pedestrians as “limited by the feasibility of uninhibited walking”. Furthermore, their research concluded that the upper density limit is reached when it lies between 1.6 and 1.8  $\frac{people}{m^2}$ . This then corresponds to a static load valued at 1100 to 1400  $\frac{N}{m^2}$ . However, it is assumed that 1  $\frac{people}{m^2}$  is more realistic and is therefore the chosen value (Bachmann & Ammann, 1987).

## 2.5 Interaction mechanisms

The development of pedestrian induced vibrations is a result of interaction between the pedestrian generating an action and the movement of the underlying surface. On the other hand, the presence of other pedestrians can also influence the interaction of the rest of the pedestrians and thus two interaction mechanisms in this chapter will be discussed.

### 2.5.1 Humans-structure interaction – HSI

The human system, and the structural system, in this case a pedestrian bridge, are working together as a unified system. The HSI is therefore implemented in vibration calculations because it is possible to assess how these two systems responds to each other. In figure 2.9 Ding Zhou et al. illustrates how the human body and the bridge can be modelled as different structural models which can then be combined to simulate the effect of a coupled model with its own effective mass  $M$ , stiffness  $K$  and damping  $C$  (Zhou, et al., 2015).

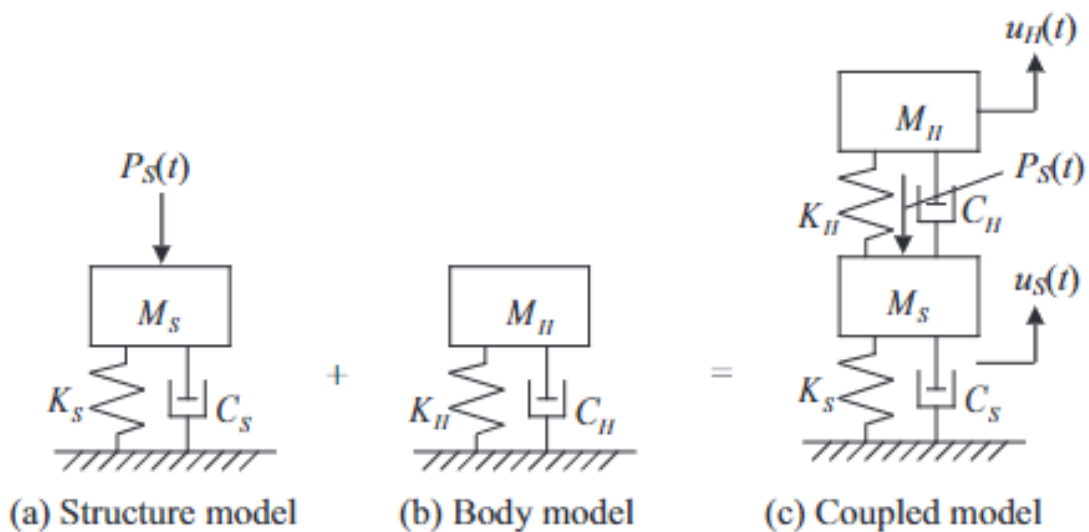


Figure 2.9: Comparison of two models for human-structure interaction as well as coupled model based on the structure and body.



There are several studies conducted on this phenomenon. General knowledge in the field indicates that the pedestrian on the bridge will add to the structural damping and mass, this however is accepted in low frequencies caused by vertical vibrations. In 2005 Zivanovic et al. illustrated in a report how damping was 10 times greater when pedestrians walked with imperfection due to the vibration caused (Zivanovic, et al., 2005). This was done in their report researching the Human-structure interaction in footbridges. On the other hand, Tubino from the university of Genoa explained that the HIS in the vertical direction increased the structural damping for lighter footbridges because of the natural frequency being close to the mean pedestrian frequency (Tubino, 2017). Different studies show how understanding this phenomenon can account to greater extent in understanding the vibration and prevention of discomfort on pedestrian bridges.

#### 2.5.2 Human-Human Interaction – HHI

Pedestrians under no influence of others or obstacles may walk freely in velocity as well as in characteristics. Pedestrian bridges often consist narrow passages. These narrow passages could lead to restrictions on the pedestrian if the bridge suddenly is densely populated and may therefore influence their action on the bridge. Thus, the HHI is mainly influenced by the pacing of the pedestrian as well as the crowd on the bridge. In other words, with the increase of the people on the bridge, the stepping frequency decreases leading to less pacing as well.

An effective way to depict the traffic of the pedestrians using the bridge is by determining the number of people on the bridge at the same time. This is called the bridge density and is often illustrated as “*d*” in many guidelines that will be assessed later. The density is calculated as pedestrians per square meter and increases with the crowd on the bridge since there are more pedestrians on each square meter. Figure 2.10 from a PhD thesis written by Ingólfsson at the Technical University of Denmark illustrates how the increasing density on the bridges affects the pacing rate and accounts for the probability as well (Ingólfsson, 2011).

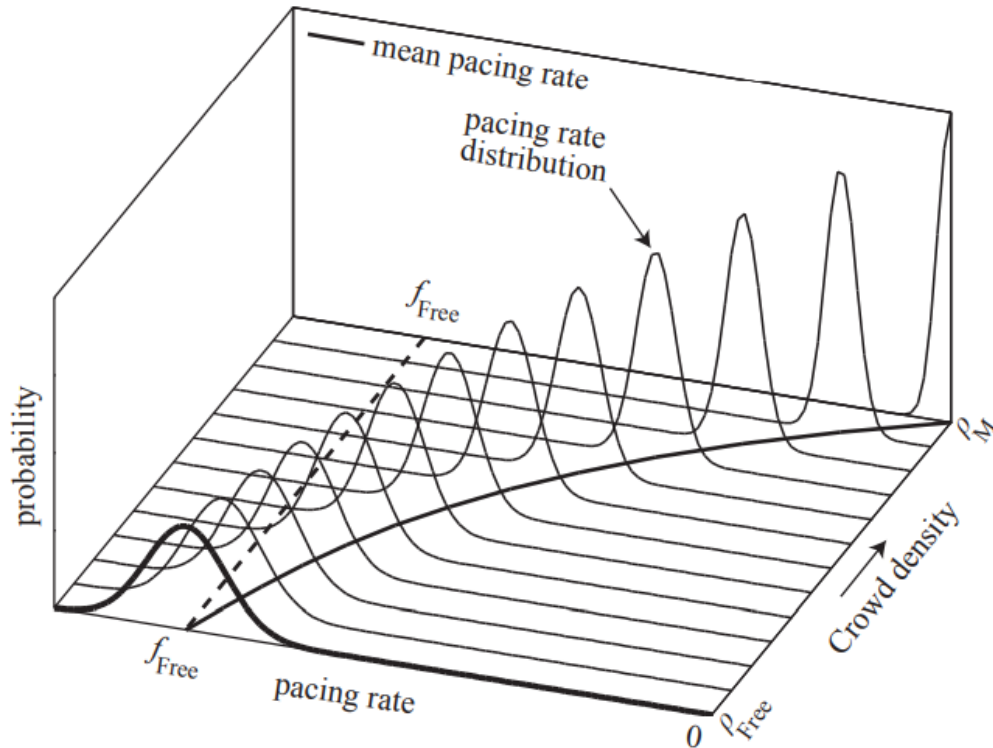


Figure 2.10: The relationship between the average crowd density and distribution of step frequency illustrated in a schematic view (Ingólfsson, 2011).

## 2.6 Bridges in different construction systems

Bridges come in many shapes and forms and are often used to express architectural desires freely. However, one thing that is always found in bridge structures is the two main components of the bridge. A bridge is divided into two components, those being the superstructure and the substructure. The superstructure of the bridge is often referred to as the main part where the slab is supported and stabilized so the load on the bridge is transferred to the substructures. The superstructure is composed of decks, supporting systems like girders and trusses as well as furniture like barriers and luminaires. The specific component varies with the material and type of bridge in question.

The second component is the substructure. This is the part of the bridge that supports the superstructure. The load from the superstructure is distributed to the foundations of the

bridge. Substructures mainly consists of, Piers, wing walls abutments footings and piles. One thing they have in common is the process of distributing the load to the ground.



*Figure 2.5: the figure illustrates the placement of the different structures described above. The figure is extracted from Hartford County (Miller, u.d.)*

### 2.6.1 Pedestrian bridges

Pedestrian bridges also known as footbridges are bridges classified for pedestrians with the sole purpose of getting pedestrians from one point to another. In locations with other traffic such as cars, trains, metros etc. pedestrian bridges allow pedestrians to cross without interfering with vehicular traffic and avoiding pedestrian accidents and injuries. Footbridges come in many forms and shapes and are often made with varied materials which are steel, concrete, and timber. And each respective material has different type of design concepts.

#### Steel bridges:

Pedestrian bridges are many times constructed in steel. This is because steel bridges can be constructed in several diverse ways making them architectural beauties to look at and explore. They can either be constructed in long spans or smaller and shorter bridges. This is a result of

the many different construction system available when designing a steel bridge. Steel bridges can consist of composite beams, cables, box girders, and trusses. The latter is often implemented in smaller pedestrian bridges and one of the bridges discussed in this thesis is a truss bridge.

#### Timber bridges:

Different from both steel and concrete, timber is exceptional due high stiffness and strength to weight ratios (Norsk Limtreprodusenters forening, 2015). Compared with for example steel, steel is relatively heavy, making timber an efficient material when for instance designing construction with spans up to 150 m. the use of timber in construction system is growing due to the environmental difficulties in the society today, but this sub-chapter will focus on glulam in timber bridges (Norsk Limtreprodusenters forening, 2015). When choosing a type of glulam bridge, there is several factors that needs to be considered. Those are spans, type of traffic, ground conditions, height clearance and economics.

#### Transverse prestressed glulam bridges:

One of the studied bridges in this thesis is a timber bridge consisting of a transverse prestressed glulam slab, therefore this section briefly considers such design choice in timber and explains the construction type.

A prestressed glulam bridge consists of a nail-laminated deck. Here several glulam beams on high edge are nailed together, side by side. The construction acts as a road surface but has its limitation in terms of both span and loading. Adding a twist on this simple solution is to brace the planks. This is done with steel rods replacing the nails described earlier. The twist then braces the system thus increasing the loading capacity. This type of construction method is referred to as Transverse prestressed glulam bridges and depending on the desired span depends on the number of glulam beams or planks (Norsk Limtreprodusenters forening, 2015).

In practical terms, the building of the structure is easy, and the stiffness of the deck is enhanced in its own plane eliminating in reducing the need for bracing. However, the difficulties lie in avoiding moisture. In other words, it is important to prevent water to penetrate the construction. One other downside is post-tensioning. It is necessary to tension the rods to keep the tension level the same between the lamellae.

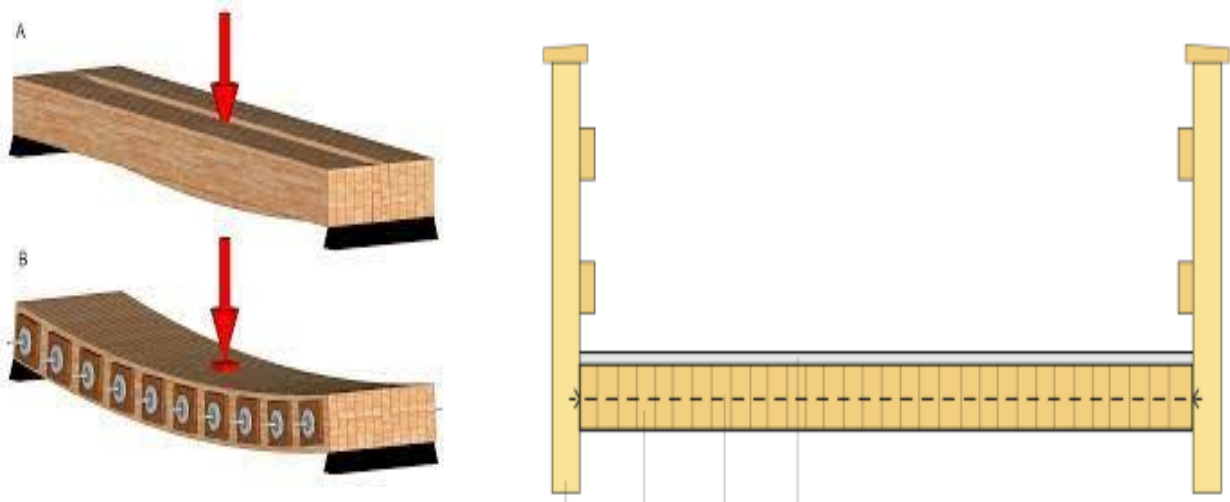


Figure 2.6: Examples of pre-stressed transversal glulam slab. Illustration to the left is extracted from a doctorate thesis (Ekholm, 2013) and from a glulam book: "Limtreboka" (Norsk Limtreprodusenters forening, 2015)

## 3 Methodology

### 3.1 Choice of method

The choice of methodology may depend on the purpose of the thesis. The two methods often used in academic writing are qualitative and quantitative methods. However, sometimes a combination of the two is possible.

Quantitative methodology is commonly applied to experiments, fieldwork, and testing (Grønmo, 2023). Here the purpose is to gather information based on observations and findings. This method is often used when gathering information and structuring them to make the results more concrete and verifiable. Qualitative methodology on the other hand is a method that takes previous knowledge and builds on it to for development (Grønmo, 2023). This method is often based on beliefs and theories that are difficult to quantify. Therefore, it makes it somehow subjective and different people have different opinion on the given information.

A combination of both the quantitative and the qualitative methods can under many different circumstances be the most fulfilling way of conducting research. By combining both own research whilst looking at different literature on the matter beforehand, a solid background teamed up with further study enhances solution to the problem under study.

This thesis takes on the challenge of field experimental campaign of the vibration serviceability performance of different pedestrian bridges developed with different structural systems and materials. Reviewing the literature about the matter and evaluating various findings, the thesis takes on further studies to validate previous results and help understand the vibration behaviour of two different pedestrian bridges in terms of construction materials and configurations. Furthermore, due to conducting field experiments numerical and modelling in FE programs, this thesis will use both qualitative and quantitative methodology.

## 3.2 Thesis approach

The work for this thesis is divided into four major phases. First, the literature review. This reflects that gathering information and planning is crucial to move on to the next phase.

The second phase involves field testing, where physical tests were conducted on physical bridges and assessed later using OMA tools. The time-history data provided the parameters necessary for the estimation of VDV, RMS and peak acceleration calculations.

The third phase consisted of using results from the field test in calibrating numerical models developed with an engineering FEM software that enables various parametric studies regarding the modal analysis.

The fourth phase presents the results from the respective OMA and the FEM models and compare them through various analysis and evaluations. Finally, a comparison of both the load models and comfort criteria concerning one of the bridges is made to assess the accuracy and robustness of other guidelines on the matter.

### 3.2.1 Field tests

Field tests were conducted on two different bridges in Norway. These are bridges made of different construction systems as well as different materials. This is to assess the vibration performance of pedestrian bridges designed and built with different systems and materials. The field test is conducted with vibration sensors (accelerometers) mounted on the bridge decks, and the bridges subjected to different activities such as walking and running to mimic the everyday use of the bridges.

## Description of the bridges:

### Timber bridge: Nordre Finstad Footbridge

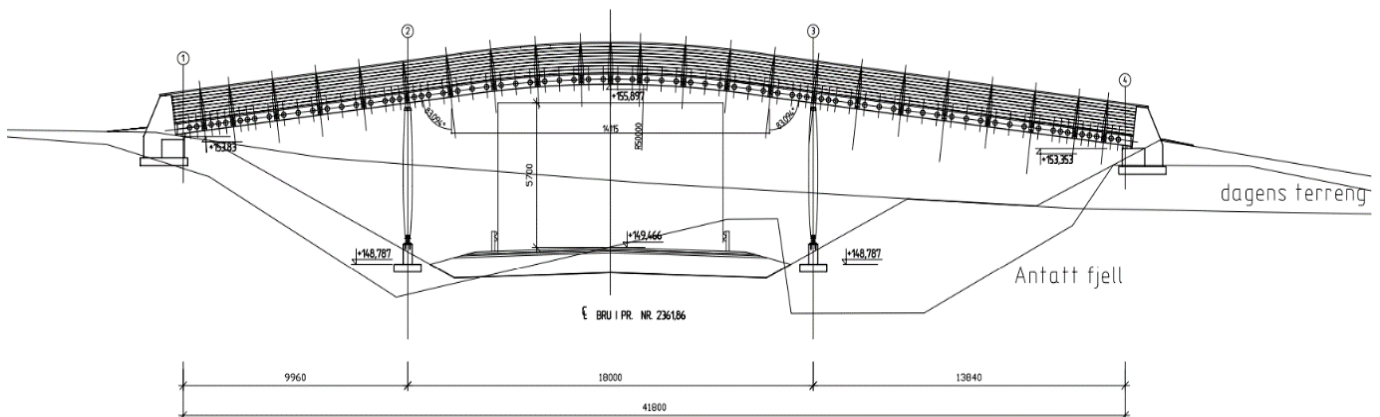


Figure 3.1: Nordre Finstad bridge photographed from the road below, and blueprints of the bridge () courtesy of Viken Municipality

Nordre Finstad footbridge is on a highway in "Finstad" in Northern Follo Municipality in Viken county. The length of the bridge is approximately 41.8 m according to the blueprints, but the as built was measured to be about 40 meters. The bridge is divided into three spans: two end spans and one main span as shown in Figure 3.1. The end spans were physically measured on site to be approximately 10 m each and the main span 20 m. In elevation the footprint of the bridge is curved, and the height of the crown is estimated to be approximately 6.4 meters from the top of the asphalt of the underpass highway.



The superstructure of the bridge is constructed with different materials. However, the deck is glulam-dominated and is referred to as a timber bridge in this thesis. The focus in this study is vertical vibration assessment of the bridge which effectively involves the deck. The glulam deck is a transverse pre-stressed with a 40 mm asphalt overlay. The thickness of the deck excluding the asphalt layer on top, is approximately 40 centimetres thick. In terms of width, the deck is 3 meters wide.

The bridge is held up by oval columns and made from glulam and are both illustrated in Figure 3.1. The columns are oval-shaped, with the most minor diameter measuring 250 mm and the most oversized diameter measuring 400 mm. They are connected to a square-shaped concrete cast and through a locking bolt on each side of the glulam beam. The substructure is made of two abutments and two intermediate piers as shown in Figure 3.1. The abutments are constructed from concrete whilst the piers are made of double glulam columns with pier caps on which sits the deck. The pier columns are anchored into concrete foundations. It is worth noting that timber and concrete should not be in direct contact due to moisture from the concrete because the wood will suck the water out of the concrete. Timber columns are separated from the concrete with connections where the distance between the timber and the concrete is between 150 to 300 mm. For more details on the bridge, see Appendix A for detailed blueprints.

Steel truss bridge: Asper bridge

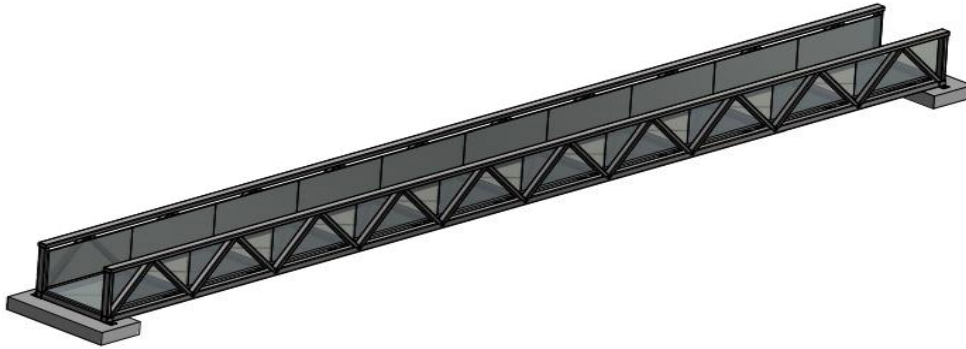


*Figure 3.2: Modelled bridge extracted from the blueprints, courtesy of Statens Vegvesen – Norwegian Public Road Administration.*



*Figure 3.3: Photographs of the bridge on the left side of the road (top) and the span of the bridge crossing the river (bottom).*

The second bridge considered in this study is the steel bridge located in Kråkstad, also in Northern Follo Municipality, Viken County. It is one of two bridges on each side of the road that crosses Kråkstad river that runs beneath the bridge. The bridge was measured to be approximately 22 m in length by 1.5m width. It is a single span and may be described as a simply supported system. The superstructure consists of steel deck of a grillage with a 40mm depth. The deck is supported on steel floor beams which in turn transfer loads to two main trusses forming the main supporting system. Diagonal bracings between each floor beam in steel are also found under the grillage. The truss is made of different hollow sections, all of which have a thickness of 12mm:

- Top chord: 200x100mm
- Bottom chord: 150x150mm
- Floor beams: 100x150mm
- Diagonal beams: 150x100m

The bracings, as well as different details, are visible in the blueprints and pictures found in Appendix B.

### Acceleration measurements

The field tests are based on the vertical vibration assessment of the bridges under operating conditions. The process explained in shorts steps as follows:

During the test, the bridge deck is partitioned into strips along the span and across the width forming a grillage system. The intersection of the partitions was considered as the locations of degrees of freedom at which sensors were located for vibration measurements. Double sided tapes were employed on those locations to enable the attachment of the sensors to the deck as shown in Figure 3.4. In all, ten sensors were employed for the test with eight serving as roving sensors and the remaining two as reference sensors. One of the reference sensors, was in the middle span near the centre and the other located in the first end span about one-third from the edge and near the middle of that span.



*Figure 3.4: illustration of placement of the double-sided tape for securing the sensors.*

As shown above, the sensors had to be secure enough because to avoid second order effects during the measurements.



*Figure 3.5: Distribution of the sensors on the timber bridge with the same spacing and distances.*

The sensors are accelerometers that measure the acceleration induced by the activity on the bridge. They were placed in intervals depending on the width of the bridge as well as the length of it. On both bridges, the eight roving sensors were distributed as sets 2 with four sensors on each row spaced 2.5 meters in between in length and spaced evenly in terms of width. For the spacing across the width, it was 1 m on the timber bridge; and 0.5 m on the steel bridge. Figure 3.5 illustrates how the sensors was set up in rows on the timber bridge. The reference sensors are marked with a red ribbon for identification to prevent tempering with them whilst transferring the roving ones as may be seen in figure 3.6. The sensors are connected to a data logger system from *the QuantumX* family via cables. From the data logger is in turn connected to a computer for data procurement. For more information on the accelerometer and amplifiers se Appendix C.



*Figure 3.6: Reference sensor marked with a red ribbon.*

After the sensor placement and testing of the data acquisition system, two tests were performed for each test set-up on the timber bridge. The first test involved a person of about 100 kg or 0.98 kN running, while the second test accounted for the same person walking. On the steel bridge, running was not convenient and was therefore substituted with heel drop in the middle. The measurements were done in intervals of two minutes, and after 4 minutes of

testing, the sensors were re-located to the following marked set of points to repeat the procedure for all test set-ups. Figure 3.7 illustrates the whole procedure made on the timber bridge and how the data is captured from the accelerometers.

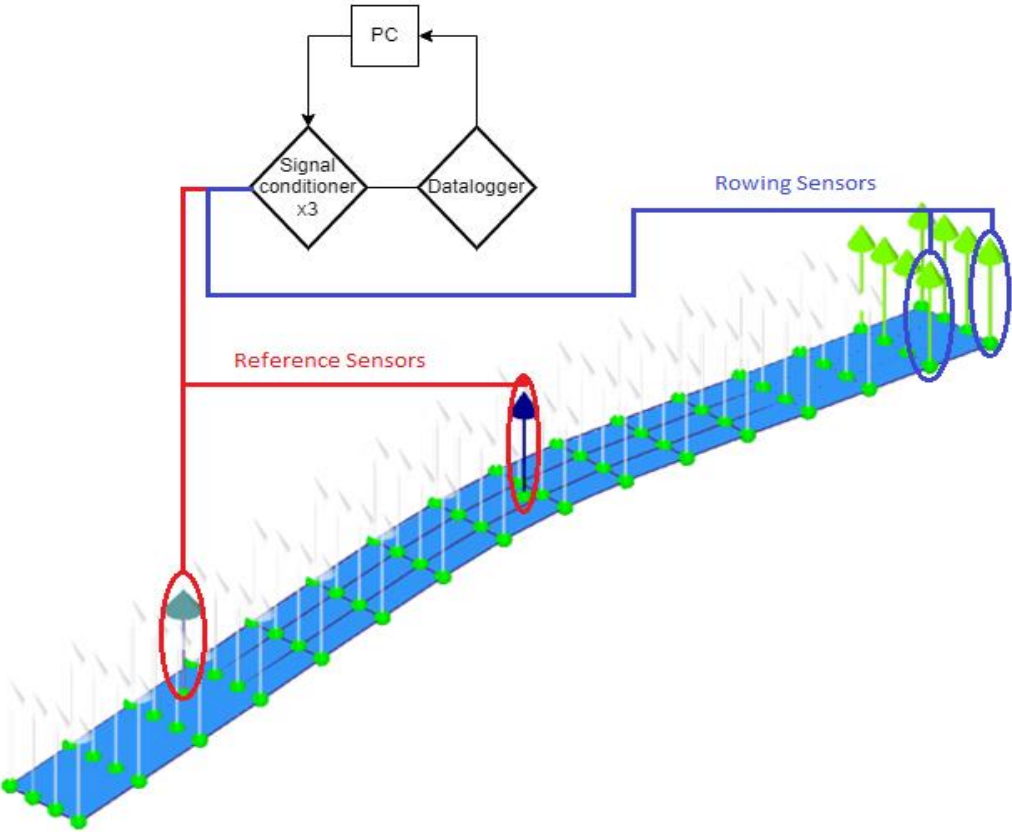


Figure 3.7: The testing procedure illustrated with roving sensors, reference sensors and data readers.

## Signal Processing

The commercial software ARTeMIS modal was used in processing the data and capturing modal characteristics of the two pedestrian bridges. The software has a two-in-one in-built facility called the Tester, and the Extractor. In the Tester, the geometry of the system can be prepared, followed by test measurements and assignments of the degrees of freedom. The Extractor takes over and conducts the signal processing and analysis using the various in-built algorithms such as the EFDD and the SSI.

## ARTeMIS – OMA

After the measurements, the results were taken and placed in a model of the deck constructed in ARTeMIS. The model is based on the dimensions of the deck and the coordinates of both the roving and reference sensors to make the results as realistic as possible. For the vertical vibration under consideration, only the deck was needed in ARTeMIS and is therefore the only thing constructed in the program.

In developing the geometry points representing the sensor locations were created. These are points acting as the nodes. After that, lines are connected through the nodes before applying surfaces on the connections. The result is the finished geometry that was used in the analysis and is illustrated in Figure 3.8.

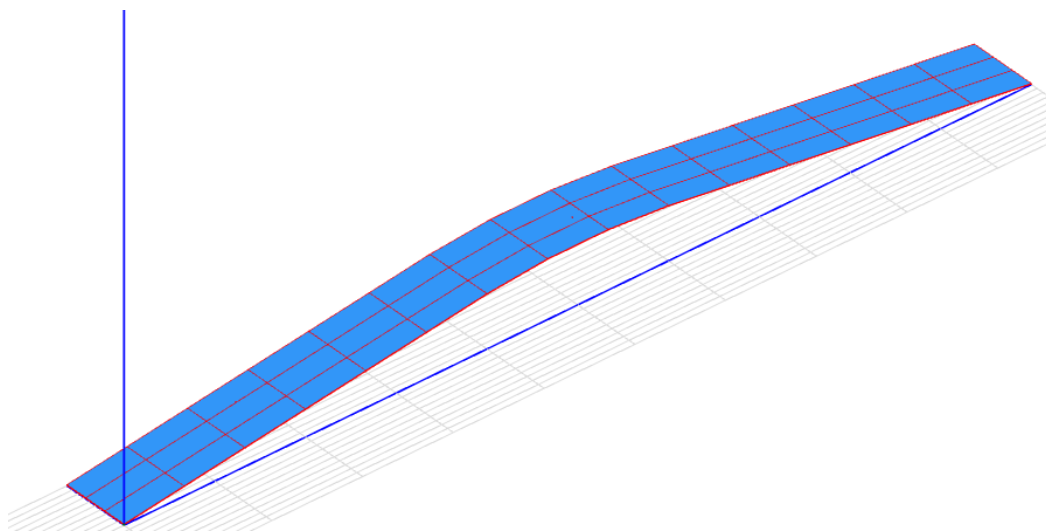


*Figure 3.8: The finished geometry for the timber deck with nodes, lines, and surfaces.*

The next step is to connect the recorded field measurements to each test and each sensor. The data recorded are converted from a text file to data with the help of the ARTeMIS program. They are manually connected to each reference point as DOFs. as Figure 3.9 illustrates. The highlighted 8 points (green) act as the eight measuring sensors placed on the bridge, and each sensor is connected to the data extracted from the sensor with the exact placement on the field test. The two sensors in blue are the reference sensors on the bridge.

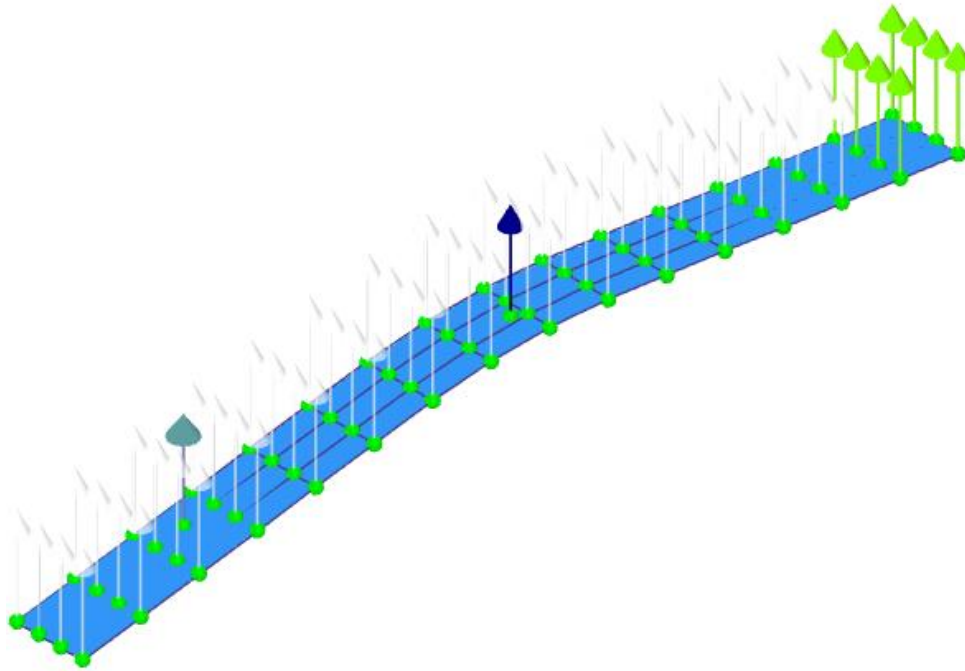


*Figure 3.9: The placement of reference and roving sensors on the bridge according to the physical placement on the bridge deck*

The data was then assigned to each DOF, that resulted in the mode shapes and the frequencies. The given data was then extracted from the software. ARTeMIS estimates the frequencies with the damping ratio and illustrates their respective mode shapes in both the time domain (SSI) and frequency domain (EFDD).



### 3.2.2 Numerical Analyses: FEM-Modelling – SAP2000

Following the field test, Finite Element (FE) numerical models of the bridges were developed for further studies. The bridges were modelled in SAP2000, and a modal analysis was performed, resulting in frequencies and mode shapes which were verified with the tests result.

The procedure is explained in the steps below:

**Grid and measurement definition** – First, the bridge deck's width, and length are marked in the Z, Y and Z direction.

**Material definition** – The materials used in the bridge's structure are then defined with their density and E-modulus. This reflects that the glulam and steel components were considered as isotropic.

**Definition of sections and areas** – Here, the different sections of the structure are defined. Beams, decks, and truss members are then defined and assigned the required material properties defined beforehand. Furthermore, the beams and truss members are represented with beam elements, while the deck are modelled as either thick or thin shells. The 400mm glulam deck was modelled as a thick shell because of the G-modulus. It plays a crucial role for the deformation and choosing a thick shell account for the through thickness. On the other hand, the Steel deck was modelled as a thin shell because of the 40 mm thin and because the deck was isotropic meaning the G-modulus is not as important.

**Modelling of the structure** – Using the grid and measurements, the bridge is modelled with the sections and areas previously mentioned.

**Dividing the areas for a finer mesh** – The bridge deck or area is then divided into sections to provide a finer mesh when it is time to analyse. The mesh size was chosen based upon the

length and width of the deck. The area was divided into equal sized pieces in the X and Y direction based upon the dimension of the bridge.

- The timber bridge was divided into 500 mm in both X and Y direction.
- The steel bridge was divided into 1000mm in the X direction and 500 mm in the Y direction.

Analysis with different mesh sizes were conducted. However, the changes in the mesh sizes did not influence the results significantly. In terms of calculating the MAC value, the area was divided in accordance with the sections represented in the ARTeMIS program to get the dynamic displacement values in the same points of interest.

**Assigning boundary conditions** – Boundary conditions were assigned at the abutment and the piers of the Timber bridge. Being a continuous system, the left abutment was assigned with a pin support, while the two inner piers and the right abutment were modelled as rollers. The steel bridge on the other hand was considered a simply supported situation, therefore the boundary conditions were simplified as pin/roller on the left and right abutment, respectively.

**Assigning a mass source** – Whilst SAP200 estimates the stiffness of the system from the material properties and member cross-sections, it requires a definition of a mass source to perform the modal analysis. Therefore, the mass source assigned is the dead load of the system.

**Running modal analysis** – Modal analysis was conducted setting the analysis option in the Z direction based on the objective of extracting the vertical vibrations characteristics of the system.

The goal was to access how each system behaves and whether and changes in certain parameters affects the modal characteristics. The FE models were validated with the experimental results which provided a basis for the parametric studies.

### Parametric studies

The FEM models are then extended by developing new models with different dimensions and configurations to assess the effect of changes in various parameters in the modal behaviour of the bridges.

### Time-history analysis

The VDV and the RMS are found based on the time-history analysis from the field tests. The field test resulted in the acceleration at each second of the activity. With the help of a Python script, the VDV, RMS and peak acceleration values were calculated from the test results. The script calculated the values for each sensor in each test. Figure 3.10 illustrates how the sensors in each test were set up for a better understanding of the figurines and tables presented later. Tests one, two, seven and eight are the test performed on the two side spans (light orange). Tests three, four, five and six (blue) are the test performed on the main span. The red and blue parts are divided by a thick line acting as the boundary conditions on the bridge. In the Figure below the numbers 1 – 8 represent the roving sensors.

Test 1		Test 2		Test 3		Test 4		Test 5		Test 6		Test 7		Test 8	
1	5	1	5	1	5	1	5	1	5	1	5	1	5	1	5
2	6	2	6	2	6	2	6	2	6	2	6	2	6	2	6
3	7	3	7	3	7	3	7	3	7	3	7	3	7	3	7
4	8	4	8	4	8	4	8	4	8	4	8	4	8	4	8

Figure 3.10: an overview of the test placements. This acts as a basis for the time-history results presented later.

### 3.2.3 Guideline evaluation

The comforts criteria and load models of several international and national guidelines were evaluated concerning the chosen bridges. Calculated results from the comfort criteria and load models were then compared and evaluated against each other to give a broader understanding of the differences and similarities found in the respective guidelines.

## 4 Existing and emerging methods of assessing pedestrian and other bridge vibration performance

Footfall impacts such as from walking, jogging and other human activities are the expected dynamic forces for evaluating vibration serviceability of pedestrian bridges. Different guidelines and technical codes provide ways of assessing vibrations of pedestrian bridges. However, there is divergence in the methods presented in the various design guidelines. This chapter summarizes available and emerging approaches based on the comfort criteria of each respective guideline.

The guidelines presented in this chapter are:

- Statens Vegvesen Handbooks
- The Eurocodes
- The UK-NA to Eurocode 1
- ISO 10137
- SÉTRA Technical guide: Assessment of vibrational behaviour of footbridges under pedestrian loading
- JRC – Design of Lightweight Footbridges for Human Induced Vibrations

Only excitation in the vertical direction will be assessed in this chapter.

#### 4.1 Statens Vegvesen Handbooks:

Since the field tests and the bridges under investigations are in Norway, the Norwegian official guidelines are included in this chapter. The official Norwegian administration for regulation in accordance with design of all public roads and bridges is called “Statens Vegvesen.” This is the Norwegian public roads administration. The public roads administration issues design regulations for public projects in Norway. These regulations are called “håndbøker.” which is translated as handbooks. Therefore, throughout the chapter the regulation will be referred to as handbooks.

Handbook N400: Bridge design – Design of bridges, ferry terminals, and other load-bearing structures is the latest handbook issue that was issued in April 2015. The handbook mentions the following (Statens Vegvesen, 2015):

*“Pedestrian and bicycle bridges that are sensitive to oscillations must be assessed with regard to the comfort of road users. Dynamic loads from wind and traffic must be assessed in both vertical and horizontal directions.*

*NS-EN 1990:2002/A1:2005+NA:2010, point A2.4.3.2 has recommendations on comfort criteria for pedestrians.”*

In other words, Handbook N400 refers to Eurocode 0 – *Basis of structural design* in terms of the comfort criteria. The Eurocodes are assessed later, with regards to the reference from the Norwegian Handbook. However, the Norwegian Public roads administration issued an older version of the same guideline called *Handbook N185*. This version was issued in October 2009 and replaced the N400 mentioned above. Therefore, N185 may be applied in this study.

In section 5.1.3.2 regarding oscillations in footbridges, handbook 185 states that oscillation-sensitive footbridges should be designed so that the reference acceleration,  $a_r$  fulfils the following (Statens Vegvesen, 2009):

$$a_r \leq 0,25 f^{0,7782} \quad [m/s^2] \quad (4.1)$$

Where  $f$  is the first natural frequency for oscillation in the vertical direction given in Hz.

The reference acceleration however calculated as in equation (4.2):

$$a_r = 4\pi^2 f^2 W_s K \psi r \quad [m/s^2] \quad (4.2)$$

Where:

$f$  is the first natural frequency for oscillation in the vertical direction given in Hz,

$W_s$  is the static deflection [m] for a point load equal to 700 N,

$K$  is a factor that depends on the total spans number and the ratio of the span length and is and can be calculated in Table 4.1,

$\psi$  is the dynamic factor that depends on the span length and the damping ratio  $\xi$ , se figure tt,

$\xi$  is the damping ratio of the construction,

$r$  is the correction factor for the reference acceleration; function of  $f$  [Hz]:

$$r = \begin{cases} 1,0 & ; f \leq 4 \\ 3,0 - f/2 & ; 4 < f < 6 \\ 0,0 & ; f \geq 6 \end{cases}$$

Footbridges with the first vertical natural frequency,  $f$ , greater than 6 Hz is not considerable in the oscillation calculations and are therefore neglected.

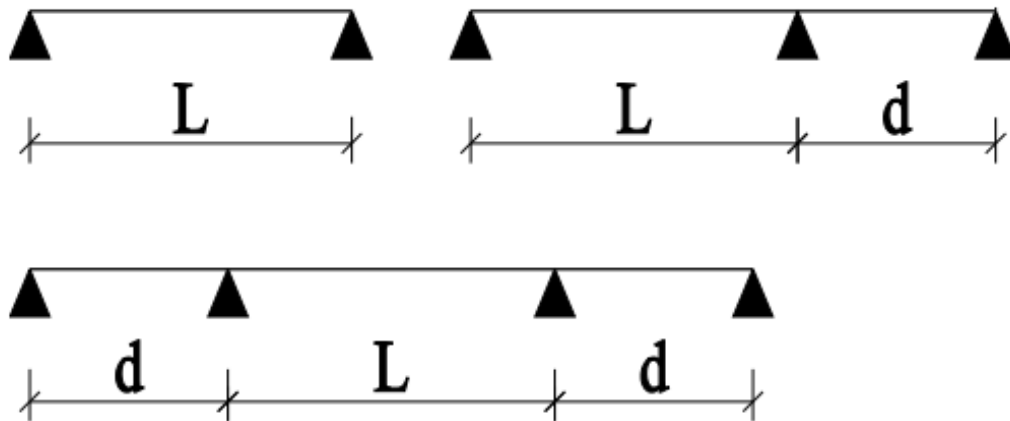


Figure 4.1: the ratio for span and width,  $d/L$  to determine the value for  $K$  in equation 4.2.

Table 4.1: determination of factor  $K$  based on the span width ratio in Figure 4.1. If there is only one slab, the factor for  $K$  is 1.0.

$\frac{d}{L}$ (See figure 4.1)	$K$	
	2 spans	3 spans
1,0	0,70	0,60
0,8	0,92	0,82
0,6	0,96	0,92
0,4	0,96	0,92
0,2	0,95	0,92

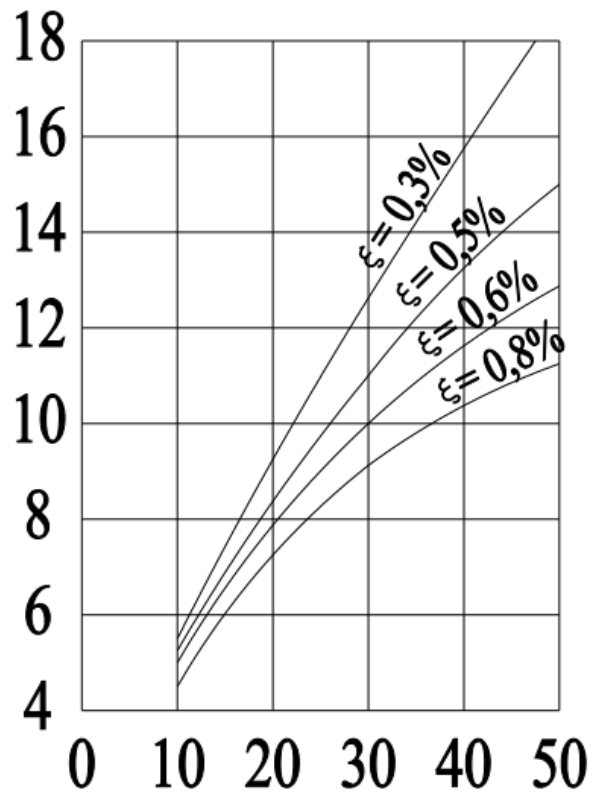


Figure 4.2: Dynamic factor load factor  $\psi$  at the y-axis can be extracted depending on the span length  $L$  on the x-axis due to the damping  $\xi$ .

## 4.2 Eurocodes

The Eurocodes are the European standards implemented for structure design. These standards have been developed and revised by the European Committee for Standardisation and are the most dominant construction guidelines for building. The Eurocodes are divided into ten respective guidelines, but not all of them are as relevant in terms of design of pedestrian bridges. The relevant guidelines for this section are the following:

- Eurocode 0 - NS-EN 1990 - Basis for Structural Design
- Eurocode 1 - NS-EN 1991 - Actions on Structures
- Eurocode 5 - NS-EN 1995 - Design of Timber Structures

In addition to the Eurocode, each country has its own annex that adds information and expands the content of the Eurocode accordingly. The UK national annex is relatively more detailed in the manner of vibrational assessment due to pedestrian loading and is therefore given detailed attention. See Chapter 4.3 for further information.

Section 5.7 of Eurocode 1 states that; *“Appropriate dynamic models of pedestrian loads, and comfort criteria should be defined.”* The same section also notes that the annex in each respective country may indicate their own criteria. The same section also mentions that Eurocode 0 Annex A2 is available for further definitions.

In Eurocode 0 Annex A2 it is described that the maximum acceleration is the key factor when determining the comfort criteria. Chapter A2.4.3.2 of EN 1990-A2 recommends that the comfort criteria should be according to values for the acceleration [ $m/s^2$ ] as follows (European Committee For Standardization, 2016):

- 0.7 for vertical vibrations
- 0.4 for crowds (this is an exceptional condition)

The same chapter recommends that the comfort criteria may be adequate if the fundamental frequency is less than 5 Hz for vertical vibrations.



Nevertheless, Annex B of EN 1995-2, suggest a method for calculating the acceleration on timber bridges. This model applies to timber bridges with simply supported beams and/or truss system made from timber (European Committee for Standardization, 2010).

First each pedestrian crossing the bridge has a predicted vertical acceleration given in  $m/s^2$ .

The vertical acceleration is defined as follow due to different frequency ranges:

$$a_{vert,1} = \frac{200}{M\xi} \text{ for } f_{vert} \leq 2.5 \text{ Hz} \quad (4.3)$$

$$a_{vert,1} = \frac{100}{M\xi} \text{ for } 2.5 \text{ Hz} < f_{vert} \leq 5.0 \text{ Hz} \quad (4.4)$$

$$a_{vert,1} = \frac{600}{M\xi} \text{ for } 2.5 \text{ Hz} < f_{vert} \leq 3.5 \text{ Hz} \quad (\text{running or jogging}) \quad (4.5)$$

$M$  is the total mass of the bridge [kg],

$\xi$  is the damping ratio given in Table 4.2,

$f_{vert}$  is the fundamental natural frequency in vertical direction [Hz]

Table 4.2: Damping ratios for timber bridges according to Eurocode 5.

Type of timber structure	Damping ratio [%]
Structures without Mechanical Joints	1.0
Structures with Mechanical Joints	1.5

In the case where more than one pedestrian is to be considered, the acceleration may be defined as:

$$a_{vert,n} = 0.23a_{vert,1}nk_{vert} \quad (4.6)$$

Where:

$n$  is the number of pedestrians,

$a_{vert}$  is the vertical acceleration for one person crossing the bridge determined according to either Equation (4.3) or (4.4).

$k_{vert}$  is a coefficient found with respect to  $f_{vert}$  in Figure 4.3,

The number of pedestrians,  $n$ , should be accounted as:

- $n = 13$  for a distinct group of pedestrians
- $n = 0.6A$  for a continuous streams of pedestrians

Where  $A$  is defined as the area of the bridge deck in  $m^2$ .

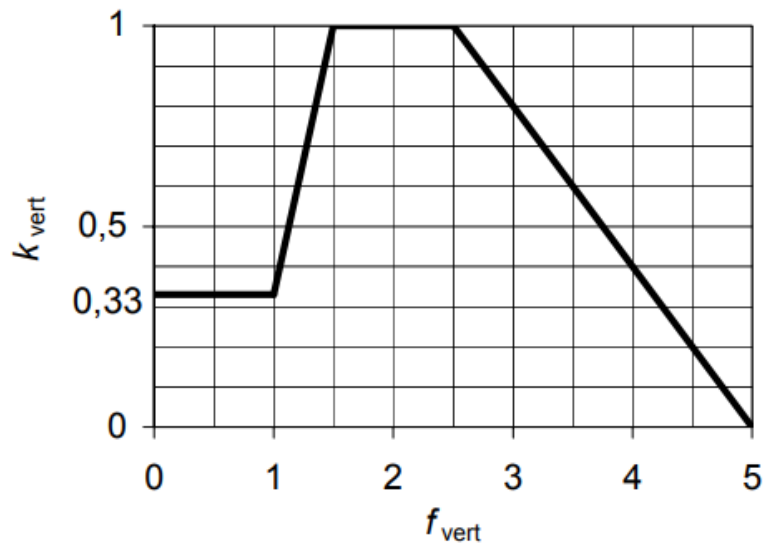


Figure 4.3: Graph that gives  $k_{vert}$  depending on  $f_{vert}$

### 4.3 UK – NA to Eurocode 1

As previously mentioned in chapter 4.2, the UK national annex for the Eurocode addresses the problem of pedestrian traffic in a more detailed manner, compared to the international Eurocode. In general, this is addressed in Eurocode 1 part two: EN 1991-2 “Actions on structures - Part 2: Traffic loads on bridges” (British Standard Institution , 2008). The annex states that “Dynamic models for pedestrian loads and associated comfort criteria may be considered based on two distinct analyses:”

- the determination of the maximum vertical deck acceleration and its comparison with the comfort criteria
- An analysis to determine the likelihood of large synchronized lateral responses.

A load model and a comfort criterion for only the vertical direction would be addressed as it is the focus of this thesis.

To fulfil the SLS criteria, the UK-NA provides values for the maximum acceleration derived from the load models based on the actions induced by pedestrians on the bridges. The acceleration limit is illustrated as:

$$a_{limit} = 1.0k_1k_2k_3k_4 \quad (4.7)$$

Where  $k_1$ ,  $k_2$ ,  $k_3$  and  $k_4$  are the response modifiers taken from the tables 4.3, 4.4, and 4.5 in which:

$k_1$  is the site usage factor found in Table 4.3,

$k_2$  is the route redundancy factor found in Table 4.4,

$k_3$  is the height of structure factor found in Table 4.5,

$k_4$  is an exposure factor which is to be taken as 1.0 unless determined otherwise for the individual project.

However, the acceleration limit should lie between:

$$0.5 \text{ m/s}^2 \leq a_{limit} \leq 2.0 \text{ m/s}^2 \quad (4.8)$$

Table 4.3: Recommended values for the site usage factor  $k_1$ .

Bridge function	$k_1$
Primary route for hospitals or other high sensitivity routes	0,6
Primary route for school	0,8
Primary routes for sports stadia or other high usage routes	0,8
Major urban centres	1,0
Suburban crossings	1,3
Rural environments	1,6

Table 4.4: Recommended values for the route redundancy factor  $k_2$ .

Route redundancy	$k_2$
Sole means of access	0,7
Primary route	1,0
Alternative routes readily available	1,3

Table 4.5: Recommended values for the structure height factor  $k_3$ .

Bridge height	$k_3$
Greater than 8 m	0,7
4 m to 8 m	1,0
Less than 4 m	1,1

#### 4.4 ISO 10137

The international Organization for Standardization, ISO, is one of many standards produced by an organization that belongs to no government whatsoever. ISO 10137 covers matters related to “Bases for design of structures - Serviceability of buildings and walkways against vibrations».

To maintain the comfort criteria according to ISO 10137, the acceleration of the bridge is dependent on the natural frequency of the structure. The acceleration implemented in the ISO is the weighted acceleration known as RMS. Furthermore, the critical frequency plays a significant role in the comfort criteria, whereas the criteria is based on this critical frequency. The critical frequency domain lies between 4 Hz and 8 Hz according to ISO 10137. However, the relevant acceleration criteria are found in frequencies between 1 to 4 Hz ( (International Organization for Standardization - ISO, 2007)).

In terms of absence of more “definitive” data, the standard recommends the following for the vertical vibrations for walkways over roads:

- The levels should not exceed the acceleration multiplied by a factor of sixty.
- If the person is standing still on the bridge, a factor of thirty will then be adequate.

Table 4.6 gives an overview of the calculated weighted accelerations according to Figure 4.4. The weighted accelerations (RMS) are either multiplied by 60 or 30 depending on the activity of the bridge as described in the section above.

Table 4.6: An overview of calculations for different frequency ranges according to Figure 4.4.

Direction	Multiplier	Frequency	Acceleration [m/s <sup>2</sup> ]	Acceleration criteria [m/s <sup>2</sup> ]
Vertical	30	1	0.01	0.03
	60			0.06
	30	4 – 8	0.005	0.15
	60			0.3
	30	80	0.05	1.5
	60			3

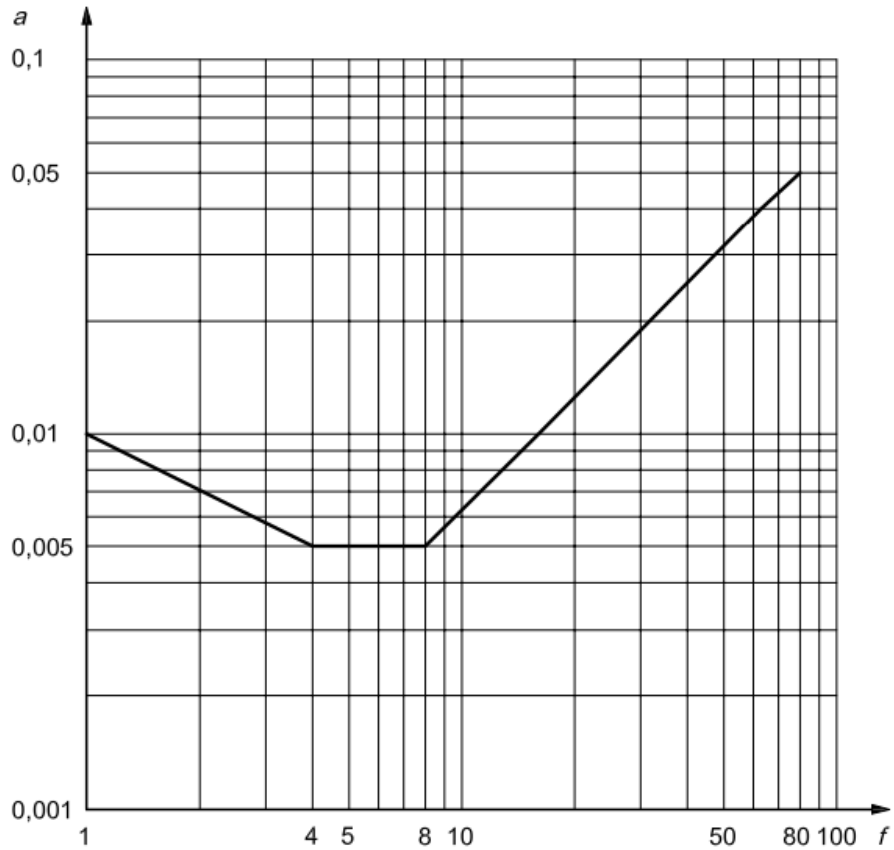


Figure 4.4: The acceleration in the vertical direction based on the frequency ranges. This is the basis for calculations in Table 4.6.

#### 4.5 SÉTRA Technical guide: Assessment of vibrational behaviour of footbridges under pedestrian loading

SÉTRA is the short form of *service d'Études techniques des routes et autoroutes* and is the French translation for “The Technical Department for Transport, Roads and Bridges Engineering and Road Safety.” This is a French technical guide under the directorate of infrastructure and transportation in France. The report is constructed with respect to the methodology used on the Solferino bridge in Paris and with the help of measurements and laboratory-conducted tests.

The footbridge class is first determined of each individual project. The class determines the level of traffic the bridge can bear, and the respective classes goes as follows (Source):’

- *Class IV: seldom used footbridge, built to link sparsely populated areas or to ensure continuity of the pedestrian footpath in motorway or express lane areas.*
- *Class III: footbridge for standard use, which may occasionally be crossed by large groups of people but that will never be loaded throughout its bearing area.*
- *Class II: urban footbridge linking up populated areas, subjected to heavy traffic and that may occasionally be loaded throughout its bearing area.*
- *Class I: urban footbridge linking up high pedestrian density areas (for instance, nearby presence of a rail or underground station) or that is frequently used by dense crowds (demonstrations, tourists, etc.), subjected to very heavy traffic.*

SETRA states that the concept of comfort should be specified. In other words, each project should define the level of comfort desired based on the three comfort levels given in the guideline. The levels are described as follows (French Ministry of Transport and Infrastructure, 2006):

- *Maximum comfort: Accelerations undergone by the structure are practically imperceptible to the users.*
- *Average comfort: Accelerations undergone by the structure are merely perceptible to the users.*
- *Minimum comfort: under loading configurations that seldom occur, accelerations undergone by the structure are perceived by the users, but do not become intolerable.*

Figure 4.5 below give the acceptable acceleration levels due to the comfort level aspired. The colours represent the comfort ranges, where green is maximum comfort and red is no comfort at all.

Acceleration ranges	0	0.5	1	2.5
Range 1	Max			
Range 2		Mean		
Range 3			Min	
Range 4				

Figure 4.5: Acceleration ranges for vertical vibrations and their respective comfort ranges.

SÉTRA advises that the natural frequency for footbridges within Class I to III should be determined in the vertical direction. The frequency is determined based on the following mass assumptions:

- Empty footbridge
- Footbridge loaded throughout its bearing area, to the tune of 700 N pedestrian per square meter ( $70 \text{ kg/m}^2$ )

The same colours for ranges explained in Figure 4.5 are applied in Figure 4.6, where Range 4 (green) is a negligible risk of resonance and Range 1 (red) is the maximum risk of resonance.



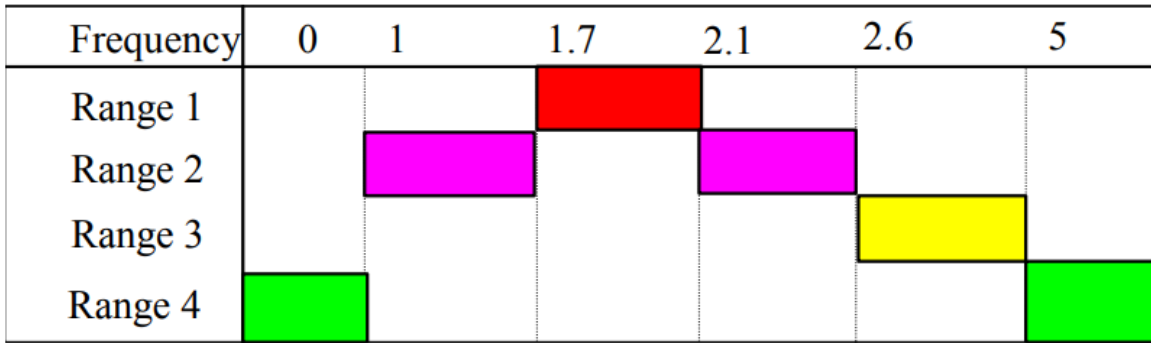


Figure 4.6: Risk ranges for frequency in the vertical direction according to SÉTRA.

The guideline also provides a method for calculating the acceleration. For a footbridge with constant inertia on two supports the acceleration can be calculated as described in Equation (4.9):

$$a_{max} = \frac{1}{2\xi} \frac{4F}{\pi\rho S} \quad (4.9)$$

Where:

$\xi$  is the damping ratio of the structure given in Table 4.7,

$F$  is the linear load on the bridge, set as 700 N as this is the mass assumption of the guideline,

$\rho S$  is the total linear density given in kg/m.

Table 4.7: Advised damping ratios ( $\xi$ ) for different materials according to SÉTRA.

Construction type	Average $\xi$
Reinforced concrete	1,3%
Pre-stressed concrete	1,0%
Mixed	0,6%
Steel	0,4%
Timber	1,0%

#### 4.6 JRC – Design of Lightweight Footbridges for Human Induced Vibrations

In 2009 The European Commission proposed a design guideline for footbridges subjected to human induced vibrations. Within the European Commission is a scientific group for research based on the European norms. The Joint Research Centre, or JRC, produced a guideline and called “Design of Lightweight Footbridges for Human Induced Vibrations” (JRC Scientific and Technical Reports, 2009).

The JRC defines an acceleration limit as degrees of comfort for the vertical direction. The guideline defines each in its respective class where CL 1 is the maximum, and CL 4 is the unacceptable. Table 4.8 illustrates the different values in accordance with the respective classes.

*Table 4.8: Comfort classes and their respective degrees of comfort followed by the acceleration value for the vertical direction.*

Comfort class	Degree of comfort	Vertical $a_{limit}$ [ $m/s^2$ ]
CL 1	Maximum	< 0.5
CL 2	Medium	0.5 – 1.00
CL 3	Minimum	1.00 – 2.50
CL 4	Unacceptable	> 2.50

Like SÉTRA, the JRC guideline includes ranges for the natural frequencies in the vertical direction and is illustrated in Table 4.9:

*Table 4.9: Frequency range for the vertical direction according to the JRC guideline*

Direction	Frequency range
Vertical	$1,25 \text{ Hz} \leq f_i \leq 2,3 \text{ Hz}$

Like other guidelines presented the JRC includes advised damping ratios for different materials. Both the damping ratios` average and minimum values are illustrated in Table.

*Table 4.10: Different materials` minimum and average damping ratios according to the JRC guideline.*

Construction type	Minimum $\xi$	Average $\xi$
Reinforced concrete	0,8%	1,3%
Prestressed concrete	0,5%	1,0%
Composite steel concrete	0,3%	0,6%
Steel	0,2%	0,4%
Timber	1,0%	1,5%
Stress-ribbon	0,7%	1,0%

#### 4.7 Compendium of Comfort criteria:

Under this section, a summary of the different guidelines' comfort criteria will be presented chronologically in accordance with their chapter order. The comfort criteria of each guideline were taken out of their respective tables and figures and then calculated to be presented in Table 4.11 and 4.12.

*Table 4.11: Summary of all acceleration limits in the presented guidelines*

Guideline	Criteria
Statens Vegvesen	$a_r \leq 0,25 f^{0,7782}$
Eurocodes	$a < 0.7 \text{ m/s}^2$
UK – national annex	$0.5 \text{ m/s}^2 \leq a_{limit} \leq 2.0 \text{ m/s}^2$
ISO 10137	$0.15 \text{ m/s}^2 \leq a_{limit} \leq 0.6 \text{ m/s}^2$
SÉTRA Technical guide	$0.5 \text{ m/s}^2 \leq a_{limit} \leq 2.5 \text{ m/s}^2$
JRC	$0.5 \text{ m/s}^2 \leq a_{limit} \leq 2.5 \text{ m/s}^2$

*Table 4.12: Summary of available frequency ranges in the guideline mentioned in Chapter 4.*

Guideline	Frequency [Hz]
Eurocode 0	$f < 5$
SÉTRA*	$0 < f \leq 1$ or $5 < f$
ISO 10137	$1 \leq f \leq 4$
JRC**	$1.25 \leq critical \leq 2.3$

\*These are values where resonance is negligible

\*\* These are values where the frequency is critical.

## 5 Results and Discussion

In this chapter all the adequate and comparable results from the OMA models are presented and discussed. Then the FE-model are validated by comparison to the OMA model for further usage and research. It is strongly advised for the reader to read Chapters 2 and 4 to understand the theory and guideline statements before reading the results in this chapter.

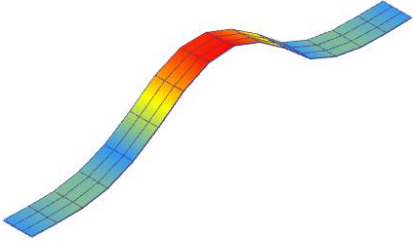
### 5.1 Field experiment results – OMA

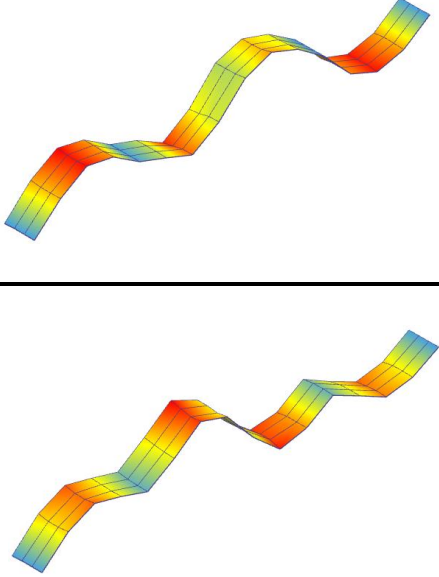
In the following section the field results from the two different field experiments are assessed and presented in table form. The result for both running and walking are presented. The first three modes in timber bridge and the fundamental mode in the steel bridge were identified and are presented with the necessary parameters.

#### 5.1.1 Timber bridge:

The result from both running and walking on the timber bridge are shown in Table 5.1 in terms of the natural frequencies, damping ratios and the complexity of the mode given in ARTeMIS modal.

*Table 5.1: An overview of the field test results with all parameters and mode shapes for both running and walking.*

Mode	Activity	Domain	Frequency [Hz]	Damping [%]	Complexity [%]	Mode shape
1	Walking	EFDD	3.429	4.851	0.15	
		SSI	3.165	5.267	1.417	
		Average	3.297	5.059	0.7835	
	Running	EFDD	2.625	4.288	0.036	
		SSI	2.678	7.085	0.103	
		Average	2.652	5.687	0.0695	
2	Walking	EFDD	7.445	3.605	0.902	
		SSI	7.444	2.205	8.928	
		Average	7.446	2.905	4.915	

3	Running	EFDD	7.658	2.244	8.862	
		SSI	7.457	3.528	15.217	
		Average	7.558	2.886	12.040	
	Walking	EFDD	9.194	2.603	10.811	
		SSI	9.587	3.303	18.902	
		Average	9.391	2.953	11.425	
Running	EFDD	10.205	1.972	1.772		
	SSI	10.034	4.596	1.971		
	Average	10.120	3.284	1.872		

To validate that the frequencies for both activities were adequate both mode shapes and frequencies were compared and found out to be similar in terms of values and shapes. It is only in the first mode that the walking and running frequency have noticeably different values in frequency, but the compatibility in this case is over 80 percent, meaning that together with the mode shape both activities are eligible for further comparison. The reason for the differences in the natural frequency values for the first mode may be that during walking it is perceived that the pedestrian is in contact with the system consistently therefore imposing additional mass. The significant differences in frequencies are only found in the fundamental frequency of the running and walking cases and does not apply for the rest of the modes. In the case of running the damping for first mode is relatively higher compared to the damping of the other modes. Whilst it is over 7% for SSI and recorded 4.3 % in EFDD as seen in Table 5.1. Generally, the average damping from the various techniques for walking is less than the damping for running for all the modes identified. Furthermore, the reason for a higher recorded damping for running may be due to the fact that when the user of the bridge jogs over, one leg touches the bridge at a time compared to walking where both legs are in contact with the deck at the same time. This could therefore lead to higher damping values.

The damping of the bridge as mentioned above are great in the first mode. In the next two modes the damping of the bridge decreases. Figure 5.1 shows a linear decrease in damping for EFDD as the frequency increased. Figure 5.2 shows that the damping ratio in the SSI for all modes is higher than damping in the EFDD. However, the rate of increase and decrease is the same for both the EFDD and the SSI.

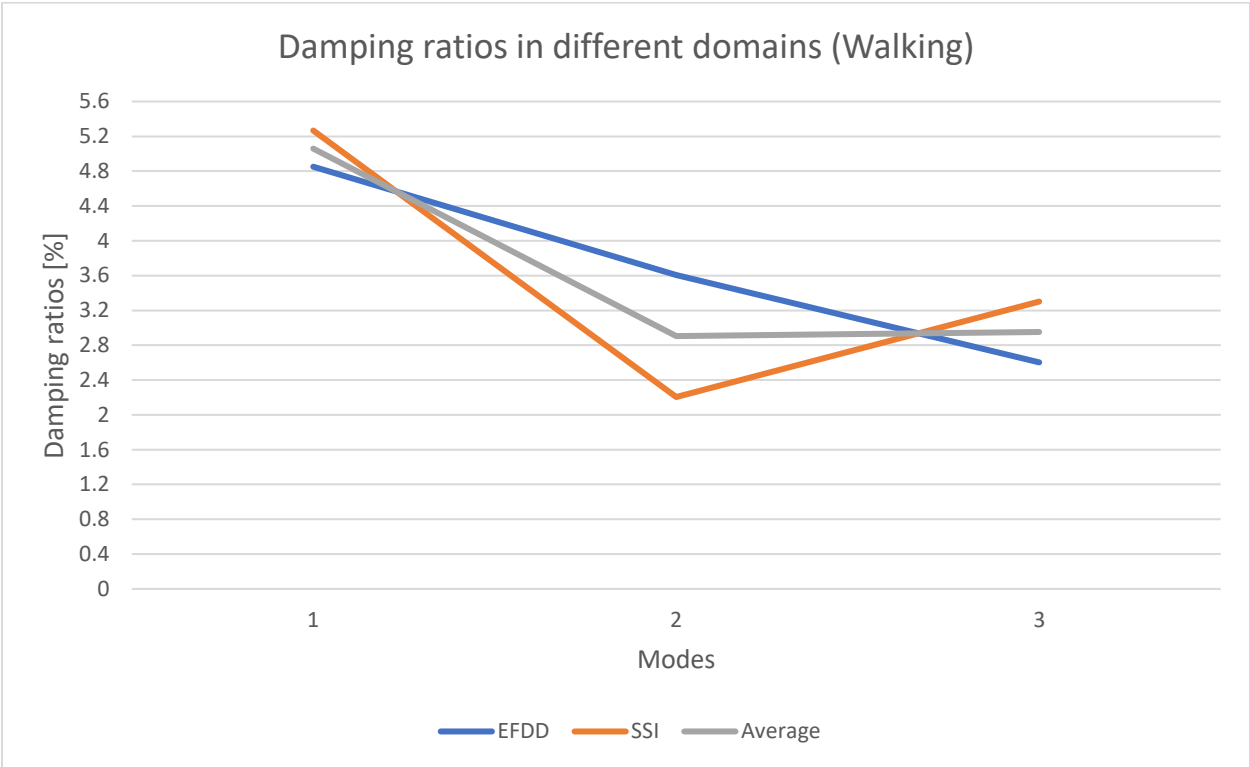


Figure 5.1: A graph of the damping development for each mode in the walking scenario. Values are based on field test from Table 5.1.

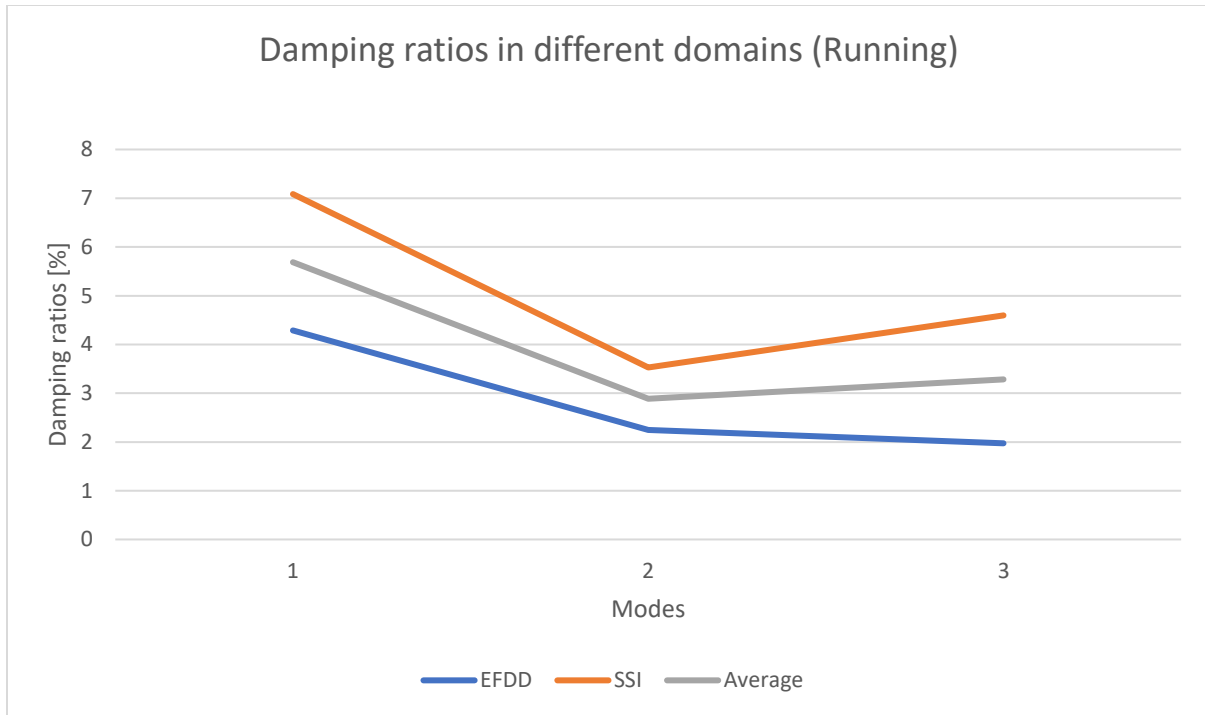


Figure 5.2: A graph of the damping development for each mode in the running scenario. Values are based on field test from Table 5.1.

Some of the guidelines mentioned in chapter 4 include damping ratios for different materials and Table 5.2 presents the values for timber structures:

Table 5.2: Damping ratios for timber in three of the guidelines mentioned in Chapter 4.

Guideline	Damping ratio [%]
Eurocode 5	1
Eurocode UK-NA	1.5
SÉTRA	1

All the average damping values in both running and walking exceeds the damping ratios advised in the guidelines. In other words, the values recommended in the guidelines are low and further work on the damping matter should take place to assess more realistic values.



The complexity of the mode shapes is low. The average complexity is illustrated for each mode and activity and neither average complexity of both activities exceeds a complexity of 13%. The highest complexity value is 18%. As may be seen from Table 5.1, as the mode order increased the complexity increased as well and the time domain (SSI) had the highest complexities in each of the modes illustrated in Table 5.1. In general, however, the complexities were not out of order for the mode shapes. 18% as the highest may be considered adequate, meaning the mode shapes may be taken as reasonable for further research.

Likewise with the damping ratios mentioned earlier, some of the different guidelines discussed offer suggestions and comment on fundamental natural frequencies in the vertical direction. These are found in Table 5.3:

*Table 5.3: Frequency ranges based on guidelines presented in Chapter 4.*

Guideline	Frequency [Hz]
Eurocode 0	$f < 5$
SÉTRA*	$0 < f \leq 1$ or $5 < f$
ISO 10137	$1 \leq f \leq 4$
JRC**	$1.25 \leq \textit{critical} \leq 2.3$

\*These are values where resonance is negligible

\*\* These are values where the frequency is critical.

As illustrated in the table above, the fundamental frequency is within the ranges of all guidelines and is excluded from and critical frequency. In the SÉTRA guideline if the value of natural frequency lies between 2.6 and 5, then the risk of resonance is minimum and can be in most cases neglected.

## Field test results up to 100 Hz:

In each test, frequency graphs were extracted for modes in ARTeMIS. Looking at Figures 5.3 and 5.4, the modes are marked with text over the amplitudes where there is suspected to be a mode shape. A high precise amplitude usually results in a good mode shape. The figures below (Figures 5.3 and 5.4) represent both the running and walking scenario, respectively for the timber bridge.

Both graphs showed that both field test results (walking and running) produced three modes that were comparable. In figure 5.3, the amplitude before Mode 1 when investigated had the same shape and may be a result of a bouncing effect. The rest of the of the peaks were found to be rigid body and localised modes. Thus, for both running and walking only three modes with well-defined mode shapes were observed.

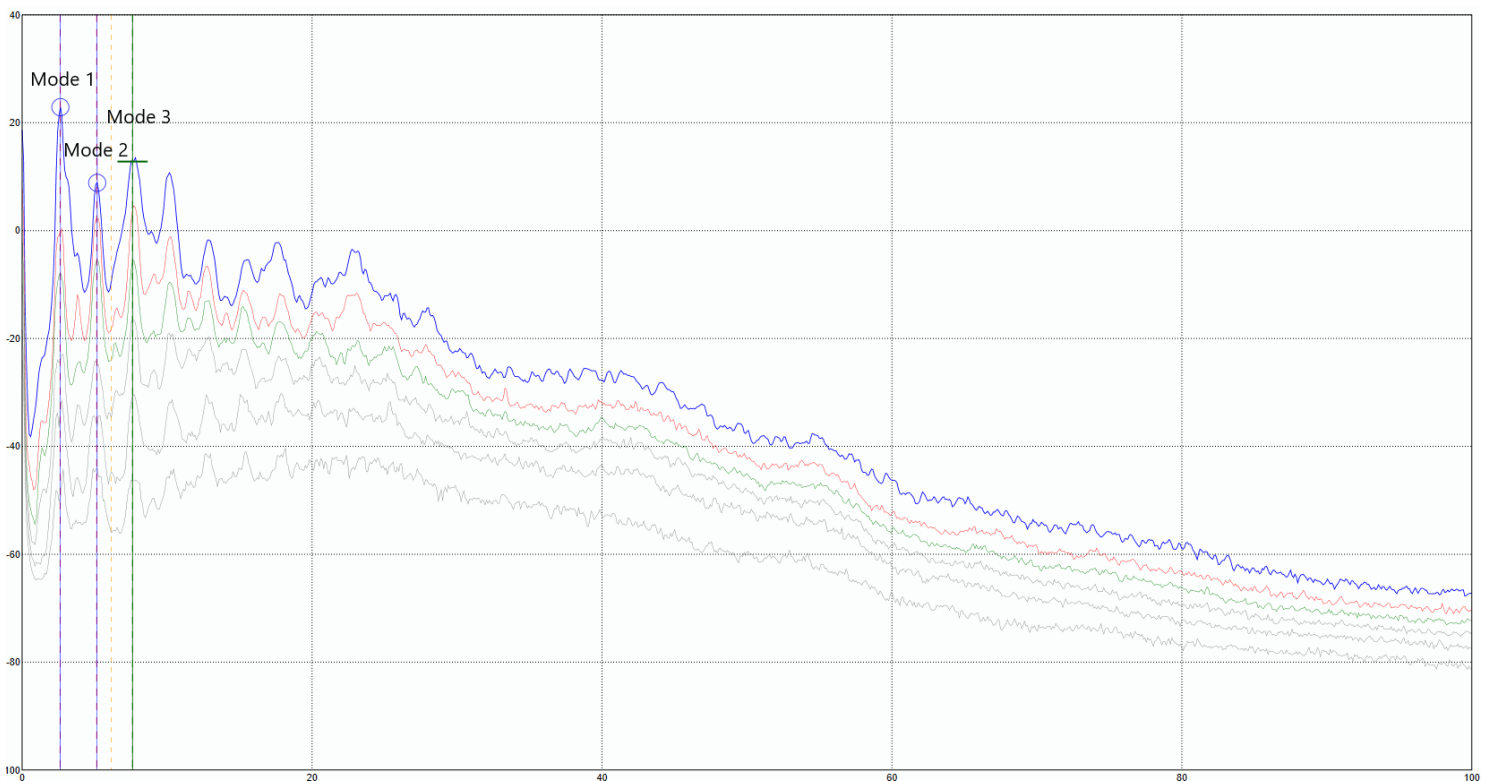


Figure 5.3: Illustrates the frequency graph for running from ARTeMIS with marked amplitudes.

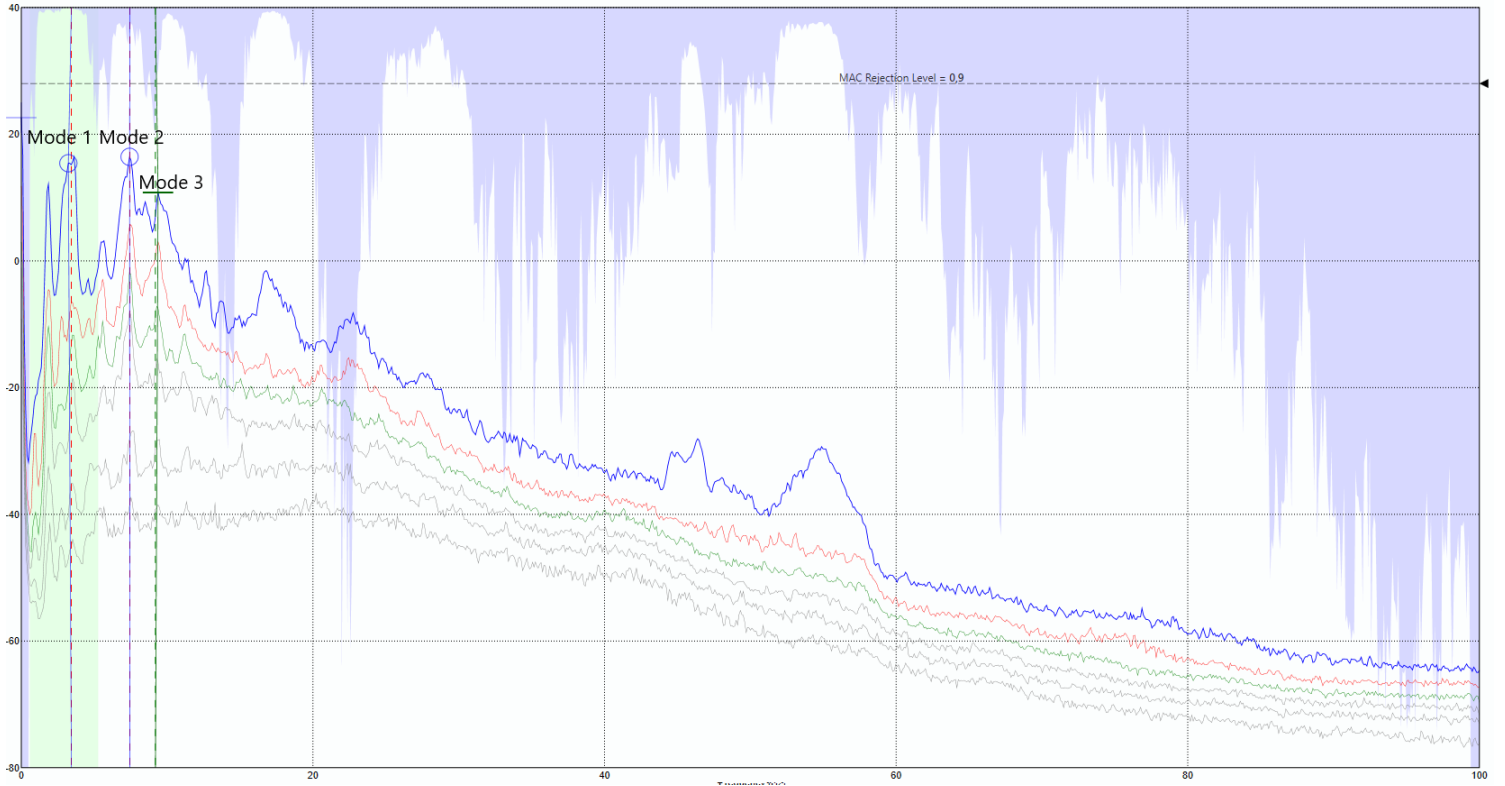


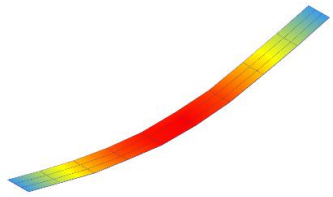
Figure 5.4: Illustrates the frequency graph for walking from ARTeMIS with marked amplitudes.

### 5.1.2 Steel bridge

The fundamental frequencies and mode shapes were almost identical in the walking and heel drop scenario. The complexity of the mode shape was lower than 1% in all cases, as Table 5.4 illustrates. Analysis showed complex localized higher order modes. This may be attributed to the fact that the bridge deck consisted of grillage pieces that were not connected in manner that enables activation of the whole deck in unison with respect to the higher modes thus, resulting in inadequate mode shapes with high complexity and no damping values.

Table 5.4 summarizes the fundamental modal parameters for the steel bridge. The frequencies, damping and mode shapes are similar in both activities (walking and heel-drop) and the complexity of the first mode in both scenarios are low for the mode shape.

*Table 5.4: An overview of the field test results with all parameters and mode shape for both running and heel-drop for the steel bridge.*

Mode	Activity	Domain	Frequency [Hz]	Damping [%]	Complexity [%]	Mode shape
1	Walking	EFDD	6.739	4.489	0.123	
		SSI	6.665	2.150	0.274	
		Average	6.7155	3.320	0.199	
	Heel drop	EFDD	6.499	2.973	0.161	
		SSI	6.518	2.774	0.098	
		Average	6.5085	2.874	0.130	

The highest recorded damping was 4.489% in the EFDD and on average it was 3.320 %. Table 5.5 provides recommended damping ratios in two of the guidelines discussed earlier:

*Table 5.5: Advised damping values for steel in UK-NA and SÉTRA.*

Guideline	Damping ratio [%]
Eurocode UK-NA	0.5
SÉTRA	0.4

Looking at the ratios compared to the ratios acquired through testing, the test values are relatively high. There is no doubt that the grillage problem that occurred within the testing

ground resulted in relatively high damping due to friction. Another reason can be the thickness of the grillage. As described in Chapter 3.2.1, the deck/grillage was only 40 mm thick resulting to clear vibration when crossing it and the flexibility coupled with higher footfall forces may generate high damping in the EFDD from ARTeMIS and other signal processing methods.

## 5.2 Time history calculations: VDV and RMS

Time-history responses were assessed in the case of the timber bridge. Measurements from the field test accelerometers were used to calculate the VDV and RMS. The calculations were made in both scenarios, running and walking. The results and calculations in each scenario are presented individually before they are compared to the ISO 10137 values for RMS and VDV.

The RMS values provided are found in chapter 4.4 Figure 4.4 where the comfort criteria are the weighted acceleration in the vertical direction that in the ISO is calculated RMS. This is calculated as  $0.3 \frac{m}{s^2}$ . Table 5.6 on the other hand provides the recommended VDV values from Table C.2 in ISO 10137:

*Table 5.6: VDV values ( $m/s^{1.75}$ ) above which various degrees of adverse comments may be expected in residential buildings.*

Place	Low probability of adverse comments	Adverse comments possible	Adverse comments probable
Residential buildings 16 h day	0.2 to 0.4	0.4 to 0.8	0.8 to 1.6
Residential buildings 8 h day	0.13	0.26	0.51

### 5.2.1 Walking

#### VDV

Figure 5.5 gives an overview of the VDV calculated based on the field test recordings for walking on the timber bridge. A high VDV value will give the most discomfort; therefore, looking at test 7 and sensor 8, the highest VDV value is found there.

Test 1		Test 2		Test 3		Test 4		Test 5		Test 6		Test 7		Test 8	
0.110	0.104	0.112	0.100	0.068	0.069	0.099	0.100	0.083	0.084	0.096	0.106	0.124	0.164	0.084	0.048
0.093	0.108	0.104	0.095	0.047	0.065	0.087	0.081	0.079	0.080	0.081	0.098	0.105	0.132	0.075	0.051
0.080	0.111	0.097	0.085	0.061	0.066	0.086	0.087	0.082	0.084	0.079	0.110	0.114	0.142	0.075	0.050
0.072	0.091	0.101	0.082	0.067	0.071	0.092	0.093	0.083	0.089	0.076	0.086	0.148	0.189	0.082	0.056

Figure 5.5: The different VDV values calculated on each of the sensors distributed on the bridge deck for walking.

As Figure 5.5 implies the Highest VDV value in the walking scenario was  $0.189 \text{ m/s}^{1.75}$ .

The ISO 10137 gives values for the VDV. However, these values are meant for residential buildings. Nevertheless, when comparing the maximum value to the ISO requirements illustrated in Table 5.6 in Chapter 5.2, it is shown that the greatest VDV value recorded on the timber bridge lies between the two most extreme cases for residential stays. In other words, the VDV values are more than adequate for the walking scenario.

#### RMS

On the other hand, the RMS is another time history response implemented to measure the comfort of the bridge. By implementing the same methodology in the RMS category, the highest recorded acceleration is  $0.1439 \text{ m/s}^2$ . This is found and illustrated in Figure 5.6 and in test 6 and sensor one particularly.

Test 1		Test 2		Test 3		Test 4		Test 5		Test 6		Test 7		Test 8	
0.0905	0.0785	0.0900	0.0864	0.0804	0.0610	0.0891	0.1029	0.0358	0.0373	0.1378	0.1439	0.0485	0.0515	0.0580	0.0360
0.0655	0.0665	0.0770	0.0770	0.0623	0.0609	0.0919	0.0853	0.0454	0.0296	0.1133	0.1261	0.0777	0.0634	0.0484	0.0463
0.0623	0.0774	0.0640	0.0612	0.0780	0.0670	0.0815	0.0937	0.0622	0.0370	0.1074	0.1368	0.0629	0.0662	0.0444	0.0474
0.0504	0.0520	0.0679	0.0449	0.0836	0.0691	0.0754	0.0486	0.0416	0.0460	0.0885	0.1023	0.0655	0.0496	0.0343	0.0336

Figure 5.6: The different RMS values calculated on each of the sensors distributed on the bridge deck for walking.

When evaluating the calculated RMS in accordance with ISO 10137, the maximum value extracted by the graph is found in Figure 4.4 in Chapter 4.4 was  $0.3 \frac{m}{s^2}$ . This is found by multiplying the acceleration with a multiplier of sixty, as the standard described in Chapter 4.4. Furthermore, it is then concluded that the calculations meet the requirement of the RMS acceleration as well.

### 5.2.2 Running

#### VDV

At first, glance, comparing walking and running implies a higher acceleration when running. Thus, the VDV and RMS calculated values would naturally be higher than those calculated when walking on the bridge. Figure 5.7 gives values for the VDV in the running case.

Test 1		Test 2		Test 3		Test 4		Test 5		Test 6		Test 7		Test 8	
0.07444	0.19185	0.2706	0.19642	0.0776	0.20765	0.35213	0.40434	0.32257	0.25953	0.14873	0.10315	0.19227	0.25324	0.16063	0.05947
0.06396	0.18082	0.26069	0.1901	0.06115	0.19744	0.34135	0.3999	0.3247	0.25686	0.14653	0.07121	0.18674	0.24298	0.15528	0.05121
0.05928	0.17694	0.2633	0.18943	0.07678	0.19689	0.33747	0.40333	0.32543	0.2678	0.15132	0.0795	0.18915	0.24792	0.15925	0.04858
0.0208	0.1894	0.27194	0.2081	0.08699	0.21113	0.34036	0.41327	0.33142	0.27787	0.15697	0.05112	0.19143	0.2651	0.17721	0.04642

Figure 5.7: The different VDV values calculated on each of the sensors distributed on the bridge deck for running.

The highest VDV value calculated in the running scenario was  $0.41327 \frac{m}{s^{1.75}}$ , more than two times greater than the value calculated for walking. The value is found in test four, and the whole test gives higher values than the other sensors. Test four is in the middle of the bridge, and it makes sense that the acceleration is higher in the middle of the span, where there may be more sway compared to other parts of the bridge.

Comparing that to the values for comfort in residential stay, the VDV value calculated is adequate for residential stay at 16 hours with adverse comments possible as the Standard describes. In other words, some users may find discomfort when jogging on the bridge.

## RMS

As previously mentioned, the highest values are more significant regarding VDV and RMS and the highest RMS value  $0.1526 \frac{m}{s^2}$ . The highest RMS value and the highest VDV is located within the same test area as Figure 5.8 illustrates. However, a value of  $0.1526 \frac{m}{s^2}$  does not exceed the comfort criteria in the standard, and the value is still, therefore, adequate in the case of the RMS criterium.

Test 1		Test 2		Test 3		Test 4		Test 5		Test 6		Test 7		Test 8	
0.1120	0.1060	0.0546	0.0414	0.0775	0.0831	0.1381	0.1497	0.1164	0.1414	0.0658	0.0563	0.1105	0.1250	0.1000	0.0686
0.0740	0.1208	0.0725	0.0489	0.0782	0.0986	0.1394	0.1385	0.1198	0.1103	0.0491	0.0350	0.1198	0.1328	0.0714	0.0610
0.0579	0.0886	0.0727	0.0484	0.1060	0.1038	0.1277	0.1526	0.1193	0.0966	0.0733	0.0442	0.0965	0.1308	0.0771	0.0481
0.0097	0.0348	0.0671	0.0466	0.1198	0.1226	0.1037	0.0979	0.1008	0.1159	0.0602	0.0312	0.0546	0.0727	0.0919	0.0562

Figure 5.8: The different RMS values calculated on each of the sensors distributed on the bridge deck for running.

### 5.2.3 Summary: Time-History

At last, both the VDV and RMS values were controlled and found to be adequate compared to the measured and calculated values illustrated in Figures 5.5 and 5.6 for walking. The Highest VDV value is on the 7<sup>th</sup> test and the highest RMS is on the 6<sup>th</sup> test compared to the highest VDV and RMS values for running located at the 4<sup>th</sup> test. Test number 4 is in the middle of the bridge. Both the RMS and the VDV values calculated was at the middle of the bridge for the running scenario. That is reasonable because of the increased sway and motion on that part of the bridge.

On the other hand, the running scenario was not adequate regarding the VDV values. However, the RMS values were adequate within a good margin. One may argue that Table 5.6 is for residential buildings and therefore not applicable to bridges. However, comparisons are made to Table C.2 in the ISO since no provisions are made for VDV limits on bridges. Also, because the VDV is a measure for longer exposure, it is speculated that satisfying the VDV limits are likely to provide comfort to pedestrians on the bridge in terms of vibration serviceability.



The reason behind so low RMS values may be the modal damping recorded in the bridge due to the thick timber slab and the asphalt layer on top of the slab. Combining those two factors could lead to recordings giving lower accelerometer and RMS values.

### 5.3 Numerical results – FEM

Under this section the numerical results from SAP2000 are presented. The frequencies and their respective mode shapes are presented in tables. Both the timber and steel bridge are presented and evaluated separately

#### 5.3.1 Validation of FE models

Before using the FE model, it is important to validate it. The validation is done so further use of the model is justified other studies. The frequencies and mode shapes extracted from the OMA results and the parameters from the modal analysis performed in SAP2000 are compared to validate the model. In addition to comparing the frequencies and mode shapes the MAC for each mode is calculated to examine as further verification of the model.

#### Timber bridge:

The FE results are compared with results of both the running and walking tests in terms of the natural frequencies, MAC and for the mode shapes. Good correspondence is obtained between FE and experimental results as seen in Table 5.7, 5.8 and 5.9.

Table 5.7: Timber bridge comparison of Field test results and FE-Model for mode one.

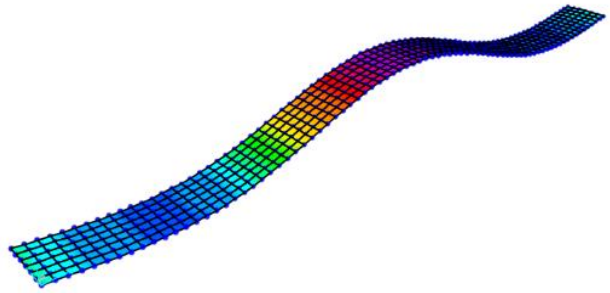
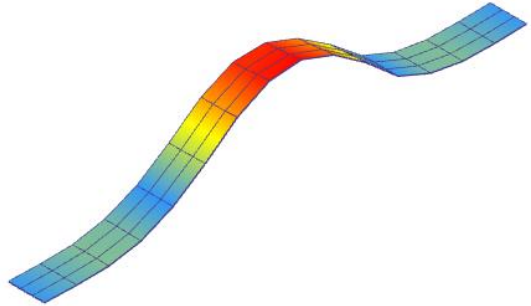
Mode	Program	Frequency		Mode shape
1	SAP2000 – FEM	$f: 3.2538 \text{ Hz}$		
	ARTEMIS – OMA	Walking	% variance	
		$f: 3.254 \text{ Hz}$	0.006%	
		Running	% variance	
$f: 2.6515 \text{ Hz}$	22.71%			
MAC	Walking		Running	
	0.99210251 = 99.21%		0.9921502 = 99.22 %	

Table 5.8: Timber bridge comparison of Field test results and FE-Model for mode two.

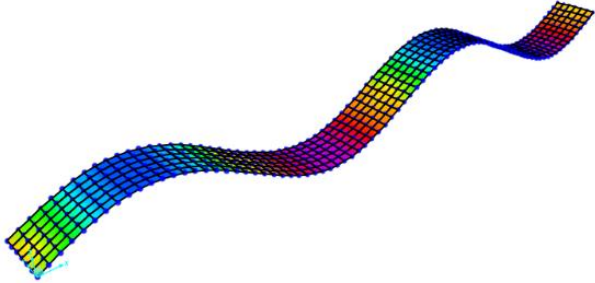
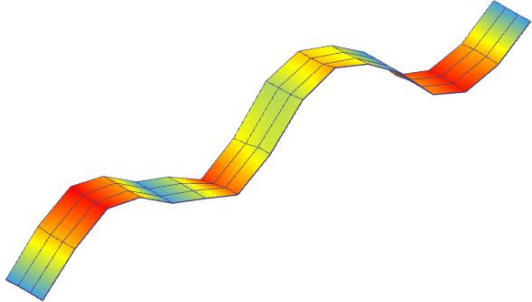
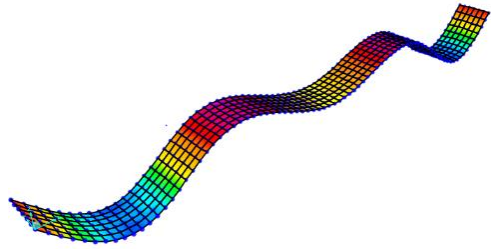
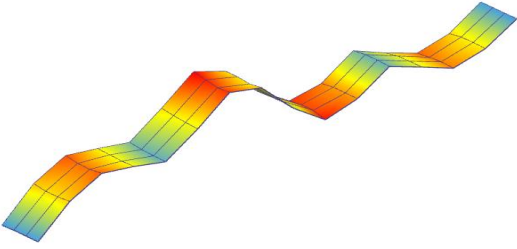
Mode	Program	Output		Mode shape
2	SAP2000 – FEM	$f: 8.3013 \text{ Hz}$		
	ARTEMIS – OMA	Walking	% variance	
		$f: 7.446 \text{ Hz}$	11.48%	
		Running	% variance	
$f: 7.5575 \text{ Hz}$	9.842%			
MAC	Walking		Running	
	0.96134312 = 96.13 %		0.96858902 = 96.9%	

Table 5.9: Timber bridge comparison of Field test results and FE-Model for mode three.

Mode	Program	Frequency		Mode shape
3	SAP2000 – FEM	$f: 10.5498 \text{ Hz}$		
	ARTEMIS – OMA	Walking	% variance	
		$f: 9.391 \text{ Hz}$	12.34%	
		Running	% variance	
$f: 10.120 \text{ Hz}$	4.247%			
MAC	Walking		Running	
	0.227712 = 22.8 % SAP (4) and ARTEMIS (3): 0.597327 = 59.7%		0.030682 = 3.0682 % SAP (4) and ARTEMIS (3): 0.913924 = 91.4 %	

The timber bridge had three identified modes in the field tests which compare very well in terms of mode order, modal shapes, and natural frequencies with the numerical modal model results. The discrepancies observed between the FE models and the test results may be attributed to assumptions made in boundary conditions, material properties and geometry simulation as the curvature in elevation was ignored.

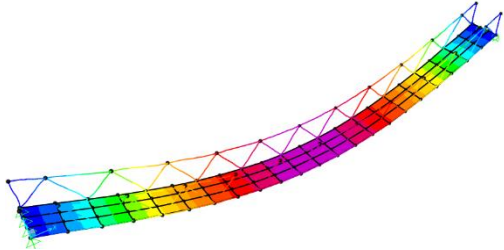
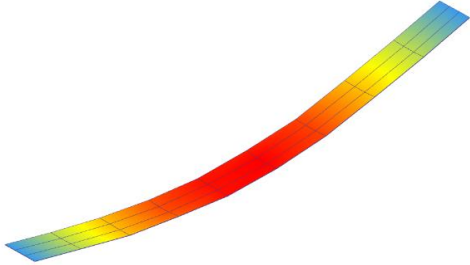
The Modal Assurance Criterion – MAC is also on par with the two first modes. That means that the mode shapes are more than 99 % compatible between the FEM and OMA models in both the running and the walking scenarios for the first two modes. However, for the other higher order modes the MAC correspondence between FE and test mode shapes were relatively low. This reflects that further updating of the FE model may be required. For instance, in the case of walking, the MAC for mode three with regards to the FE test is 22.8%, and in the case of

running 3.0682%. These values are low and may not be within an acceptable ratio. However, by comparing mode 4 in SAP2000 and mode 3 from the test results, it was observed that the MAC value rose to almost 60 % in walking and over 91 % in running. It may be speculated that the dynamic displacements constituting modes three and four appear to interact in manner that influences each other.

**Steel bridge:**

As Table 5.10 illustrates, in comparison the steel bridge`s frequencies and mode shapes for both walking and heel drop corresponds with the frequencies and mode shapes extracted in the FE model. this is visible for the frequencies where the frequency discrepancies were on average 3.7%. The MAC values are almost 99% in both cases meaning the mode shapes also align in both respective programs. Nevertheless, as mentioned earlier because of the localized modes, only the fundamental mode may not be enough to validate the FE model with the field experimental results.

*Table 5.10: Steel bridge comparison of Field test results and FE-Model for mode one.*

Mode	Program	Output		Mode shape
1	SAP2000 – FEM	Frequency, $f$ : 6.8554 Hz		
	ARTEMIS – OMA	Walking	% variance	
		6.7155 Hz	2.08%	
		Heel drop	% variance	
$f$ : 6.5085 Hz	5.33%			
MAC	Walking		Heel drop	
	0.98988307 = 98.988 %		0.99922939 = 99.922 %	

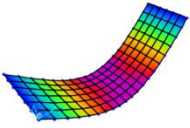
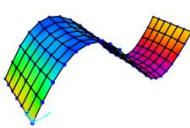
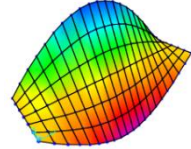
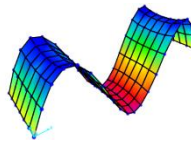
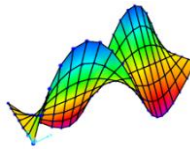
#### 5.4 Effect of changes in span length

This section conducts a parametric study on the timber bridge to evaluate and understand how changes in the bridge span affect the modal characteristics of the system. The timber bridge was remodelled as a single span, considered as simply supported whilst maintaining the thickness and width of the deck. The focus of the study was how the frequencies and modes changed depending on the variation of span length. The study evaluated spans starting at 10 meters, and the deck was increased by 5 meters up to 25 meters to evaluate frequencies, mode shapes, and the number of modes participating with frequencies up to 100 Hz.

The results are presented in tables with the necessary parameters for each span. The first five modes as presented for each span, but other higher modes are commented upon. The mode order is chronologically. However, the modes are presented in the format of  $(m, n)$  which means number of half sin waves in the span ( $m$ ) and width ( $n$ ) direction, respectively.

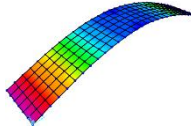
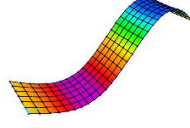
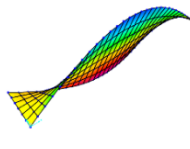
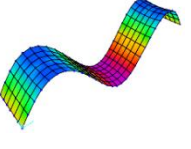
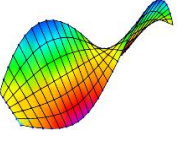
The shortest span was 10 meters, resulting in the highest stiffness. A high stiffness naturally results in higher frequencies, as illustrated in Table 5.11. For all the studied spans, the two first modes had half-sine curvatures along the span as may be seen in the tables. However, up to 20 metres, mode three had one half-sine wave along the span with two half sine waves in the direction of the width. This reflects that when the span increased to 25 meters mode three and four interchanged positions on the mode order. When the span was set to be 10m, available modes up to 100 Hz were five modes.

Table 5.11: Parametric study result for timber deck span 10 m.

Length of deck: 10 m					
Mode order	1	2	3	4	5
Mode	1,1	2,1	1,2	3,1	2,2
$f$ [Hz]	8.29941	33.27165	36.71491	74.63543	78.12752
Mode shape					
Modes up to 100 Hz: 5 modes					

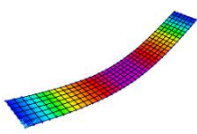
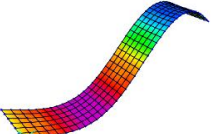
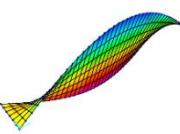
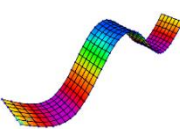
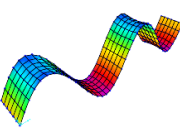
Increasing the span from 10 m to 15 m resulted in the same mode shapes but the fundamental frequency reduced by more than 50%. Furthermore, when the span was at 15m length, the modes up to 100 Hz increased from 5 to 8.

Table 5.12: Parametric study result for timber deck span 15 m.

Length of deck: 15m					
Mode order	1	2	3	4	5
Mode	1,1	2,1	1,2	3,1	2,2
$f$ [Hz]	3.68481	14.7728	24.3466	33.2797	50.1172
Mode shape					
Modes up to 100 Hz: 8 modes					

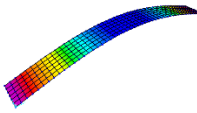
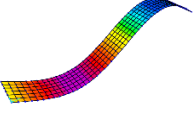
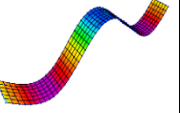
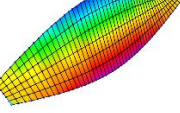
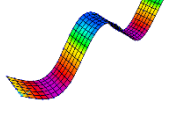
With the span at 20 m the fundamental frequency decreased by about 43 % compared to the 15 m span. It may be observed that as the span decreases the corresponding reduction in the fundamental natural frequencies is not regular. This may be due to increases in mass without the corresponding increases in stiffnesses. For number of modes with frequencies up to 100 Hz, two additional modes are added to the number.

Table 5.13: Parametric study result for timber deck span 20 m.

Length of deck: 20m					
Mode order	1	2	3	4	5
Mode	1.1	2.1	1.2	3.1	4.1
$f$ [Hz]	2.07176	8.30067	18.24844	18.7075	33.2837
Mode shape					
Modes up to 100 Hz: 10 modes					

Considering a system with span 25 m, the fundamental frequency is 1.326 Hz a reduction of about 36% with respect to the 20 m span system and about 84% when compared with the initial span of 10 m. The mode quantity increased from 5 at 10 m to 14 modes as the span was set to 25m. Thus, an increase of 15 meter resulted in 9 additional modes.

Table 5.14: Parametric study result for timber deck span 25 m.

Length of deck: 25m					
Mode order	1	2	3	4	5
Mode	1.1	2.1	3.1	1.2	4.1
$f$ [Hz]	1.32561	5.30873	11.96202	14.60272	21.29151
Mode shape					
Modes up to 100 Hz: 14 modes					

It is important to note that with increased number of modes within a particular cut-off frequency range, there is likely to be amplification of motion responses. This is because the motion perceptible at any instance may be due to the participation of all modes within the cut off range. The practical implications are that long span pedestrian bridges without adequate stiffnesses and damping may cause discomfort to pedestrians due to amplification of motion responses such displacements and accelerations.



As the results from the parametric study imply, a shorter span results in a higher frequency as the stiffness is inversely related to the span length. Furthermore, for all the other higher modes, the natural frequencies increase as the span decreases. As Figure 5.9 illustrates, the increases in the modal natural frequencies for each span is progressive and becomes almost linear in the case of the 25 m system. Modal separation could also be a source of vibration problems. This is because it could lead to coupling and hence amplification as it increases the risk of interference.

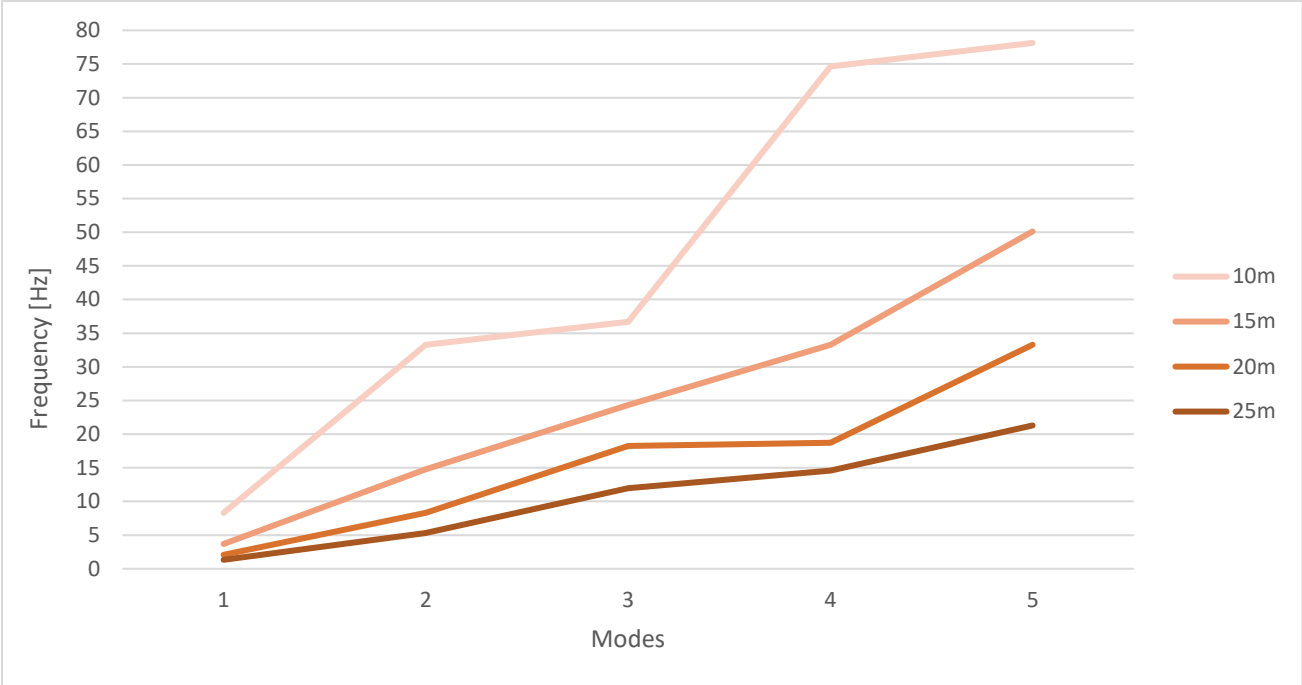


Figure 5.9: The graph represents the frequencies at each mode for the different spans studied.

## 5.5 Guideline Evaluation

This section will present the comfort criteria and acceleration calculations of the guideline and compare them to the peak acceleration calculated based on the field results. It is strongly advised to read Chapter 4 for a better understanding of the comfort criteria and to understand why the decisions done in this chapter were made.

### 5.5.1 Comfort Criteria

As mentioned earlier, the comfort criteria presented in Table 5.15 are compared to the peak acceleration values of the timber bridge's walking and running scenarios. Only the highest peak acceleration is compared because if the highest peak accelerations are adequate, all other calculated accelerations on the deck will also be adequate.

*Table 5.15: Acceleration limits in the comfort criteria for guidelines presented in Chapter 4.*

Guideline	Criteria
Statens Vegvesen	$a_r \leq 0,25 f^{0,7782}$
Eurocodes	$a < 0.7 \text{ m/s}^2$
UK – national annex	$0.5 \text{ m/s}^2 \leq a_{limit} \leq 2.0 \text{ m/s}^2$
ISO 10137	$0.15 \text{ m/s}^2 \leq a_{limit} \leq 0.6 \text{ m/s}^2$
SÉTRA Technical guide	$0.5 \text{ m/s}^2 \leq a_{limit} \leq 2.5 \text{ m/s}^2$
JRC	$0.5 \text{ m/s}^2 \leq a_{limit} \leq 2.5 \text{ m/s}^2$

### 5.5.2 Peak acceleration:

Figures 5.10 and 5.11 illustrate the bridge deck's acceleration values for walking and running, respectively. Whilst in the VDV and RMS the highest response occurs in test 7 for walking and test 4 for running, the same thing applies to the peak accelerations. For the walking scenario the highest acceleration is  $0.434 \text{ m/s}^2$  and for the running it was calculated as  $0.6712 \text{ m/s}^2$ .

## Walking

Test 1		Test 2		Test 3		Test 4		Test 5		Test 6		Test 7		Test 8	
0.124	0.165	0.187	0.163	0.112	0.146	0.179	0.199	0.134	0.117	0.225	0.178	0.274	0.351	0.15	0.054
0.105	0.157	0.169	0.151	0.088	0.157	0.171	0.178	0.145	0.115	0.176	0.149	0.248	0.285	0.121	0.057
0.09	0.159	0.153	0.136	0.109	0.152	0.165	0.204	0.168	0.143	0.18	0.162	0.328	0.342	0.136	0.061
0.081	0.138	0.159	0.131	0.127	0.156	0.177	0.195	0.158	0.17	0.184	0.133	0.419	0.434	0.164	0.062

Figure 5.10: Calculated peak walking acceleration for all field tests conducted on the timber bridge.

## Running

Test 1		Test 2		Test 3		Test 4		Test 5		Test 6		Test 7		Test 8	
0.1637	0.4568	0.3468	0.3228	0.1579	0.3335	0.486	0.6712	0.4136	0.3476	0.2481	0.1564	0.4253	0.4686	0.2976	0.1021
0.1069	0.4089	0.3659	0.3133	0.1434	0.3066	0.5849	0.6269	0.4195	0.354	0.2265	0.1084	0.4066	0.4415	0.2632	0.087
0.0873	0.3714	0.3638	0.3116	0.1683	0.289	0.5606	0.6569	0.4349	0.3401	0.2379	0.1157	0.3924	0.4411	0.2933	0.0738
0.0395	0.296	0.3603	0.3653	0.209	0.3509	0.4902	0.4908	0.4208	0.3744	0.2202	0.1047	0.3886	0.4375	0.3789	0.0821

Figure 5.11: Calculated peak running acceleration for all field tests conducted on the timber bridge.

Handbook N185 of Statens Vegvesen, Eurocode 5-2, The UK-NA, and SÉTRA all present methods to calculate the acceleration limit in their respective guidelines. The results from the calculations are presented with the guideline's corresponding acceleration criteria in Table 5.16. For theory on calculations see chapter 4.1 and 4.2 and see Appendix D for the calculations.

Table 5.16: Comparison of calculated acceleration and the guideline of each guideline presented in Chapter 4.

Guideline	Criteria [ $m/s^2$ ]	Calculated value [ $m/s^2$ ]
Handbook N185	$a_r \leq 0,25 f^{0,7782}$ = 0.6262	$a_r = 0.559$
Eurocode 5-2	$a < 0.7$	$a_{vert} = 0.3472$   $a_{vert,jog} = 2.083$
UK-NA	$0.5 \leq a_{limit} \leq 2.0$	$a_{limit} = 1.69$
SÉTRA Technical guide	$0.5 \leq a_{limit} \leq 2.5$	$a_{max} = 0.844$

From the results for acceleration for both respective guidelines, it is evident that the calculated acceleration for jogging in Eurocode 5-2 is too high compared to the one for walking. The jogging acceleration is almost three times the value of the comfort criteria in the Eurocodes. The reason may be the damping factor that is recommended in the Eurocode. The Eurocode recommends a damping ratio of 1.5%. That is a significant decrease compared to the 5.687 % recorded in the field test. The acceleration value drops to  $0.5495 \frac{m}{s^2}$  by implementing the experimental damping ratio. This acceleration value is satisfied compared to the limit from Table 5.16 and is used later for further comparison.

In Handbook 185, the dynamic load factor is governed by the damping in the guideline, as explained in Chapter 4.1. By choosing a damping factor close to 1% when the longest span of the bridge is 20 m, the dynamic load factor ( $\psi$ ) extracted from Figure 4.2 in Chapter 4.1 is seven, resulting in a calculated acceleration of  $0.559 \frac{m}{s^2}$ . However, mentioned earlier, a damping factor of only 1% did give fair value in this case. Nonetheless, a higher damping ratio would give more conservative values resulting in a lower acceleration for future comparison.

The UK-NA uses a method consisting of multiplying factors to determine an estimation of an acceleration limit. The factors are based on the bridge dimensions, usage, and environment. The calculated limit is shown in Table 5.16 and is adequate within the limit presented in the National Annex of the Eurocode. However, this is a much higher acceleration than the other values in the table and may seem incorrect compared to other values.

The calculations done based on the SÉTRA's calculation method also gave adequate values within the guidelines' own acceleration limits. Compared to for example the UK-NA, the SÉTRA's acceleration is half the value of the UK-NA and closer in comparison to the other guidelines, however it is still higher and does not fall under the Eurocodes limit.

### 5.5.3 Comparison of Guidelines and Peak Accelerations

Table 5.17 and Table 5.18 illustrates the comfort criteria limits and the calculated accelerations provided in Eurocode 5-2, Handbook N185, UK- NA and SÉTRA for both walking and jogging as well as the calculated peak acceleration calculated from the field tests as well.

*Table 5.17: Comparison of acceleration from field tests, calculated acceleration according to guidelines, and acceleration limits for walking.*

Guideline	Criteria	Calculated value [ $m/s^2$ ]	Peak acceleration [ $m/s^2$ ]
Handbook N185	$a_r \leq 0,25 f^{0,7782}$	0.559	0.434
Eurocodes	$a < 0.7 m/s^2$	0.3472	0.434
UK – National Annex	$0.5 m/s^2 \leq a_{limit} \leq 2.0 m/s^2$	1.69	0.434
ISO 10137	$0.15 m/s^2 \leq a_{limit} \leq 0.6 m/s^2$	-	0.434
SÉTRA Technical guide	$0.5 m/s^2 \leq a_{limit} \leq 2.5 m/s^2$	0.844	0.434
JRC	$0.5 m/s^2 \leq a_{limit} \leq 2.5 m/s^2$	-	0.434

The peak acceleration in the walking tests were just below the different guideline limits. The UK-NA, SÉTRA, and the JRC all have minimal limits of  $0.5 m/s^2$ , and a value of  $0.434 m/s^2$  falls short of their limit, implying that the acceleration could lead to critical frequencies that lead to the discomfort of the pedestrian crossing the bridge. Nevertheless, the peak acceleration for walking satisfied the limits in Handbook 185N and in the Eurocodes. However, only the Eurocode 5-2 calculation method for acceleration aligns somewhat with the walking frequency. As Figure 5.10 illustrates, the calculated acceleration is in the same ballpark as many of the values of test 7. This was the test area with the highest recorded accelerations.

Table 5.18: Comparison of acceleration from field tests, calculated acceleration according to guidelines, and acceleration limits for running.

Guideline	Criteria	Calculated value [ $m/s^2$ ]	Peak acceleration [ $m/s^2$ ]
Statens Vegvesen	$a_r \leq 0,25 f^{0,7782}$	0.559	0.6712
Eurocodes	$a < 0.7 m/s^2$	0.5495	0.6712
UK – National Annex	$0.5 m/s^2 \leq a_{limit} \leq 2.0 m/s^2$	1.69	0.6712
ISO 10137	$0.15 m/s^2 \leq a_{limit} \leq 0.6 m/s^2$	-	0.6712
SÉTRA Technical guide	$0.5 m/s^2 \leq a_{limit} \leq 2.5 m/s^2$	0.844	0.6712
JRC	$0.5 m/s^2 \leq a_{limit} \leq 2.5 m/s^2$	-	0.6712

The running values, on the other hand, were all within the acceleration range of all guidelines. However, the limit of the Eurocode was  $0.7 m/s^2$  compared to  $0.6712 m/s^2$ ; the calculated acceleration for running was just below the Eurocode limit for vertical vibration. Compared to other guidelines and the UK-NA, the Advised criteria of Eurocode 0 may need to be higher and could lead to implications in other projects.

By implementing the effective damping ratio from the field tests, the running acceleration decreased from  $2.083 m/s^2$  to  $0.5495 m/s^2$ . Thus, making the calculated value within the acceleration limit proposed by the Eurocode as illustrated in table 5.19.

The calculated values based on the frequencies in Handbook 185 and Eurocode 5-2 (including field test damping) for running were close compared to those based on the field test. Figures 5.11 shows that many accelerations in the middle of the spans are close in values. In other words, both the Eurocode 5-2 and Handbook N185 calculations align with the values of the field tests for running. The calculations based on SÉTRA's method is close to the recorded running acceleration. However, increasing the damping of Equation (4.9) in Chapter 4.5 from on 1% to 1.5%, the value decreases from  $0.844 m/s^2$  to  $0.563 m/s^2$ . In other words, the advised average damping value of 1% in SÉTRA is not as accurate as 1.5 % for this timber bridge.

The calculated value in the UK-NA is still relatively high compared to the recorded peak acceleration for running. However, as previously mentioned the calculations made in the UK-NA consists of multiplication factors based on the bridge dimensions, usage, and environment. Therefore, making the value an estimation.

## 6 Conclusions and Further Work

### 6.1 Deductions from results

The main objective of this thesis was to contribute to the global community researching vibrational matters of pedestrian bridges. The goal was to see how the modal characteristics of different pedestrian bridges changed with the implementation of new systems and materials. Other parameters were assessed and extracted from various analysis methods. The parameters were then compared to different comfort criteria of various national and international guidelines considering the vibrational matter of pedestrian bridges. The analysis was performed on two bridges in Viken Municipality in Norway—one in timber, and the other in steel. Field tests were performed on both bridges under normal operational conditions before the bridges were modelled in an FE-software and verified with the experimental results. After the verification, parametric studies were conducted on the timber bridge.

Some limitations were experienced in this thesis. Time was an essential factor that limited some of the planned work. Secondly, the weather in and around Ås, Norway was unstable this spring, resulting in time delays in the field experiment that limited the available time at hand. Last but not the least, the issue regarding the localized higher order modes of the steel bridge also made a comparison of the steel bridge limited. The grillage on the bridge was not continuous, leading to unsatisfactory results.

It was discovered in the experimental tests that the frequencies in both running and walking were corresponding in terms of values and mode shapes for the timber bridge. Similar coherence was also observed for the fundamental frequency of the steel bridge excited under walking and heel-drop.

The correspondence between the test and FE modal model for the timber bridge indicated the capabilities of FE software programs in simulating pedestrian bridges capable of representing real structures. The MAC was also calculated and showed that the modal shapes observed for both walking and running were matched each other.

Time-history responses were calculated and assessed for accelerations regarding running and walking. The implementation of VDV for pedestrian bridges has not been researched much in the past and it was shown in this thesis that it is applicable and satisfying as the VDV limits are likely to provide comfort to pedestrians on the bridge in terms of vibration serviceability. Parametric studies of different span length of the bridge showed that long span pedestrian bridges without adequate stiffnesses and damping may cause discomfort to pedestrians due to amplification of motion responses such as displacements and accelerations. However, Shorter spans resulted in higher frequencies because the stiffness is inversely related to the span length. It was noted that a source of problem could be Modal separation that could lead to coupling and hence amplification as it increases the risk of interference.

Accelerometers recordings of responses were found to be higher in the case of excitation of running as compared to those measured from the walking footfall forces. In comparison the values for the peak acceleration due to walking were observed to be comparable to calculated accelerations based on guideline provisions from Handbook N185, Eurocodes. However, peak acceleration limits for walking according to the UK-NA, the SÉTRA, and the JRC were not satisfied. The values were too low and did not fall within their limited range of acceptable comfort criteria. On the other hand, the running acceleration satisfied all comfort criteria of the guidelines. However, recommended damping ratios in the guidelines did not correspond with the effective dampings of the field experimental results. Upon substituting the field evaluated damping ratios in the formulas from the guideline's calculated accelerations are found to be comparable to the recorded peak acceleration in the field test as shown in Appendix D.



## 6.2 Further work: Recommendations

In the future, this thesis can be used as a cornerstone for further work on the matter of vibrations on pedestrian bridges. However, some limitations were met and limited the possible research that could be done. However, there are some recommendations for additional work that can be done in future reports:

- For further excitation and different frequency ranges, the implementation of a shaker could lead to exciting results. The performance of a shaker was experienced at the London Millennium Bridge and led to discoveries regarding the frequencies that simple human excitation could not.
- This thesis did not account for pedestrian loading as a group of people and therefore did not account for synchronization and accelerations regarding more than one pedestrian. Loading as a result of density increase is an occurring problem and may open doors for a broader perspective on the matter of vibrations in pedestrian bridges.
- As this thesis took upon the comfort criteria of said guidelines, the loading models were sadly not applied to the Finite Element Model. Due to the limitation of time and weather delays, as mentioned earlier, this was neglected. Nevertheless, for future work, the application of load models and comparing them to the comfort criteria of different bridges could lead to solutions many guidelines could find interesting.
- The vibrations investigated in this thesis were only in the vertical direction. It is possible to research the lateral direction for lateral vibration as well. The dominating problem in the London Millennium Bridge was the lateral vibrations, and many bridges excite oscillations in the lateral direction as well. This could therefore lead to discoveries on how to assess a matter that leads to discomfort for pedestrians.

## References

- Allemang, R. J., 2003. The Modal Assurance Criterion (MAC): Twenty years of use and abuse. *Journal of Sound and Vibration*, Januar.
- Altunişik, A. C., Bayraktar, A., Sevim, B. & Özdemir, H., 2011. Experimental and analytical system identification of Eynel arch type steel highway bridge. *Journal of Constructional Steel Research* 67, 16 July, pp. 1912-1921.
- Andriacchi, T., Ogle, J. & Galante, J., 1977. Walking speed as a basis for normal and abnormal gait measurements. *Journal of Biomechanics* 10, pp. 261-268.
- Bachmann, H. & Ammann, W., 1987. Vibration In Structures - Induced by Man and Machines. *Structural Engineering*.
- Bin Zahid, F., Ong, Z. C. & Yee Khoo, S., 2020. A review of operational modal analysis techniques for in-servicemodal identification. *Journal of the Brazilian Society of Mechanical Sciences and Engineering*, 7 July.
- Blanchard, J., Davies, B. L. & Smith, J. W., 1977. Design criteria and analysis for dynamic loading of footbridges. *Proceedings of the DOE and DOT TRRL Symposium on Dynamic Behaviour of Bridges*, 19 May, pp. 90-106.
- Brincker, R. & Ventura, C., 2015. *Introduction to Modal Analysis*. 1. ed. West Sussex : John Wiley & Sons Ltd.
- British Standard Institution , 2008. *UK National Annex to Eurocode 1: Actions on structures - Part 2: Traffic loads on bridges* , London: British Standard Institution - BSI.
- BSI - British Standars, 2008. *BS 6472: Guide To Evaluation of Human Exposure to Vibration in Buildings - Part 1*, London: BSI - British Standars.
- Chopra, A. K., 2014. *Dynamics of Structures - Theory and Applications to Earthquake Engineering*. 4. ed. Harlow: Pearson Education Limited.

CSI - Knowledge Base, 2022. *SAP2000*. [Online]

Available at: <https://wiki.csiamerica.com/display/sap2000/Home>

[Accessed 04 May 2023].

Dallard, P. F. A. J. et al., 2001. The London Millennium bridge: pedestrian-induced lateral vibration. *Journal of Bridge Engineering* 6, pp. 412-417.

Ekhholm, K., 2013. *Performance of Stress-Laminated-Timber Bridge Decks*, Gothenburg: Department of Civil and Environmental Engineering - Chalmers University of Technology .

European Committee for Standardization, 2010. *EN 1995-2 Eurocode 5: Design of timber structures - Part 2: Bridges*, Europe: European Committee for Standardization.

European Committee For Standardization, 2016. *EN 1990: Eurocode - Basis of structural design* , Europe: European Committee For Standardization.

Ewins, D. J., 2000. *Modal Testing: Theory, Practice and Application*. 2. ed. Baldock: Research Studies Press LTD..

French Ministry of Transport and Infrastructure, 2006. *Service d'Études Techniques des Routes et autoroutes - SÉTRA Technical guide*, Paris: French Ministry of Transport and.

Galbraith, F. & Barton, M., 1970. Ground loading from footsteps. *Journal of the Acoustic Society of America* 48, pp. 1288-1292.

García, D., Rosales, M. & Sampaio, R., 2018. Uncertainties in The Dynamic Behaviour of Timber Footbridges Considering Human Structure Interaction. *Mecánica Computacional Vol XXXVI*, 9 November, pp. 693-702.

Grønmo, S., 2023. *Kvalitativ metode*. [Online]

Available at: [https://snl.no/kvalitativ\\_metode](https://snl.no/kvalitativ_metode)

[Accessed 25 March 2023].

Grønmo, S., 2023. *Kvantitativ metode*. [Online]

Available at: [https://snl.no/kvantitativ\\_metode](https://snl.no/kvantitativ_metode)

[Accessed 25 March 2023].

Harper, F. C., Warlow, W. J. & C. B. L., 1969. *The forces applied to the floor by the foot in walking*, London: Department of Scientific and Industrial Research.

Huebner, K. H., Dewirst, D. L., Smith, D. E. & Byrom, T. G., 2001. *The Finite Element Method For Engineers*. 4. ed. Canada: John Wiley & Sons Inc..

IEEE, 2020. *The Advantages of the Finite Element Method*. [Online]

Available at: <https://innovationatwork.ieee.org/the-advantages-of-fem/>

[Accessed 24 April 2023].

Ingólfsson, E. T., 2011. *Pedestrian-induced lateral vibrations of footbridges*, Lyngby: DTU - Danmarks Tekniske Universitet.

International Organization for Standardization - ISO, 2003. *ISO 2631: Mechanical vibration and shock - Evaluation of human exposure to whole-body vibration*, Geneva: International Organization for Standardization - ISO.

International Organization for Standardization - ISO, 2007. *ISO 10137: Bases for design of structures - Serviceability of buildings and walkways*, Geneva: International Organization for Standardization - ISO.

Jacobsen, N.-J., Andersen, P. & Brincker, R., 2007. *Using EFDD as a Robust Technique for Deterministic Excitation in Operational Modal Analysis*, Aalborg: Aalborg University.

JRC Scientific and Technical Reports, 2009. *Design of Lightweight Footbridges for Human Induced Vibrations*, Luxembourg: European Commission.

Matsumoto, Y., Nishioka, T., Shiojiri, H. & Matsuzaki, K., 1978. Dynamic design of footbridges. *IABSE Proceedings, No. P-17/78*, pp. 1-15.

Miller, R. M., n.d. *Bridge Construction & Materials*. [Online]

Available at: <https://www.harfordcountymd.gov/654/Bridge-Construction-Materials>

[Accessed 02 Mai 2023].

Newland, D. E., 1993. *Random vibrations, spectral and wavelet analysis*. 3. ed. Harlow: Pearson Education Limited.

Norsk Limtreprodusenters forening, 2015. *Limtreboka*. 1. ed. s.l.:Norsk Limtreprodusenters forening.

Pavic, A., Armitage, T., Reynolds, P. & Wright, J., 2002. Methodology for modal testing of the Millennium Bridge, London. *Structures and Buildings 152 (2)*, 2002 May, pp. 111-121.

Ramoul, A. & Spremic, M., 2021. Vibration serviceability limit state of pedestrian bridges. *Building Materials and Structures 64*, 30 September, pp. 177-183.

Ren, W. X. & Zong, Z. H., 2004. Output-only modal parameter identification of civil engineering structures. *Struct. Eng. Mech 17*, pp. 429-444.

Rivera, H., Martínez, J. & Lozano, J. Á., 2015. Translation of SAP2000 Models to Equivalent-Models for FiniteElement Command-Based Softwares. *Ideas en Ciencia*, 5 June, pp. 37-48.

Schlaich, M., 2002. Planning conditions for footbridges. *Proceedings of the International Conference on the Design and Dynamic Behaviour of Footbridges*, 20 November, pp. 40-52.

Statens Vegvesen, 2009. *Håndbok 185 - Bruprosjektering*, s.l.: Statensvegvesen.

Statens Vegvesen, 2015. *Håndbok 400 - Bruprosjektering*, Norge: Statens Vegvesen.

Stevenson, R., 1821. Description of bridges of suspension. *Edinburgh Philosophical Journal 5*, pp. 237-256.

Structural Vibration Solution - SVIBS, 2023. *Frequency Domain Decomposition*. [Online]

Available at: <https://svibs.com/frequency-domain-decomposition/>

[Accessed 23 April 2023].

Structural Vibration Solutions - SVIBS, 2023. *ARTEMIS Modal*. [Online]

Available at: <https://svibs.com/>

[Accessed 29 April 2023].

SVIBS, S. V. S. -, 2023. *Stochastic Subspace Identification*. [Online]

Available at: <https://svibs.com/stochastic-subspace-identification/>

[Accessed 27 April 2023].

Tubino, F., 2017. Human-structure interaction in pedestrian bridges: a probabilistic approach.

*Procedia Engineering, Volume 199*, pp. 2883-2888.

Ussher, E., Arjomandi, K. & Smith, I., 2022. Status of Vibration Serviceability Design Methods for Lightweight Timber Floors. *Journal of Building Engineering 50*, 29 January.

Wheeler, J. E., 1982. Prediction and control of pedestrian induced vibration in footbridges. *ASCE Journal of the*, p. 2045–2065.

Zhou, D., Han, H. J. T. & Xu, X., 2015. Comparison of two models for human-structure interaction. *Applied Mathematical Modelling Volume 40, Issues 5-6*, 6 November, pp. 3738-3748.

Zivanovic, S., Pavic, A. & Ingolfsson, E. T., 2010. *Modelling Spatially Unrestricted Pedestrian*, s.l.: ASCE Journal of Structural Engineering, Vol. 136, No. 10, pp. 1296-1308.

Zivanovic, S., Pavic, A. & Reynolds, P., 2005. Human–structure dynamic interaction in footbridges. *Bridge engineering 158, Issue BE4*, 23 September, pp. 165-177.

Zivanovic, S., Pavic, A. & Reynolds, P., 2005. *Vibration Serviceability of Footbridges Under Human-Induced Excitation: a literature review*, Sheffield: Journal of Sound And Vibration.

# Appendix A: Blueprints for timber bridge

All the blueprints located in Appendix A and B are courtesy of Viken Municipality and Statens Vegvesen - Norwegian Public Road Administration in Norway.

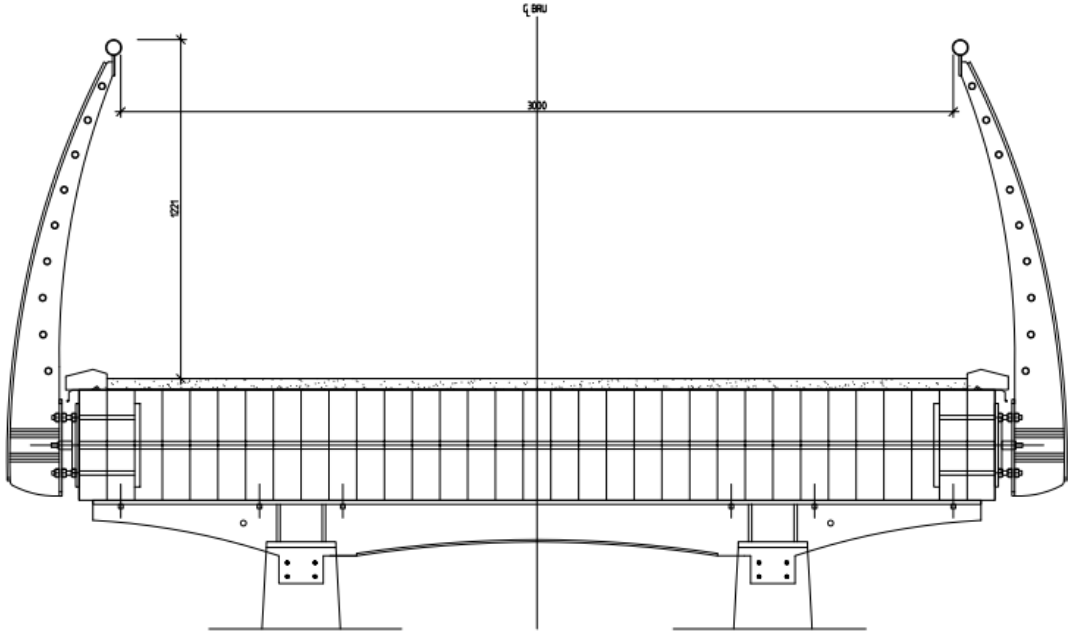


Figure A. 2: Cross section of the timber bridge deck blueprints courtesy of Viken Municipality

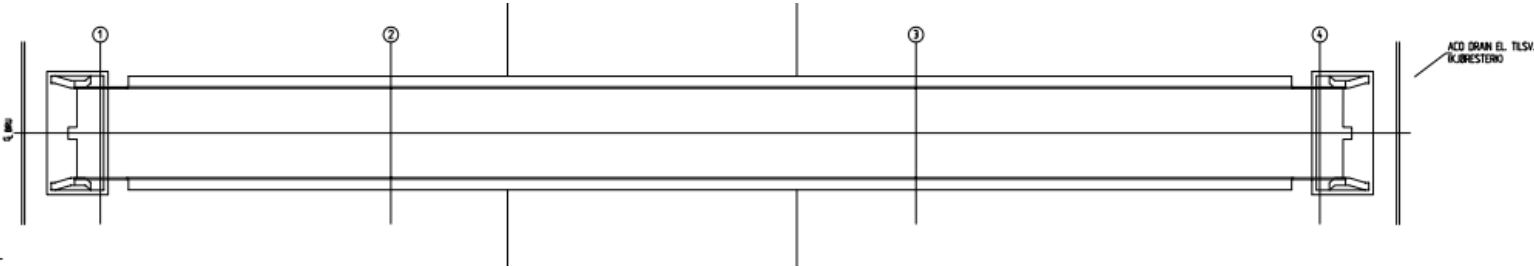


Figure A. 1: The timber bridge deck seen from the above.

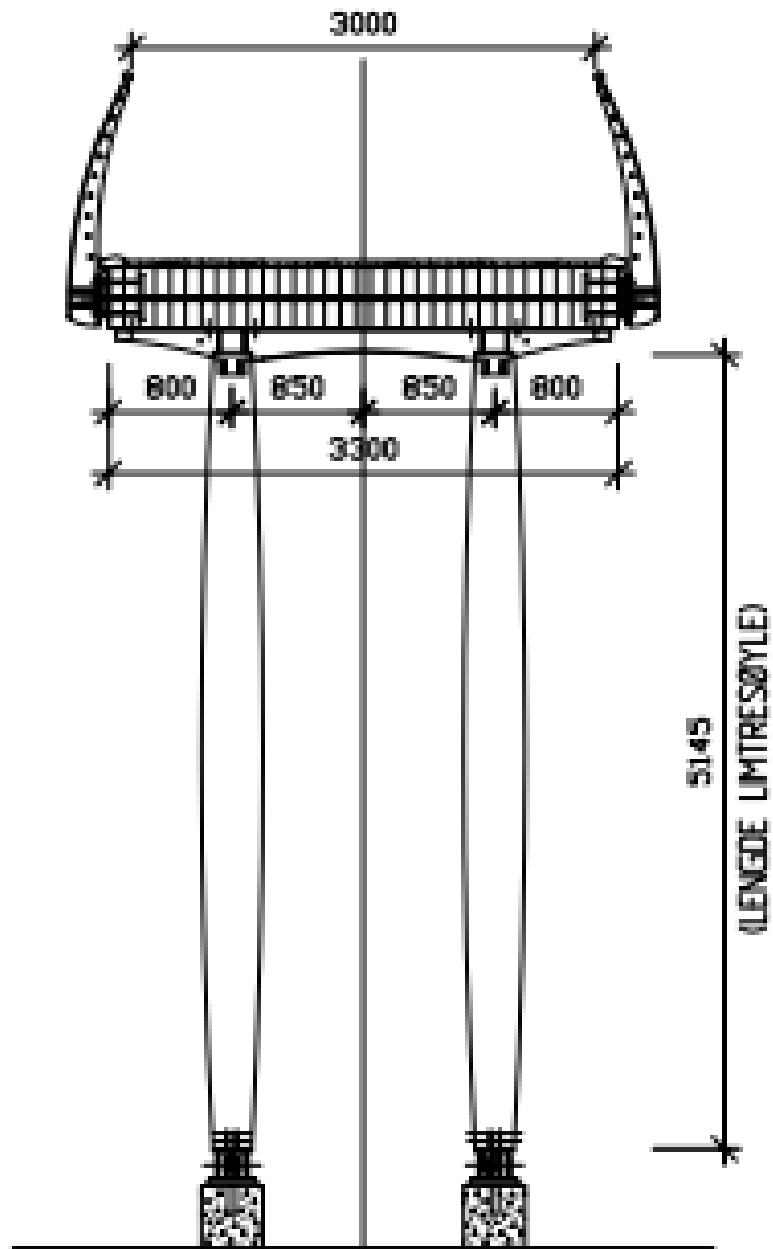
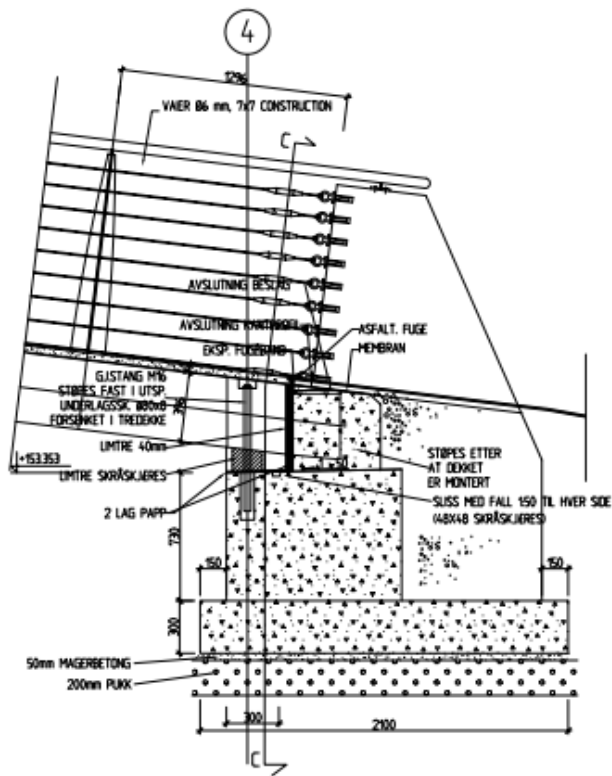
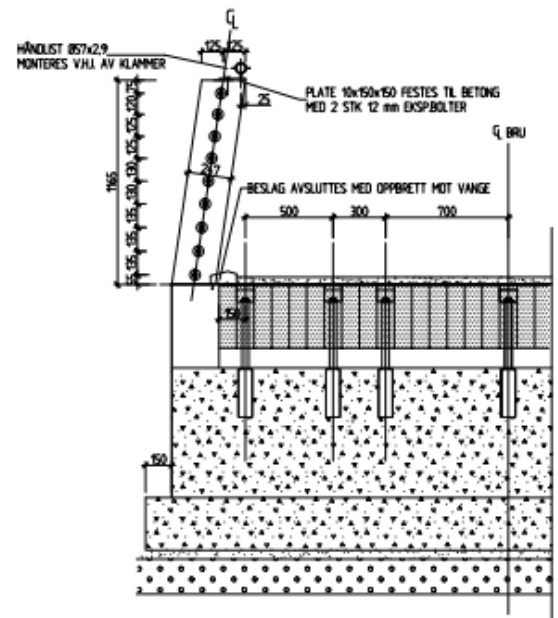


Figure A. 3: Cross section of the timber bridge including deck and columns.





DETALJ NR 1 - FUNDAMENT I AKSE 4  
1:20



SNITT C-C  
1:20

Figure A. 4: Longitudinal section (left) and cross section (right) of the concrete abutments on each side of the timber bridge.

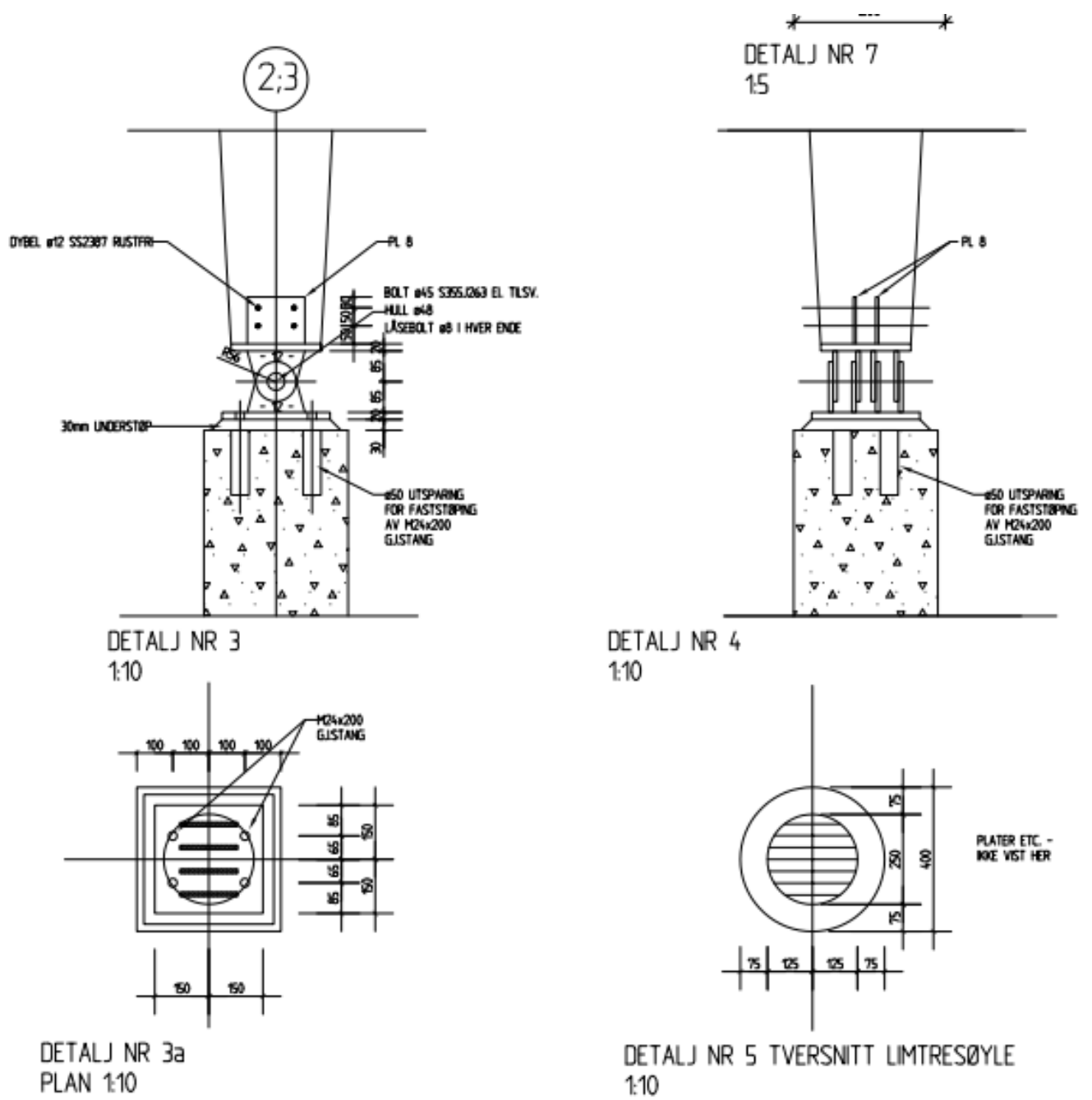


Figure A. 5: Illustrations with dimensions of the oval columns and connections of the concrete fundaments.

## Appendix B: Blueprints for Steel bridge

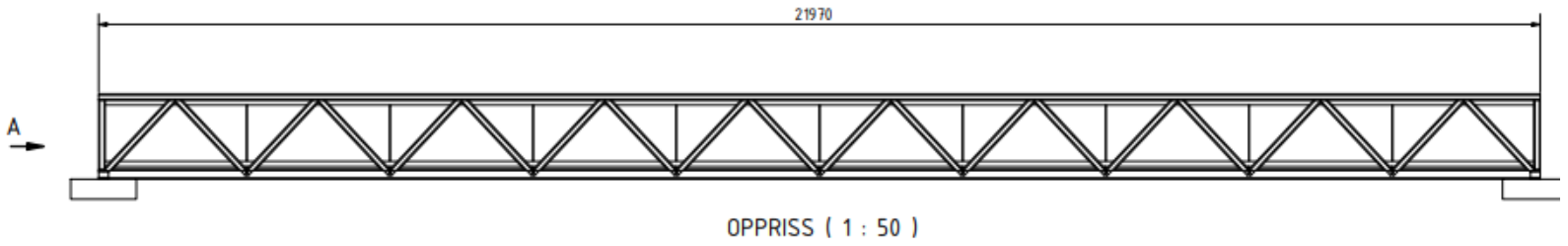


Figure B. 1: Longitudinal section of the steel bridge with truss configuration.

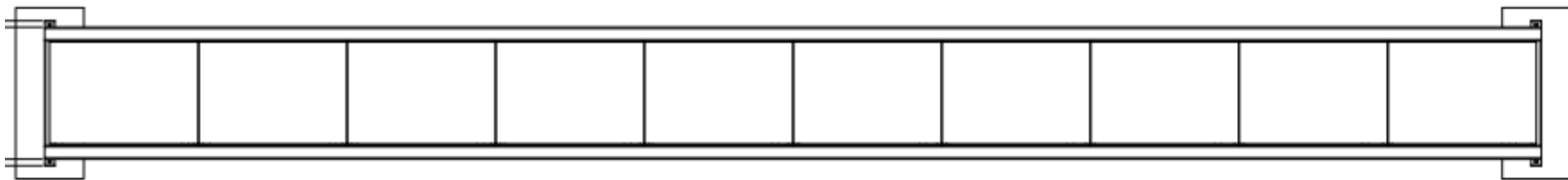


Figure B. 2: The steel bridge seen from above and marked with lines where the floor beams are placed.

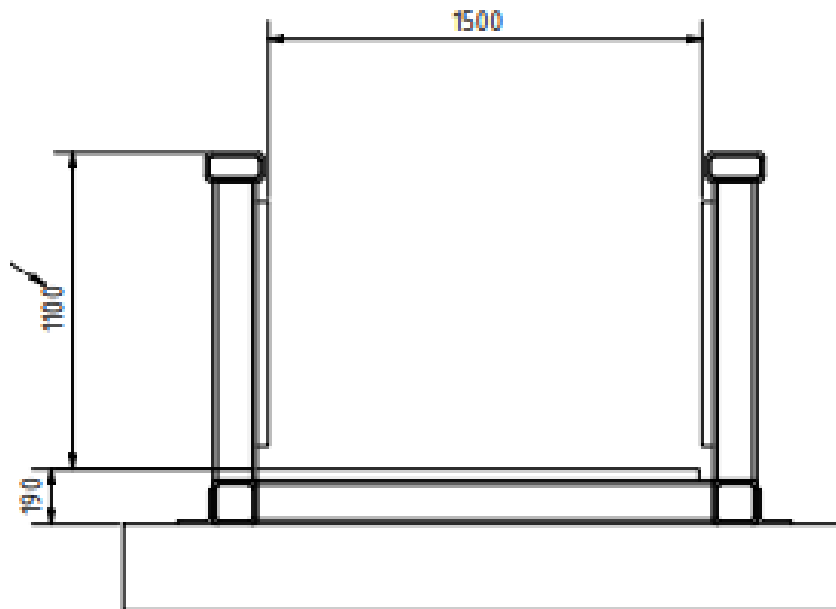


Figure B. 3: Cross section of the bridge showing both the top and bottom chords.

Appendix C: Raw data on the accelerometers and amplifiers used to conduct the field tests.

## **ACCELEROMETER, ICP®, SEISMIC**

### **Model 393B12**

Seismic, high sensitivity, ceramic shear ICP® accel., 10 V/g, 0.15 to 1k Hz, 2-pin top conn.

- Sensitivity: ( $\pm 10\%$ )10000 mV/g (1019.4 mV/(m/s<sup>2</sup>))
- Broadband Resolution: 0.000008 g rms (0.00008 m/s<sup>2</sup> rms)
- Measurement Range: 0.5 g pk (4.9 m/s<sup>2</sup> pk)
- Frequency Range: ( $\pm 5\%$ )0.15 to 1000 Hz
- Electrical Connector: 2-Pin MIL-C-5015
- Weight: 7.4 oz (210 gm)

### **Model 393B31**

Seismic, high sensitivity, ceramic flexural ICP® accel., 10 V/g, 0.1 to 200 Hz, 2-pin top conn.

- Sensitivity: ( $\pm 5\%$ )10.0 V/g (1.02 V/(m/s<sup>2</sup>))
- Broadband Resolution: 0.000001 g rms (0.000009 m/s<sup>2</sup> rms)
- Measurement Range: 0.5 g pk (4.9 m/s<sup>2</sup> pk)
- Frequency Range: ( $\pm 5\%$ )0.1 to 200 Hz
- Electrical Connector: 2-Pin MIL-C-5015
- Weight: 22.4 oz (635 gm)

*Figure C. 1: Details regarding accelerometer Model 39B31 and Model 393B12*

HBM Catman

## MX440B and MX840B universal amplifiers



### 4- or 8-channel universal amplifier of the QuantumX family

It supports the following transducer technologies:

- Full-bridge or half-bridge strain gauges (DC or 4.8 kHz carrier frequency)
- SG quarter bridge with adapter
- Current-fed piezoelectric transducers (IEPE / ICP®)
- Piezoresistive full bridge
- Resistance thermometers (PT100 / PT1000) Thermocouples (types K, N, R, S, T, B, E, J, C)
- Ohmic resistor
- Potentiometric transducers (Poti)
- Inductive half or full bridge, LVDT
- Voltage ( $\pm 100\text{mV}$ ,  $\pm 10\text{V}$ ,  $\pm 60\text{V}$ ) and Current (0 / 4 ... 20 mA, 2-/3- or 4-wire)
- Channel 5-8, in addition: frequency, counter, rotary encoder, SSI
- CAN bus

Figure C. 2: Details regarding amplifiers Model MX440B and Model MX840B

## MX1601B universal amplifier

### 16-channel amplifier of the QuantumX family

It supports the following transducer technologies:

- Current-fed piezoelectric transducers (IEPE, ICP)
- Voltage ( $\pm 100$  mV,  $\pm 10$  and  $\pm 60$  V)
- Current (0/4 ... 20 mA, 2-/3- or 4-wire)



## Precise

- Accurate measurement attributed to the 0.03 accuracy class
- Integrated delta-sigma-analog-to-digital converter (24 bit)
- Digital low-pass filters (Bessel, Butterworth, linear phase)
- Sample rates of up to 20 kS/s per channel and a signal bandwidth of up to 3 kHz
- Interference-free signal path due to electrically isolated channels
- Working standard calibration certificate according to ISO 10012 stored in the module
- DAkkS certificate (ISO 17025) from HBM on request

Figure C. 3: The specifications for the MX1601B amplifier.

Appendix D: Acceleration calculation based on the guidelines.

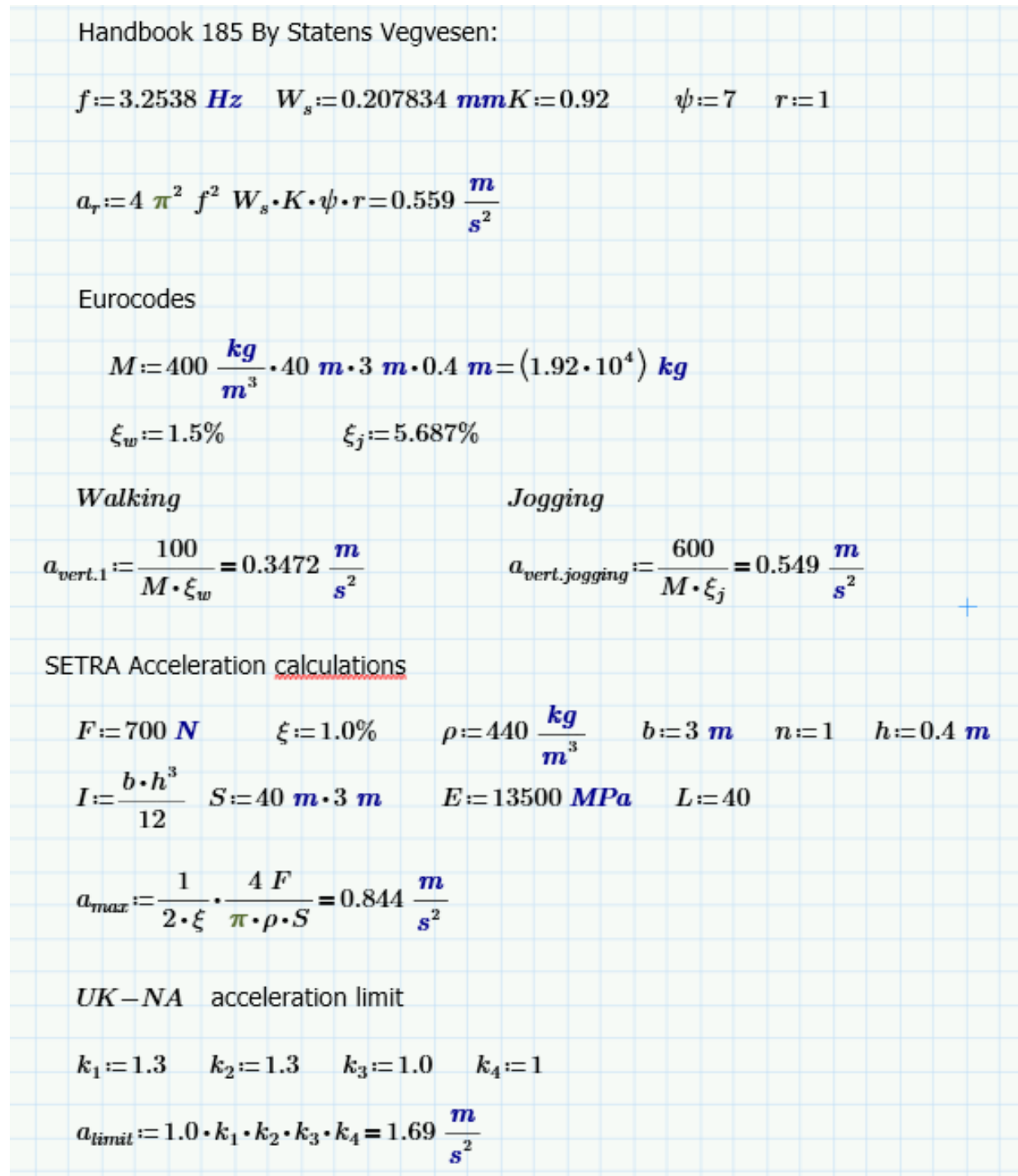


Figure D. 1: Acceleration calculations made in accordance with the guidelines presented.



**Norges miljø- og biovitenskapelige universitet**  
Noregs miljø- og biovitenskapelige universitet  
Norwegian University of Life Sciences

Postboks 5003  
NO-1432 Ås  
Norway